New Fluorescent Probes and Assays for Lactate and Hydrogen Peroxide

Dissertation zur Erlangung des Doktorgrades der Naturwissenschaften
(Dr. rer. nat.)

an der
naturwissenschaftlichen Fakultät IV
– Chemie und Pharmazie –
der Universität Regensburg

vorgelegt von

Dominik Berndt Michael Grögel

aus Deggendorf

im Juli 2011

New Fluorescent Probes and Assays for Lactate and Hydrogen Peroxide

Doctoral Thesis

by

Dominik Berndt Michael Grögel

für Kathrin

Diese Doktorarbeit entstand in der Zeit von Dezember 2007 bis Juli 2011 am Institut für Analytische Chemie, Chemo- und Biosensorik an der Universität Regensburg.

Diese Arbeit wurde angeleitet von Prof. Dr. Otto S. Wolfbeis.

„Bei Herausforderungen geht es nicht ums Gewinnen, sondern darum, herauszufinden, was für ein Mensch man ist."[i]

Carlo Pedersoli

---

[i] Carlo Pedersoli, Lorenzo de Luca, Davidi de Filippi, „Bud Spencer – Mein Leben, meine Filme – Die Autobiographie", Schwarzkopf & Schwarzkopf, Berlin, 2011, 4. Auflage.

Danksagung

Mein erster Dank gilt meinem Doktorvater **Prof. Otto S. Wolfbeis**, der mir mit Rat und Tat zur Seite gestanden ist und es mir ermöglicht hat, die vielfältige Chemie der Farbstoffe zu entdecken. Darüber hinaus bedanke ich mich für die ausgezeichneten Arbeitsbedingungen.

Besonderer Dank gebührt **Dr. Axel Dürkop** für die sehr gute Betreuung in den vergangenen Jahren sowie der flotten, dennoch gründlichen Korrektur der vorliegenden Arbeit.

Weiterhin möchte ich mich bei **Prof. Joachim Wegener** und **Barbara Goricnik** für die gute Zusammenarbeit bei den Zelluntersuchungen mit einem meiner Farbstoffe bedanken.

Den Mitarbeitern der Zentralen Analytik gebührt ein „Vergelts Gott", weil sie mit ihren Untersuchungen zum Erfolg dieser Doktorarbeit beigetragen haben. Namentlich seien **Dr. Rudolf Vasold** (HPLC) sowie **Josef Kiermeier** und **Wolfgang Söllner** (MS) erwähnt.

Weiterer Dank gebührt **Thomas „Horst" Lang** für das eifrige Korrekturlesen meiner Dissertation. Darüber hinaus danke ich ihm sowie **Dr. Thomas Hirsch**, **Dr. Péter Kele** und **Dr. Martin Link** für die gemeinsamen Montagabende „beim Vu".

Meinem „ewigen" Laborkollegen **Lorenz Fischer** danke ich für die angenehme und kameradschaftliche Atmosphäre in unserem Labor „am Ende des Instituts". Den Doktoren **Robert Meier** und **Mark-Steven Steiner** danke ich für die Einführung in das RGB Imaging. Für das freundschaftliche Arbeitsklima am Institut ist unter anderem **Gisela Hierlmeier**, **Joachim Rewitzer**, **Angelika Stoiber**, **Sayed Saleh**, **Daniela Achatz**, **Max Oberleitner**, **Michaela Sperber** und **Dr. Judith Stolwijk** zu danken. Zum Erfolg der Arbeit haben die Azubis **Matthias Hautmann**, **Sabine Hofmeister** und **Roxanne Harteis** sowie mein österreichischer Forschungspraktikant **Norbert Galler** beigetragen.

Die schöne Zeit in Regensburg ist mit vielen Freunden und Wegbegleitern verbunden, vor allem **Dr. Thomas Ehrenschwender**, **Dr. Carolin Fischer**, **Dr. Ulrich Lange**, **Susanne Ohmayer**, **Dr. Christopher „Günni" Rose**, **Carolin Russ** und **Dr. Stefan Welsch**.

Tanti saluti ai miei amici italiani **Dr. Roberto Fanelli** e **Dr. Cristian Cattaneo**. Sind so nette Collega!

Table of Contents

1. Introduction

1.1 Aim of the Work

Increased lactate levels inside cells are closely related to tumour growth according to the Warburg hypothesis.[1, 2] While an up-regulation of glycolysis can be observed, pyruvate concentrations remain low, indicating that the tumour employs either the glycolytic pathway as a whole or other metabolic routes. The amount of blood vessels built during angiogenesis causes an oxygen gradient in tumour cells. Glucose is converted to lactate in order to produce more energy for carcinogenesis in hypoxic tumour cells.[3] In vivo studies on rat brain, whose striatum contained C6 glioma cells (brain tumour), yielded a decrease of glucose from 2.14 mM to 1.71 mM and an increase of lactate concentrations from 0.86 mM to 1.65 mM compared to a control cell line.[4] Lactate, however, needs to be withdrawn from cells due to intracellular homeostasis.[5] This is realized by a monocarboxylate transporter.[6] Thus, lactate is immediately taken up by aerobic tumour cells and subjected to the citric acid cycle to form CO_2 and $NADH/H^+$.[7] The latter is oxidized to NAD^+ and the emerging energy is harnessed by ATP-synthase to form ATP.

Enzymes are key players in carcinogenesis. In case of bowel cancer, tumour growth is regulated by DNAse X whereas metabolism is controlled by transketolase-like-1 (TKTL-1)[8]. Both enzymes are overexpressed and high lactate levels together with acetoin, diacetyl and acetyl phosphate occur as result of a changed metabolism. Therefore, TKTL-1 forms an interesting target as information about enzymatic activity relates to tumour growth. The metabolic products can be labelled with specific fluorescent probes that change their spectral properties (fluorescence intensity or lifetime) upon attachment. Probes for acetoin[9], diacetyl[10] and acetyl phosphate[11] are known and may be subjected to tumour imaging[12] by means of fluorescence microscopy in reference to the pioneering work of *Weissleder et al.* This group developed a method for imaging tumour-associated lysosomal protease activity in a xenograft mouse model *in vivo*.[13] They applied artificial enzyme substrates based on a peptide chain that bears two fluorophores whose fluorescence was quenched due to their proximity. Fluorescence is recovered once the peptide is cleaved by intracellular protease. This enables the detection of tumours even at an early stage.

Artificial enzyme substrates may alter the activity of TKTL-1, which can result in changes of glycolysis. Therefore, lactate is an interesting target in tumour diagnosis. Hence, novel luminescent probes and detection schemes for lactate were investigated in

this PhD thesis. The first part constitutes the design and development of fluorescent probes, which are attached to lactate via covalent or hydrogen bonds or coordinative interactions. Only one specific probe for lactate has been reported so far[14] illustrating how challenging lactate detection is. In the present work, a new approach should be performed using phenylboronic acids as receptor. They were to be attached to fluorophores and characterized regarding the change of spectroscopic properties upon interaction with both lactate enantiomers. The interference of saccharides on the boronic acid-lactate interaction was to be considered as well.

The second part of the PhD thesis deals with the development of an enzymatic assay for L-lactate. Lactate oxidase (LOx) catalyses the conversion of L-lactate to pyruvate under release of hydrogen peroxide (HP). A new probe for HP (HP Green) had already been prepared by Martin Link within his PhD thesis, yet more detailed investigations regarding the response of HP Green to HP in the presence and absence of horseradish peroxidase (HRP) were to be performed here. Moreover, HP Green was to be combined with HRP and LOx. In the next step, glucose oxidase (GOx) was to be utilized as a further model for oxidase based assays in general owing to the fact that it is a very stable, easy to handle enzyme that is inexpensive even in high quantities. Finally, the L-lactate assay was to be established based on all obtained results. All assays require characterization with respect to their dynamic range and their limit of detection.

1.2 Theoretical Background

Fluorescence spectroscopy has become a powerful tool as a specific and sensitive method in analytical chemistry.[15] Parker`s law expresses the correlation of fluorescence intensity and concentration of a fluorophore where F is the fluorescence intensity detected, I is the intensity of the photo-exciting light, ε is the molar absorbance, c is the concentration of the fluorophore, d is the length of the optical pathway, ϕ is the fluorescence quantum yield and k is a factor regarding the specific instrumental geometry:

$$F = I \cdot \varepsilon \cdot c \cdot d \cdot \phi \cdot k$$

Upon interaction of a fluorophore with an analyte, spectral changes on lifetime[16, 17], quantum yield[18] and/or fluorescence intensity[19], respectively occur. The latter was measured in the present work in order to prove probe-analyte interactions, establish

calibration plots or determine the kinetics. Two processes that modulate intensity are described below as well as a novel method for the visualization of luminophores. More details about probes for lactate and hydrogen peroxide are presented at the beginning of the respective chapters.

1.2.1 Photoinduced Electron Transfer

Generally, photoinduced electron transfer (PET) occurs from a PET donor to an excited fluorophore (acceptor) that quenches its fluorescence. All PET probes are based on three components that can be combined depending on the desired application. A fluorophore acts as a light-harvesting antenna and simultaneously as an electron acceptor. The number of appropriate dyes is virtually unlimited and covers the whole spectral range. Thus, the choice of the fluorophore is governed by the required excitation and emission wavelengths. The spacer consists of at least one methylene group and separates the fluorophore from the receptor. This spacer facilitates the PET effect which is a long range process.[20] The ideal number of methylene groups is 3 to 4 according to investigations on fluorescent PET probes for alkali metal ions with different spacer lengths.[21] The third unit is the receptor (electron donor) that binds or reacts with an analyte, thereby changing the PET efficiency. The molecule of interest determines the constitution of the receptor unit.[22, 23, 24] PET probes are mostly designed as "OFF-ON" fluorophores with low/no fluorescence in the unbound state and a strong fluorescence after binding to (or reaction with) an analyte (Fig. 1.1).[25]
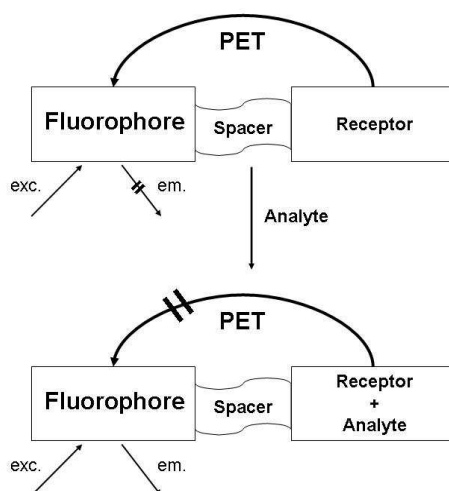
Figure 1.1. Interruption of PET after binding of an analyte to the receptor unit.

In the following, the PET effect is discussed by means of the "OFF-ON" principle, however, cases are reported for "ON-OFF" fluorophores as well.[26] Usually, the analyte-free receptor is bearing free electron pairs, e.g. at nitrogen or oxygen atoms. One of these electrons can be transferred to the partially unoccupied HOMO of the photoexcited luminophore. Back-electron transfer then can take place from the excited state of the luminophore to the HOMO of the receptor. This leads to a radiationless deactivation of the excited state, and fluorescence is quenched. If an analyte binds to the receptor, the PET is interrupted and fluorescence is turned on (Fig. 1.2). In most cases, the free electron pair of the donor is removed or blocked by the analyte either through oxidation[27, 28], covalent binding[22, 29] or noncovalent interactions[24].
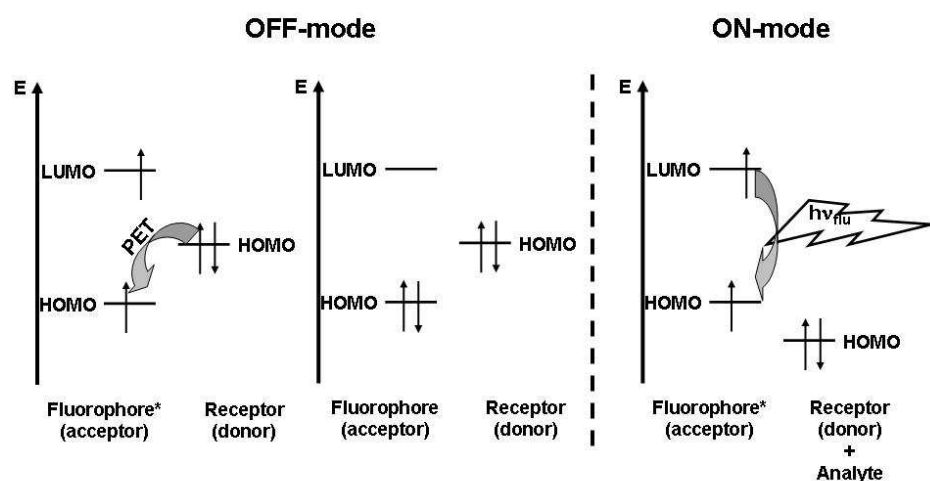
Figure 1.2. Simplified molecular orbital energy diagrams showing the relative energetic dispositions of HOMO/LUMO of the fluorophore and HOMO of the donor involved in PET. The asterisk (*) symbolizes the excited fluorophore.[31]

In the unbound state, the energy of the HOMO of the receptor lies between the energy levels of HOMO and LUMO of the fluorophore. The reaction of the receptor with the analyte shifts the energy of its HOMO to lower values, thereby stabilizing it. Ideally, it lies energetically lower than the HOMO of the fluorophore. In this case, the PET effect is completely suppressed (ON-mode).[30, 31] The comparison of the redox potentials of receptor and dye gives information about the energetic levels of the involved HOMOs according to the HOMO/LUMO concept. This is a useful criterion for the design of such triad molecules. Weller[32] has derived a quantitative approach to predict PET efficiency. In all cases, PET occurs fast and fully reversible.

In case of HP sensitive receptors, their oxidation decreases the energy level of the HOMO. *Soh et al.*[33] proved this assumption by energy level calculations using a diphenylphosphine moiety as a receptor and its corresponding oxide as a model PET system (Fig. 1.3). The probe DPPEA-HC (7-hydroxy-2-oxo-N-(2-(diphenylphosphino)ethyl)-2H-chromene-3-carboxamide) contains a redox-active diphenylphosphine group that is spaced from the coumarin fluorophore by two methylene groups. It shows a maximum in absorption at 405 nm and emits blue fluorescence with a maximum at 449 nm. Following the oxidation by HP, the fluorescence intensity is switched on with a 137-fold increase after a reaction time of 60 min at 37 °C. The dynamic response ranges from 0 to 20 µM of HP. Some ROS such as superoxide (O_2^-) and NO increase the fluorescence intensity to an extent similar to HP, while $ONOO^-$, OCl^-, $OH^·$, or $ROO^·$ do not interfere significantly. Accordingly, the coumarin based probe was the first HP sensitive PET probe that was applicable in aqueous solution.
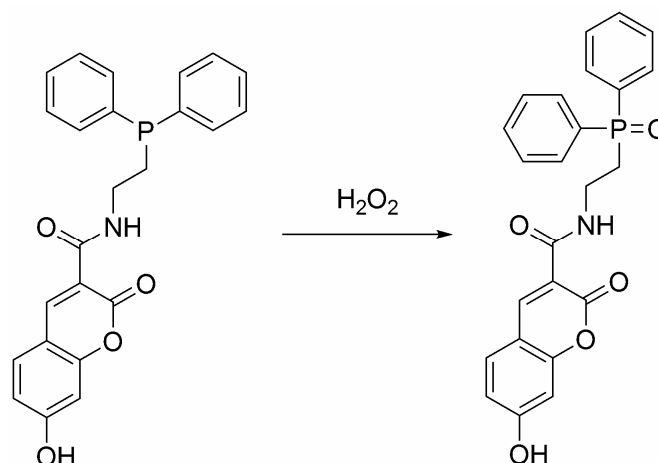
Figure 1.3. DPPEA-HC (left) reacts with HP to DPPEA-HC oxide (right).

Up to now, no PET probe for lactate is mentioned, however, manifold other fluorophores with PET are described in the literature, for instance for H^+,[34] Na^+,[35] K^+,[25] Ca^{2+},[36] Mg^{2+},[37] Ag^+,[38] Zn^{2+},[39] HPO_4^-,[40] uronic acid[41] and glucose.[42, 43] The latter makes use of boronic acid moieties[44], which partly quench fluorescence. Upon interaction with glucose, PET is suppressed and emission is enhanced. More details on the mechanism are described in chapter 4. PET probes based on naphthalimides and ruthenium(II) complexes are presented in this dissertation.

1.2.2 Internal Charge Transfer

Spectral properties can also be altered by applying an internal charge transfer (ICT). Common ICT fluorophores consist of electron-donating (δ^+) and electron-accepting (δ^-) terminal groups that are connected via a delocalized π-system. Furthermore, they contain heteroatoms (non hydrocarbons), which increase the amphiphilic character resulting in a more pronounced dipole moment of the "push-pull" system. Upon excitation, this dipole moment increases as electron density is being redistributed[45] and microenvironmental changes can be detected by absorption and/or fluorescence. Fluorescence is mostly red-shifted with increasing solvent polarity[46] because dipole-dipole interactions of fluorophore and solvent stabilize the excited S_1 state, thus lowering its energy.[30] Optical detection of solvent vapours applies environmentally sensitive ICT fluorophores like Nile Red, which was embedded in different polymers to be placed at tips of an optical fibre.[30, 47] Furthermore, the large dipole moment of ICT fluorophores renders them suitable for indicators of quickly occurring changes in the membrane potential.[48]

ICT probes for charged or neutral analytes additionally afford a receptor in order to increase the number of target species in the microenvironment which can exert stronger electric fields than solvent molecules. The integrated fluorophore-receptor system is the most common structural principle which features the same backbone of electron-donating and electron-withdrawing terminals but the receptor is integrated in one terminal or in between. Both, the wavelengths of absorption and emission are up to changes upon analyte capture depending on the position of the receptor (Fig. 1.4).[49] Binding of a cation, for instance, is likely to result in a blue shift in absorption and emission when the receptor is connected to the electron-donating terminal. The repulsive forces between the positively charged guest and the δ^+-end of the fluorophore destabilize the electronic excited S_1 state, thus increasing its energy.[30] The extent of the blue-shifted bands is related to the concentration of the cation, enabling a ratiometric analysis.[50] In contrast, fluorescence is red shifted when the electron-accepting end is carrying the cation receptor.[30] PET probes for cations do not display such shifts offering one criterion for discerning PET and ICT.
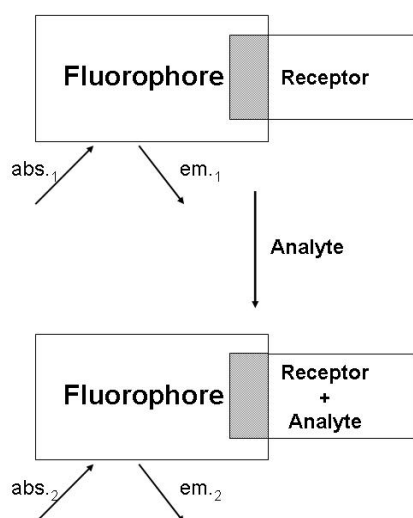
Figure 1.4. Change of spectral properties in ICT probes upon binding of an analyte to the receptor unit.[49]

Up to now, no ICT probe for lactate has been reported, however, various other species are targeted like Zn^{2+},[51] Cu^{2+},[52] saccharides[53, 54], pyrophosphate[55] and cyanide[56]. In case of HP, the ICT probe Peroxy Lucifer 1 (PL1) undergoes changes of emission colour upon reaction with HP (Fig. 1.5).[57] PL1 displays absorption and emission maxima at 375 and 475 nm, respectively. The boronate-based carbamate protecting group is cleaved off by a chemoselective reaction with HP. The electron-poor donor becomes an electron rich amine, which causes a red shift in absorption and fluorescence (to 435 and 540 nm, respectively). Ratioed emission intensities display a 12-fold increase after 2 h of reaction when 200 μM HP was added to 5 μM PL1. The probe was successfully subjected to ratiometric imaging of HP in living cells. ICT probes based on hemicyanines and aminocyanines were prepared in this work.
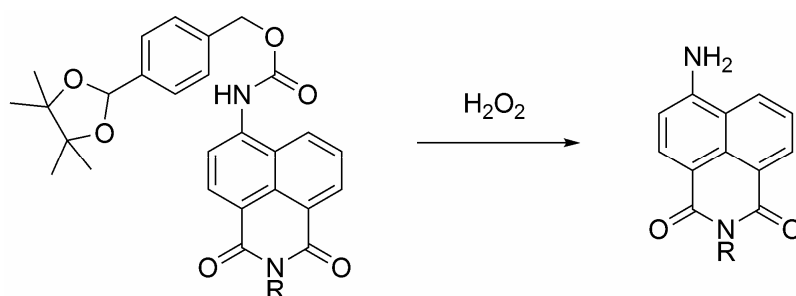
Figure 1.5. Peroxy Lucifer 1 (left) reacts with HP to an aminonaphthalimide (right).

1.2.3 Red-Green-Blue Readout of Digital Cameras

Photometers, fluorimeters and other optical instruments like microscopes are well known and established for the determination of analytical targets. They remain mostly at a fixed position which affords the user to prepare samples in proximity or to transport them to the device. In-field measurements however, need miniaturized systems that are easy to transport and to handle. Despite electrochemical methods, small optical tools or sensors are known. A recent trend in sensor technology makes use of digital cameras to substitute classic instruments.[58] The core of modern digital cameras consists of either a CCD (charge coupled device) or a CMOS (complementary metal oxide semiconductor) chip, which contains small spots (pixels) with defined areas that are sensitive to light. A Bayer filter is placed in front of every pixel, which allows transmission of either only red (R), green (G) or blue (B) light of the visible spectrum.[59] Therefore, data are recorded in three separate channels and the final colour picture is a superposition of all three RGB data sets. The RGB sensitivity of the camera covers the whole visible spectrum (Fig. 1.6) and colour information is given as brightness values in the form of histograms.[60]
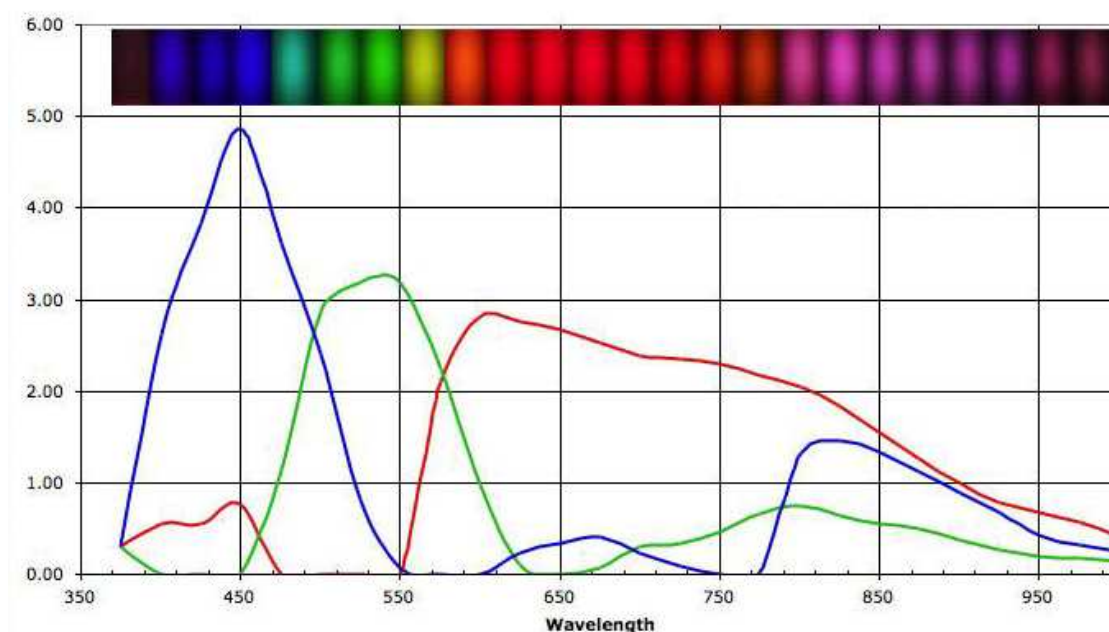
Figure 1.6. Spectral response of the Canon EOS 50D CMOS chip showing the sensitivities of the red, green and blue (RGB) channels (image taken from reference [60]).

Smart sensor design affords fluorophores, whose fluorescence matches the RGB channels. Data evaluation follows a reverse procedure: The picture is split and colour (=analytical) information of the respective channel (=histogram) can be obtained by using software like Adobe Photoshop or ImageJ. Beside mono-colour systems,[61, 62, 63] it is more common to utilize a dual colour system consisting of a sensing and a reference dye in order to enable ratiometric read-out. It is important that both fluorophores can be excited at the same wavelength and display different Stokes´ shifts, so that the emissions are stored in different memories of the RGB camera. The mean values of the histograms of sensing and reference channel, respectively, are divided to obtain ratiometric evaluation. Methods based on this principle have been successfully developed for oxygen[58], imaging of intracellular oxygen[60] or biogenic amines[64] as well as a dual RGB sensor[65] for oxygen and pH. The latter was used to monitor progress in wound healing, where small cameras simplify measurements in-field instead of bulky instruments like fluorimeters or sophisticated imaging set-ups.

In the present work, a RGB digital camera was used to follow changes of a mono-colour system in normal rat kidney (NRK) cells upon incubation with hydrogen peroxide. The fluorescence intensity was recorded in the green channel and analysis was performed with ImageJ (see chapter 2.8).

1.3 Literature

1. O. Warburg, Das Carcinomproblem. *Angew. Chem.*, **1926**, 32, 949 – 968.

2. O. Warburg, On the origin of cancer cells. *Science*, **1956**, 123, 309 – 314.

3. G. L. Semenza, Tumor metabolism: cancer cells give and take lactate. *J. Clin. Invest.*, **2008**, 118, 3835 – 3837.

4. O. Darbin, M. Lonjon, M. H. Quentien, J. F. Michiels, P. Grellier, J. Negrin, J. C. Rostain, J. J. Risso, In vivo study of tumor metabolism: an application of new multi-probe microdialysis system in the striatum of freely moving rats grafted with C6 cells. *Brain Res.*, **2000**, 881, 121 – 127.

5. X. T. Zheng, H. B. Yang, C. M. Li, Optical detection of single cell lactate release for cancer metabolic analysis. *Anal. Chem.*, **2010**, 82, 5082 – 5087.

6. V. N. Jackson, A. P. Halestrap, The kinetics, substrate, and inhibitor specifity of the monocarboxylate (lactate) transporter of rat liver cells determined using the fluorescent intracellular pH indicator, 2´,7´-bis(carboxyethyl)-5(6)-carboxyfluorescein. *J. Biol. Chem.*, **1996**, 271, 861 – 868.

7. J. C. Portais, R. Schuster, M. Berle, P. Canioni, Metabolic flux determination in C6 glioma cells using carbon-13 distribution upon [1-^{13}C]glucose incubation. *Eur. J. Biochem.*, **1993**, 217, 457 – 468.

8. S. Langbein, M. Zerilli, A. zur Hausen, W. Staiger, K. Rensch-Boschert, N. Lukan, J. Popa, M. P. Ternullo, A. Steidler, C. Weiss, R. Gobholz, F. Willeke, P. Alken, G. Stassi, P. Schubert, J. F. Coy, Expression of transketolase TKTL1 predicts colon and urothelial cancer patient survival: Warburg effect reinterpreted. *Brit. J. Cancer*, **2006**, 94, 578 – 585.

9. A. Duerkop, P. Kéle, personal communication.

10. X. Li, A. Duerkop, O. S. Wolfbeis, A fluorescent probe for diacetyl detection. *J. Fluoresc.*, **2009**, 19, 601 – 606.

11. M.-S. Steiner, A. Duerkop, Luminescent ruthenium probe for the determination of acetyl phosphate in complex biological matrices. *Analyst*, **2011**, 136, 148 – 154

12. T. Jiang, E. S. Olson, Q. T. Nguyen, M. Roy, P. A. Jennings, R. Y. Tsien, Tumor imaging by means of proteolytic activation of cell-penetrating peptides. *Proc. Natl. Acad. Sci. USA*, **2004**, 101, 17867 – 17872.

13. R. Weissleder, C.-H. Tung, U. Mahmood, A. Bogdanov Jr., In vivo imaging of tumors with protease-activated near-infrared fluorescent probes. *Nat. Biotechnol.*, **1999**, 17, 375 – 378.

14. R. Pal, D. Parker, L. C. Costello, A europium luminescence assay of lactate and citrate in biological fluids. *Org. Biomol. Chem.*, **2009**, 7, 1525 – 1528.

15. J. R. Lakowicz, Principles of fluorescence spectroscopy. 3rd edition, **2006**, Springer Science+Business Media, New York.

16. G. Liebsch, I. Klimant, C. Krause, O. S. Wolfbeis, Fluorescent imaging of pH with optical sensors using time domain dual lifetime referencing. *Anal. Chem.*, **2001**, 73, 4354 – 4363.

17. M. Wu, Z. Lin, M. Schäferling, A. Duerkop, O. S. Wolfbeis, Fluorescence imaging of the activity of glucose oxidase using a hydrogen-peroxide-sensitive europium probe. *Anal. Biochem.*, **2005**, 340, 66 – 73.

18. Z. Lin, M. Wu, M. Schäferling, O. S. Wolfbeis, Fluorescent imaging of citrate and other intermediates in the citric acid cycle. *Angew. Chem. Int. Ed.*, **2004**, 43, 1735 – 1738.

19. M. Schäferling, O. S. Wolfbeis, Europium tetracycline as a luminescent probe for nucleoside phosphates and its application to the determination of kinase activity. *Chem. Eur. J.*, **2007**, 13, 4342 – 4349.

20. A. P. de Silva, T. Gunnlaugsson, T. E. Rice, Recent evolution of luminescent photoinduced electron transfer sensors. *Analyst*, **1996**, 121, 1759 – 1762.

21. H.-F. Ji, R. Dabestani, G. M. Brown, R. L. Hettich, Spacer length effect on the photoinduced electron transfer fluorescent probe for alkali metal ions. *Photochem. Photobiol.*, **1999**, 69, 513 – 516.

22. G. J. Mohr, New chromogenic and fluorogenic reagents and sensors for neutral and ionic analytes based on covalent bond formation - a review of recent developments. *Anal. Bioanal. Chem.*, **2006**, 386, 1201 – 1214.

23. T. S. Snowden, E. V. Anslyn, Anion recognition: synthetic receptors for anions and their application in sensors. *Curr. Opin. Chem. Biol.*, **1999**, 3, 740 – 746.

24. E. V. Anslyn, Supramolecular analytical chemistry. *J. Org. Chem.*, **2007**, 72, 687 – 699.

25. H. He, M. A. Mortellaro, M. J. P. Leiner, R. J. Fraatz, J. K. Tusa, A fluorescent sensor with high selectivity and sensitivity for potassium in water. *J. Am. Chem. Soc.*, **2003**, 125, 1468 – 1469.

26. N. R. Cha, S. Y. Moon, S. K. Chang, New ON-OFF type Ca^{2+}-selective fluoroionophore having boron-dipyrromethene fluorophores. *Tetrahedron Lett.*, **2003**, 44, 8265 – 8268.

27. N. Soh, Recent advances in fluorescent probes for the detection of reactive oxygen species. *Anal. Bioanal. Chem.*, **2006**, 386, 532 – 543.

28. K. Akasaka, T. Suzuki, H. Ohrui, H. Meguro, Study on aromatic phosphines for novel fluorometry of hydroperoxides (I) – synthesis and spectral properties of diphenyl aryl phosphines and their oxides. *Anal. Lett.*, **1987**, 20, 731 – 745.

29. A. P. de Silva, H. Q. N. Gunaratne, J. L. Habib-Jiwan, C. P. McCoy, T. E. Rice, J. P. Soumillion, New fluorescent model compounds for the study of the photoinduced electron transfer: The influence of a molecular electric field in the excited state. *Angew. Chem. Int. Ed.*, **1995**, 34, 1728 – 1731.

30. A. P. de Silva, H. Q. N. Gunaratne, T. Gunnlaugsson, A. J. M. Huxley, C. P. McCoy, J. T. Rademacher, T. E. Rice, Signaling recognition events with fluorescent sensors and switches. *Chem. Rev.*, **1997**, 97, 1515 – 1566.

31. A. P. de Silva, T. S. Moody, G. D. Wright, Fluorescent PET (photoinduced electron transfer) sensors as potent analytical tools. *Analyst*, **2009**, 134, 2385 – 2393.

32. A. Weller, Electron-transfer and complex formation in the excited state. *Pure Appl. Chem.*, **1968**, 16, 115 – 123.

33. N. Soh, O. Sakawaki, K. Makihara, Y. Odo, T. Fukaminato, T. Kawai, M. Irie, T. Imato, Design and development of a fluorescent probe for monitoring hydrogen peroxide using photoinduced electron transfer. *Bioorg. Med. Chem.*, **2005**, 13, 1131 – 1139.

34. R. A. Bissell, A. P. de Silva, H. Q. N. Gunaratne, P. L. M. Lynch, G. E. M. Maguire, K. R. A. S. Sandanayake, Molecular fluorescent signalling with fluor-spacer-receptor systems: approaches to sensing and switching devices via supramolecular photophysics. *Chem. Soc. Rev.*, **1992**, 21, 187 – 195.

35. H. He, M. A. Mortellaro, M. J. P. Leiner, S. T. Young, R. J. Fraatz, J. K. Tusa, A fluorescent chemosensor for sodium based on photoinduced electron transfer. *Anal. Chem.*, **2003**, 75, 549 – 555.

36. H. He, K. Jenkins, C. Lin, A fluorescent chemosensor for calcium with excellent storage stability in water. *Anal. Chim. Acta*, **2008**, 611, 197 – 204.

37. Y. Suzuki, N. Saito, H. Komatsu, D. Citterio, T. Kubota, Y. Kitamura, K. Oka, K. Suzuki, Design and application of novel fluorescent indicators of Mg^{2+}. *Anal. Sci.*, **2001**, 17, 1451 – 1454.

38. M. Gubelmann, A. Harriman, J.-M. Lehn, J. L. Sessler, Photoinduced charge separation within a polymetallic supramolecular system. *Chem. Commun.*, **1998**, 77 – 79.

39. S. C. Burdette, G. K. Walkup, B. Spingler, R. Y. Tsien, S. J. Lippard, Fluorescent sensors for Zn^{2+} based on a fluorescein platform: synthesis, properties and intracellular distribution. *J. Am. Chem. Soc.*, **2001**, 123, 7831 – 7841.

40. M. E. Huston, E. U. Akkaya, A. W. Czarnik, Chelation enhanced fluorescence detection of non-metal ions. *J. Am. Chem. Soc.*, **1989**, 111, 8735 – 8737.

41. M. Takeuchi, M. Yamamoto, S. Shinkai, Fluorescent sensing of uronic acids based on a cooperative action of boronic acid and metal chelate. *Chem. Commun.*, **1997**, 1731 – 1732.

42. T. D. James, K. R. A. S. Sandanayake, S. Shinkai, A glucose-selective molecular fluorescence sensor. *Angew. Chem. Int. Ed.*, **1994**, 33, 2207 – 2209.

43. H. S. Mader, O. S. Wolfbeis, Boronic acid based probes for microdetermination of saccharides and glycosylated biomolecules. *Microchim. Acta*, **2008**, 162, 1 – 34.

44. T. D. James, P. Linnane, S. Shinkai, Fluorescent saccharide receptors: a sweet solution to the design, assembly and evaluation of boronic acid derived PET sensors. *Chem. Commun.*, **1996**, 281 – 288.

45. J. F. Callan, A. P. de Silva, D. C. Magri, Luminescent sensors and switches in the early 21st century. *Tetrahedron*, **2005**, 61, 8551 – 8588.

46. P. Fromherz, A. Heilemann, Twisted internal charge transfer in (aminophenyl)-pyridinium. *J. Phys. Chem.*, **1992**, 96, 6864 – 6866.

47. T. A. Dickinson, J. White, J. S. Kauer, D. R. Walt, A chemical-detecting system based on a cross-reactive optical sensor array. *Nature*, **1996**, 382, 697 – 700.

48. P. Fromherz, C. O. Müller, Voltage-sensitive fluorescence of amphiphilic hemicyanine dyes in neuron membrane. *Biochim. Biophys. Acta*, **1993**, 1150, 111 – 122.

49. A. P. de Silva, D. B. Fox, T. S. Moody, S. M. Weir, The development of molecular fluorescent switches. *Trends Biotechnol.*, **2001**, 19, 29 – 34.

50. A. P. de Silva, N. D. McClenaghan, Simultaneously multiply-configurable or superposed molecular logic systems composed of ICT (internal charge transfer) chromophores and fluorophores integrated with one- or two-ion receptors. *Chem. Eur. J.*, **2002**, 8, 4935 – 4945.

51. K. Hanaoka, Y. Muramatsu, Y. Urano, T. Terai, T. Nagano, Design and synthesis of a highly sensitive off-on fluorescent chemosensor for zinc ions utilizing internal charge transfer. *Chem. Eur. J.*, **2010**, 16, 568 – 572.

52. Z. Xu, Y. Xiao, X. Qian, J. Cui, D. Cui, Ratiometric and selective fluorescent sensor for Cu^{II} based on internal charge transfer (ICT). *Org. Lett.*, **2005**, 7, 889 – 892.

53. S. Arimori, L. I. Bosch, C. J. Ward, T. D. James, Fluorescent internal charge transfer (ICT) saccharide sensor. *Tetrahedron Lett.*, **2001**, 42, 4553 – 4555.

54. S. Arimori, L. I. Bosch, C. J. Ward, T. D. James, A D-glucose selective fluorescent internal charge transfer (ICT) sensor. *Tetrahedron Lett.*, **2002**, 43, 911 – 913.

55. Y. Sun, C. Zhong, R. Gong, E. Fu, A highly selective fluorescent probe for pyrophosphate in aqueous solution. *Org. Biomol. Chem.*, **2008**, 6, 3044 – 3047.

56. R. Badugu, J. R. Lakowicz, C. D. Geddes, Enhanced fluorescence cyanide detection at physiologically lethal levels: reduced ITC-based signal transduction. *J. Am. Chem. Soc.*, **2005**, 127, 3635 – 3641.

57. D. Srikun, E. W. Miller, D. W. Domaille, C. J. Chang, An ICT-based approach to ratiometric fluorescence imaging of hydrogen peroxide produced in living cells. *J. Am. Chem. Soc.*, **2008**, 130, 4596 – 4597.

58. X. Wang, R. J. Meier, M. Link, O. S. Wolfbeis, Photographing oxygen distribution. *Angew. Chem. Int. Ed.*, **2010**, 122, 5027 – 5029.

59. M.-S. Steiner, Optical detection of acetyl phosphate and biogenic amines. **2010**, Dissertation Universität Regensburg.

60. X. Wang, H.-H. Gorris, J. A. Stolwijk, R. J. Meier, D. B. M. Groegel, J. Wegener, O. S. Wolfbeis, Self-referenced RGB colour imaging of intracellular oxygen. *Chem. Sci.*, **2011**, 2, 901 – 906.

61. W.-Q. Deng, A. H. Flood, J. Fraser Stoddart, W. A. Goddard III, An electrochemical color-switchable RGB dye: tristable [2]catenane. *J. Am. Chem. Soc.*, **2005**, 127, 15994 – 15995.

62. S. Pang, X. Cui, J. DeModena, Y. M. Wang, P. Sternberg, C. Yang, Implementation of a color-capable optofluidic microscope on a RGB CMOS color sensor chip substrate. *Lab Chip*, **2010**, 10, 411 – 414.

63. Y. M. Shirshov, V. Y. Khoruzhenko, K. V. Kostyukevych, R. V. Khristosenko, I. A. Samoylova, A. S. Pavluchenko, A. V. Samoylov, Y. V. Ushenin, Analysis of some alcohol molecules based on the change of RGB components of interferentially colored calixarene films. *Sens. Actuat. B*, **2007**, 122, 427 – 436.

64. M.-S. Steiner, R. J. Meier, A. Duerkop, O. S. Wolfbeis, Chromogenic sensing of biogenic amines using a chameleon probe and the red-green-blue readout of digital cameras. *Anal. Chem.*, **2010**, 82, 8402 – 8405.

65. R. J. Meier, Luminescent single and dual sensors for in-vivo imaging of pH and pO_2. **2011**, Dissertation Universität Regensburg.

2. Development of Fluorescent Probes for Hydrogen Peroxide

2.1 Introduction

Hydrogen peroxide (HP) belongs to the class of the so-called "reactive oxygen species" (ROS), which also include species such as singlet oxygen, hydroxy radicals, superoxide anions, or nitric oxide. These are associated with various functions in (patho)physiological processes.[1, 2] If exposed to oxidative stress, cells can be substantially damaged if the levels of ROS exceed the tolerable physiological range.[3] HP also is vasoactive and plays key roles in inflammation and hypoxia-reoxygenation of tissues.[4, 5] Despite its hazard to organisms, HP is ubiquitous as it is a by-product of many metabolic reactions and acts as a messenger in cellular signaling.[6, 7, 8] HP also is a widely used bleaching agent and its toxicity towards microorganisms is harnessed for purposes of cleaning and disinfection. Furthermore, it is used in the production of explosives and as a rocket fuel.

Common detection schemes for HP are based on either electrochemical or optical methods. Amperometric methods are widely used because HP is monitored (continuously) either via anodic oxidation or cathodic reduction. The resulting current is dependent on the concentration of HP. Recent approaches combine either graphene[9] or silver nanoparticles[10] with classical electrode materials. Optical methods are an attractive alternative and widely used in the fields of imaging[11] or high-throughput screening[12]. Optical methods based on photometry[13] are interesting candidates but fluorometry displays higher sensitivity and can be applied to coloured and scattering media such as cells and tissue. *Maeda et al.*[14] have synthesized a number of pentafluorobenzenesulfonyl fluoresceins, so-called "off-on" fluorophores. The fluorescein backbone is connected to a quenching pentafluorobenzenesulfonyl group which is cleaved off by HP via perhydrolysis, thus regenerating the phenolic group of fluorescein. Best LOD values are 4.6 pmoles of HP. Boronic acid pinacol esters are a very promising alternative for switching off the fluorescence of fluorescein.[15] Upon perhydrolysis, non-toxic boronic acid is formed and fluorescence restored.[16, 17] While the selectivity and sensitivity of these probes is excellent, their synthesis is (partly) time consuming and laborious. EuTc, an Eu(III) complex with the antibiotic tetracycline (Tc) as a ligand is easy to prepare and displays emission at 616 nm. A 15-fold increase in fluorescence intensity is achieved when HP replaces a water molecule from the coordination site, and the LOD is 1.8 µM. However, phosphate and citrate interfere.[18, 19, 20, 21] Amplex Red is the most common used probe for HP.[22, 23, 24] It is

non-fluorescent but converted into a fluorescent product after reaction with HP in the presence of peroxidase. It has a very low LOD (50 nM) and is widely applied in microtiter plate based schemes, e.g. to determine the activity of oxidases or the concentration of their substrates. Assay kits are commercially available.[25] Other probes for HP are based on the photoinduced electron transfer (PET) effect.[26] DPPEA-HC, for instance, possesses a diphenylphosphine moiety as a receptor group that is spaced from a coumarin fluorophore by two methylene groups.[27] The fluorescence intensity of the probe depends on the PET effect exerted by the diphenylphosphine donor on the coumarin acceptor. Once the diphenylphosphine moiety is oxidized, electron transfer (and thus quenching) is blocked and fluorescence restored. The state of the art in fluorescent probes for HP has been reviewed recently.[28]

2.2 Synthesis and Characterization of HP-Probes with Redox Active *p*-Anisidine and N,N-Dimethyl-*p*-phenylene Diamine Head Groups

The aminonaphthalimide fluorophore was chosen because of its spectral characteristics and relatively facile preparation. Manifold derivatives are described in literature, e. g as an acceptor in PET probes for sensing alkaline ions[29, 30], or as an intracellular marker.[31, 32, 33] Such naphthalimides have moderate molar absorbance (7,600 L*mol^{-1}*cm^{-1}), but can be photoexcited with blue light, display strongly green and pH-independent fluorescence under physiological conditions, and a large Stokes´ shift. Then, *p*-anisidine and N,N-dimethyl-*p*-phenylene diamine, respectively, were chosen as PET quenchers that are easily oxidized by HP but are otherwise stable on air. Each redox active group was synthetically spaced from the naphthalimide fluorophore by two methylene groups. In addition, the fluorophore was equipped with a C-6 linker carrying a terminal carboxy group to impart better water solubility and to enable covalent immobilization.[34]

2.2.1 Synthesis of an HP Probe with Redox Active *p*-Anisidine Group
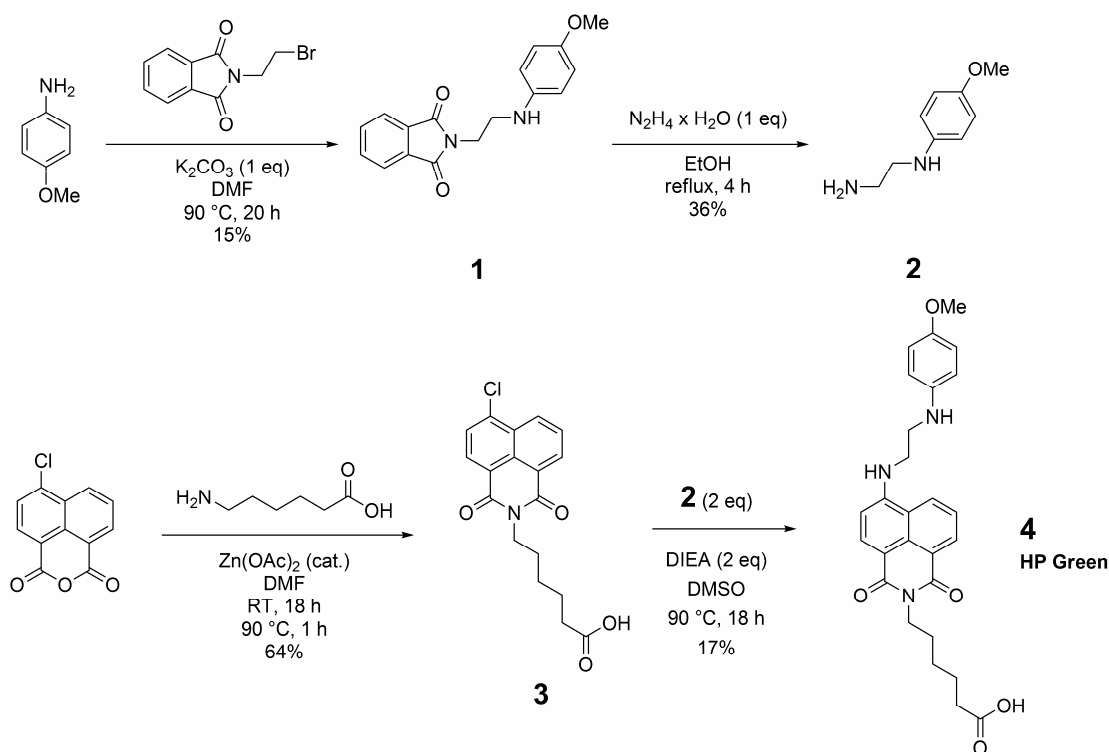
Figure 2.1. Synthetic pathway to compound **4** ("HP Green").

Compound **4** was synthesized in four steps using affordable starting materials (Fig. 2.1, developed by Martin Link[35]). *p*-Anisidine and *N*-(2-bromoethyl)phthalimide were reacted, by analogy to a related protocol,[36] to give compound **1**. Its phthalimide protective group was then cleaved off by hydrazinolysis in boiling ethanol to yield the primary amine **2**. In parallel, 4-chloro-1,8-naphthalic anhydride and 6-aminocaproic acid[37] were reacted to obtain the corresponding naphthalimide **3**. Substitution of the chloro group in **3** by the amino group of **2** in the presence of diisopropylethylamine (DIEA) yielded probe **4** in the form of a yellowish solid, which is called HP Green. Recrystallization yielded all compounds in high purity and in 44 to 78% yields. HP Green is stable for months if stored under inert gas. It is well soluble in halogenated organic solvents, ethyl acetate or polar aprotic solvents like DMF or DMSO. Aqueous stock solutions were prepared by diluting solutions in DMSO with water or buffer (usually phosphate buffered saline, PBS). The dye is soluble in water in concentrations of up to 500 µM. A 100 µM stock solution in PBS/DMSO (9:1, v/v) is stable for more than two weeks.

2.2.2 Synthesis of an HP Probe with Redox Active N,N-Dimethyl-*p*-phenylene Diamine Group
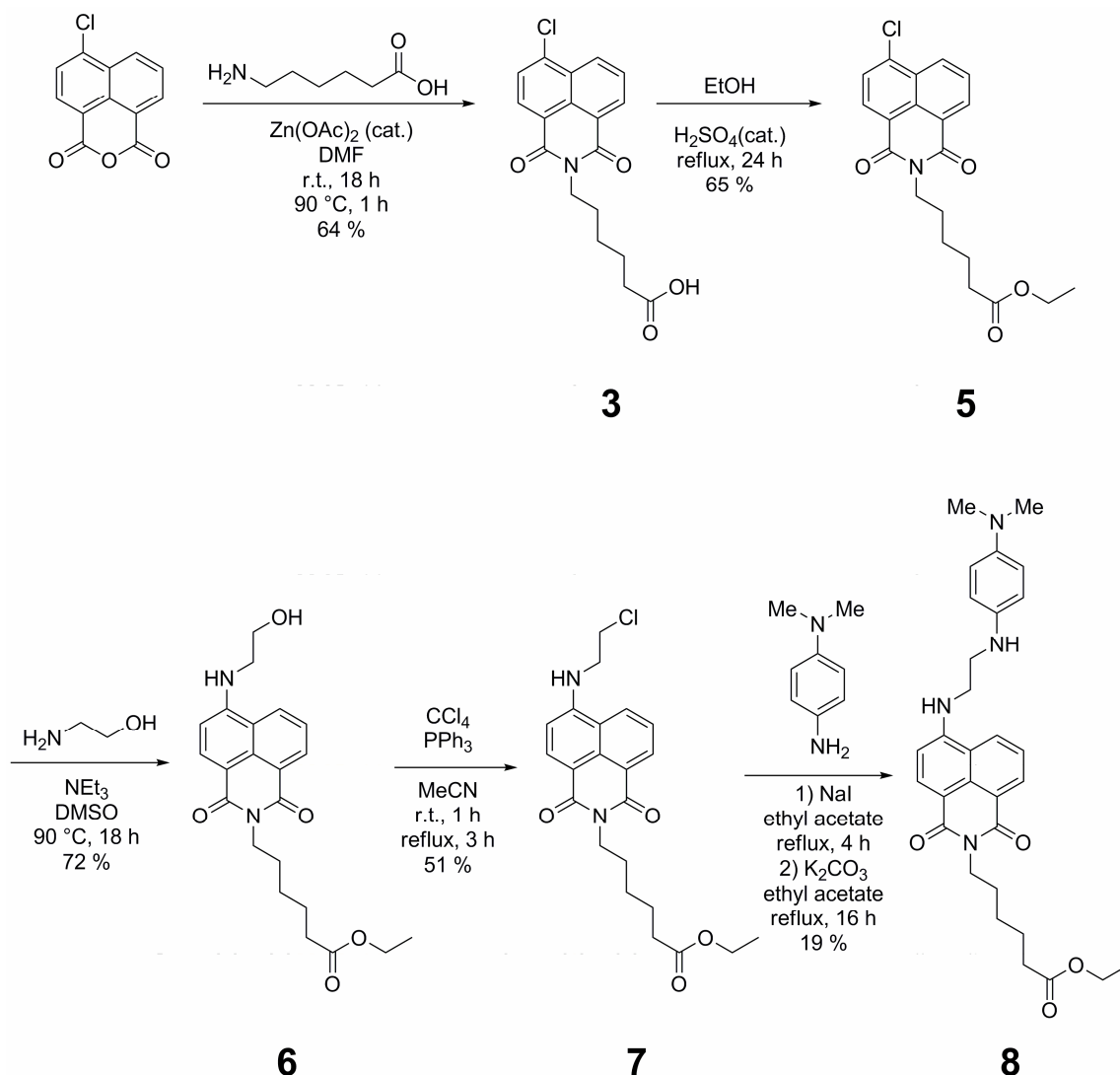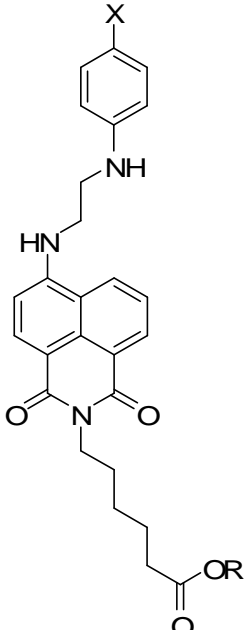
Figure 2.2. Synthetic pathway to compound **8**.

A different synthetic route than the one for HP Green was performed to yield a derivative with the N,N-dimethyl-*p*-phenylene diamine redox group (Fig. 2.2). Efforts to prepare the compound in a parallel fashion were only successful until the last step due to decomposition processes. Therefore, a step-by-step protocol (developed by Martin Link[35] and the author of this dissertation) was followed. In a first step, compound **3** was prepared from 4-chloro-1,8-naphthalic anhydride and 6-aminocaproic acid in DMF. The esterification of the carboxylic acid group was done in boiling ethanol with concentrated H_2SO_4 as catalyst to obtain the ester **5**. Then, the spacer was introduced by reacting compound **5** with ethanolamine in presence of triethylamine in DMSO to give compound

6. The hydroxy group of **6** was substituted in presence of CCl_4 and PPh_3 in acetonitrile to obtain compound **7** (with the corresponding chloro derivative). It is necessary to transform the free carboxylic acid into the ester because Appel type of reactions may occur with carboxylic acids, too, thereby forming an acyl chloride.[38] Finally, the chloro group in **7** is replaced by an iodine atom via *in situ* Finkelsteijn reaction with NaI in ethyl acetate to improve the electrophilicity of the carbon atom. Substitution of the iodo group by the aromatic amino group of N,N-dimethyl-*p*-phenylene diamine in the presence of potassium carbonate as scavenger for HCl finally yields probe **8** as ochre solid. Recrystallization was used for purification and yielded all compounds in high purity and in excellent to acceptable yields with the exception of the last step. Here, work-up with column chromatography on silica resulted in low yield (19 %), however, probe **8** showed high purity.

2.2.3 Spectroscopic Characterization – UV, Fluorescence and Effect of pH

Table 2.1. Structure, chemical and spectroscopic data of **4** and **8**, respectively, in phosphate buffered saline (PBS) of pH 7.4 (10 mM) unless noted otherwise.

	4, HP Green	**8**
formula	$C_{27}H_{29}N_3O_5$	$C_{30}H_{36}N_4O_4$
M.W. (g/mol)	475.22	516.27
	R = H[a]	R = CH_2CH_3[b]
X	OCH_3	$N(CH_3)_2$
λ_{abs} (nm)	456	452
λ_{em} (nm)	534	534
ε (L*mol^{-1}*cm^{-1})	7,600	13,700
ϕ^c	0.0032	0.014

a) H: free carboxylic acid. b) CH_2CH_3: ethyl (ester). c) Quantum yields (QY) were determined in aqueous solution with 1 % (v/v) DMSO against the reference dye fluorescein whose QY is reported to be 0.95 in 0.1 M NaOH.

The absorption spectrum of HP Green in aqueous solution of pH 7.4 has a maximum at 455 nm and the molar absorption coefficient ε is 7,600 L*mol^{-1}*cm^{-1} which is typical for aminonaphthalimides.[39, 40] Its green fluorescence has a main peak at 533 and a side peak at 580 nm. The quantum yield is 0.0032. Probe **8** displays the same emission maxima at 534 and 581 nm like HP Green but its absorption maxima is slightly blue shifted to 452 nm. Furthermore, dye **8** possesses higher values of molar absorbance ε (13,700 L*mol^{-1}*cm^{-1}) and fluorescence quantum yield ϕ (0.014). The large Stokes' shift of both probes (~ 80 nm) is favourable in terms of separating (scattered) excitation light from fluorescence (Tab. 2.1 and Fig. 2.3A). The fluorescence of both probes is strongly quenched due to photoinduced electron transfer (PET) from the redox moieties to the naphthalimide luminophore. If *p*-anisidine or N,N-dimethyl-*p*-phenylene diamine is oxidized by HP (as shown further below), PET is suppressed and fluorescence intensity increased. The mechanism of the oxidation of the probes by HP is unclear yet. By analogy to the electrochemical oxidation of *p*-anisidine[41] we assume that an instable radical cation is being formed. At pH values of ≤ 6, the PET effect is suppressed (Fig. 2.3B) due to protonation of the amino group of *p*-anisidine or the secondary amino group of N,N-dimethyl-*p*-phenylene diamine, while fluorescence is constant in the pH range from 6 to 9, thereby rendering both probes suitable for experiments at physiological pH values.
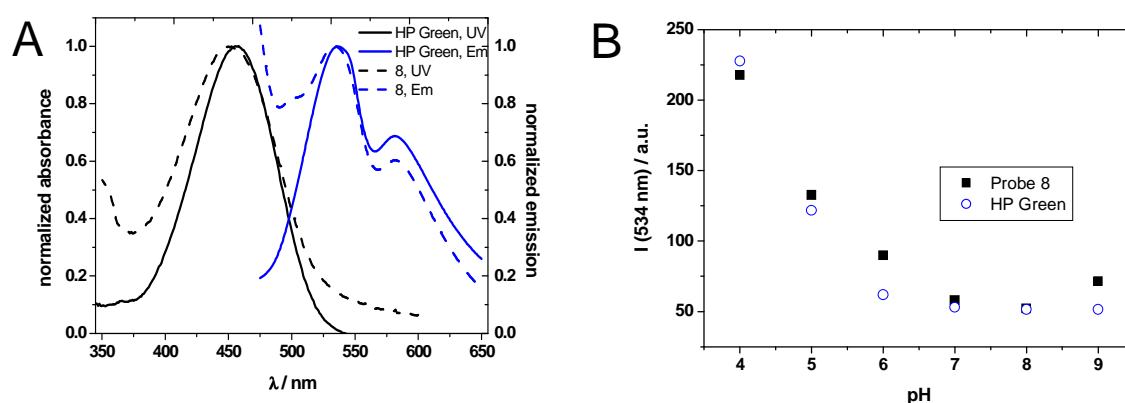
Figure 2.3. A: Absorption and emission spectra of HP Green and probe **8** (10 µM, each) in phosphate buffer of pH 7. B: Effect of pH on the fluorescence (534 nm) of HP Green and probe **8** (10 µM, each) after excitation at 450 nm.

2.3 Hydrogen Peroxide Assay using HP Green

2.3.1 Which Probe to use for the Hydrogen Peroxide Assay?
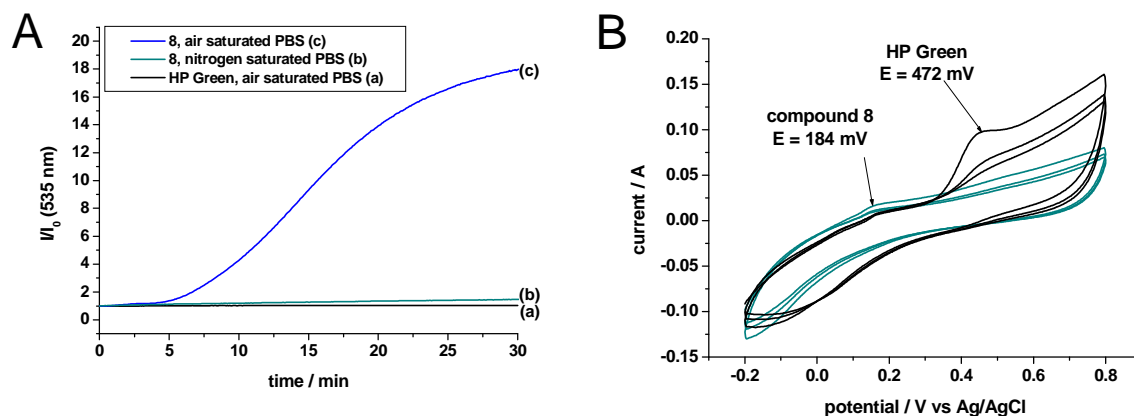
Figure 2.4. A: Time traces of the fluorescence intensity of (a) HP Green (10 µM) in air saturated phosphate buffered saline (PBS), probe **8** (10 µM) in (b) nitrogen saturated PBS and (c) air saturated PBS. B: Cyclic voltammograms of HP Green and probe **8** (50 µM, each) in PBS of pH 7.4.

It was successfully demonstrated by Martin Link[35] that HP Green reacts with HP and that it can act as probe for HP determination. Probe **8** is a derivative of HP Green and it is determined here, whether it is a potential alternative. Although the fluorescence intensity of probe **8** increased after reaction with 1 mM of HP (Fig. 6.5D), a stable blank signal is more important, which is necessary for the development of an HP assay. Therefore, the fluorescence intensity of both probes (referenced against its starting value at t = 0, Fig. 2.4A) in PBS was followed over time under constant irradiation. In case of HP Green, a weak, but continuous increase in fluorescence intensity is observed ($I/I_0 = 1.03$ after 30 min), which is caused by photooxidation from diffusing oxygen from ambient air (trace a). The fluorescence intensity of probe **8** however is strongly affected: It is raised by a factor of 18, which is higher more than 17-fold than in case of HP Green (trace c). Nitrogen saturated PBS and sealed cuvettes reduce photooxidation of probe **8** significantly but the fluorescence is still increased up to $I/I_0 = 1.45$ (trace b). It can be concluded that probe **8** is more easily oxidized than HP Green, which was conformed by cyclic voltammetry (Fig. 2.4B). The potentials of HP Green and probe **8** are 184 and 472 mV, respectively, and were measured against a silver/silver chloride reference electrode.

Furthermore, the cyclic voltammograms of both probes illustrate an irreversible oxidation because no reduction peak was detected. In conclusion, HP Green is preferably chosen as probe in assays for HP because its fluorescence remains stable and effects by photooxidation are low.

2.3.2 Response of HP Green to Hydrogen Peroxide in Absence of Peroxidase

The response towards hydrogen peroxide in the absence of peroxidase was studied by adding HP (in final concentrations of 500 or 250 µM) to a 10 µM solution of HP Green in PBS at 25 °C. Fig. 2.5A depicts the resulting time trace of the emission at 534 nm over 30 min. Fluorescence intensity increased linearly over time (30 min) indicating a slow reaction of HP Green with HP (b and c). Trace (a) in Fig. 2.5B shows the signal of a blank solution containing HP Green in buffer only. A weak but continuous increase in fluorescence intensity is observed ($I/I_0 = 1.04$ after 45 min), which is likely to be caused by autoxidation or photooxidation. A similar behaviour was reported by *Soh et al.*[27] for the DPPEA-HC probe. Traces (b) and (c) show that HP can be detected with sufficient sensitivity after a 30 min reaction time. This yields a calibration plot for HP (Fig. 2.5B) over the concentration range from 10 to 250 µM. The plot can be described by the equation $y = y_0 + A_1*exp(-x/t_1)$, with values of 1.115 ± 0.003, -0.113 ± 0.003 and 78 ± 5 for y_0, A_1 and t_1, respectively. The correlation coefficient (R^2) is 0.97.
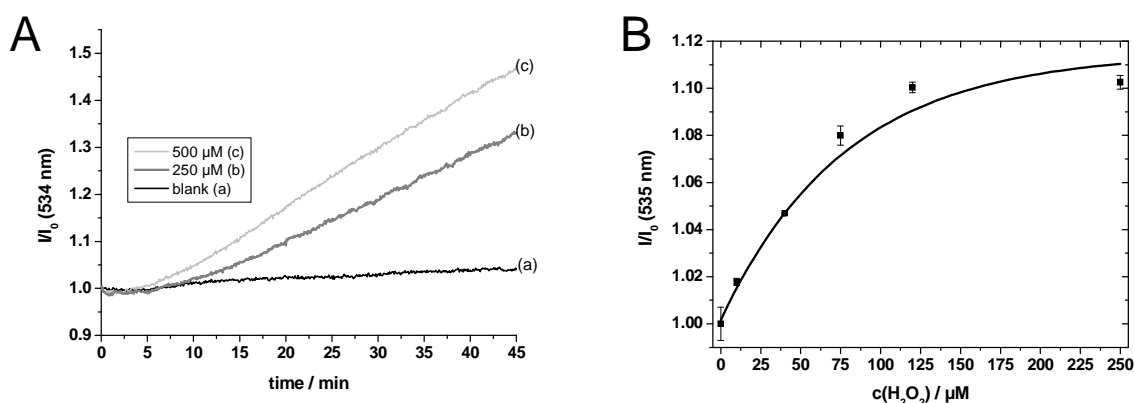
Figure 2.5. A: Time traces of fluorescence intensity after addition of (a) 0, (b) 250 µM and (c) 500 µM of HP (final concentration, each) to HP Green (10 µM) in PBS of pH 7.4 at 25 °C. B: Relative signal change of the fluorescence intensity (I/I_0) of probe HP Green at 10 µM in the presence of 0, 10, 40, 75, 125 and 250 µM HP after 30 min.

2.3.3 Response of HP Green to Hydrogen Peroxide in Presence of Peroxidase

The slow reaction of HP Green with HP and the resulting modest increase in signal suggested the use of horseradish peroxidase (HRP; E.C. 1.11.1.7). HRP is a heme peroxidase that can oxidize a wide range of phenols and anilines.[42, 43] The assay developed here follows a protocol of a ready-to-use kit.[25] HP Green was dissolved in PBS of pH 7.4 (in a final concentration of 10 µM) and various quantities of HP (in final concentrations of 0 – 30 µM) were added in the presence of 0.1 U/ml HRP. Emission and excitation spectra were recorded after 10 min of incubation at 30 °C (Figs. 2.6 and 6.5A).
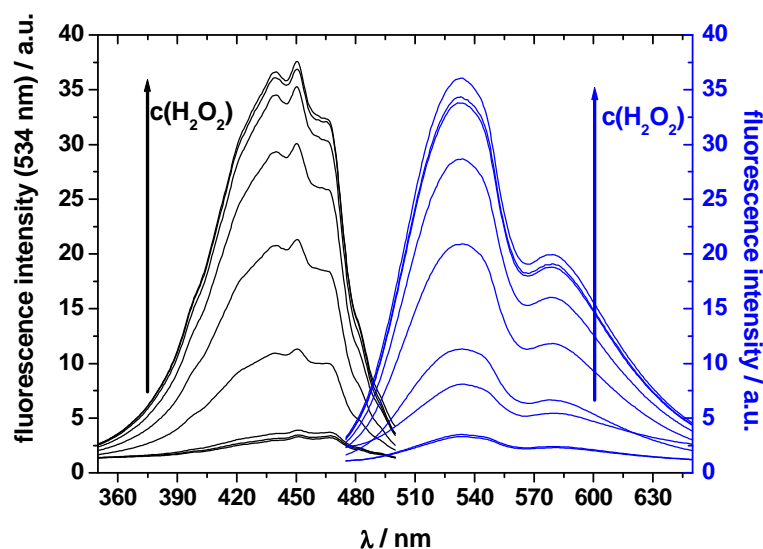
Figure 2.6. Excitation (left) and emission spectra (right) of HP Green (10 µM) after incubation for 10 min with HRP (0.1 U/mL) and HP (0 to 30 µM) at pH 7.4 and at 30 °C.

In both cases, an up to 11-fold increase of fluorescence intensity occurs at 534 nm, which is also reflected by an increase in quantum yield from 0.32% to 4%. The maxima of the fluorescence spectra remain at 534 and 580 nm, respectively, but the absorption maximum is blue-shifted from 456 to 443 nm. The molar absorption coefficient decreases from 7,600 to 5,500 L*mol^{-1}*cm^{-1} (see Tab. 2.2). Upon addition of catalase (E.C. 1.11.1.6, oxidoreductase, CAT) to a sample containing HP, HRP and HP Green, HP is decomposed to water and oxygen. Concomitantly the oxidation of HP Green is stopped (Fig. 2.7). This experiment illustrates that the fast increase in fluorescence is due to oxidation of HP Green by HP.

Table 2.2. Spectroscopic properties of HP Green before and after reaction with hydrogen peroxide (10 µM) and horseradish peroxidase (0.1 U/mL).

	λ_{abs} (nm)	λ_{em} (nm)	ε (Lmol^{-1}cm^{-1})	ϕ (%)
before	456	534	7600	0.32
after (15 min)	444	534	5500	4
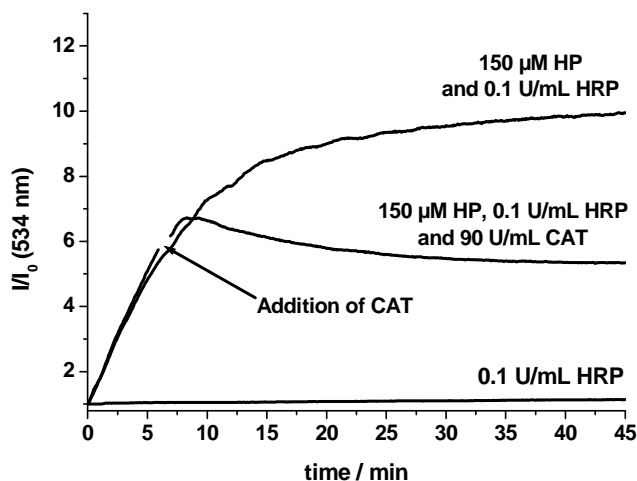
Figure 2.7. Time trace of fluorescence intensity of HP Green (10 µM), HRP (0.1 U/mL) and HP (150 µM) in PBS of pH 7.4 at 30 °C. Addition of catalase (CAT, 90 U/mL) after 6 min of reaction time will stop the oxidation of HP Green.

The kinetics of the reaction of HP Green and HP in presence of HRP was studied *via* time trace measurements and by referencing against the corresponding initial emission intensity (I/I_0) (Fig. 2.8A). First, the fluorescence of HP Green (10 µM) was monitored over 30 min at 30 °C in the presence of HRP (0.1 U/mL), but without HP (plot a). The signal is virtually stable in that I/I_0 increased by 4% only, probably due to photooxidation. Upon addition of various concentrations of HP, fluorescence intensity increases significantly. In case of 1 µM of HP, the reaction is completed after 10 min (plot b). Higher concentrations of HP require longer times for equilibration, for example 30 min in case of 5 µM HP (plot c). HP in concentrations of > 10 µM cannot be determined because no further increase of signal is observed (plots d and e, respectively). In a kinetic assay format, 10 min of incubation is adequate for a quick and sensitive determination of HP.
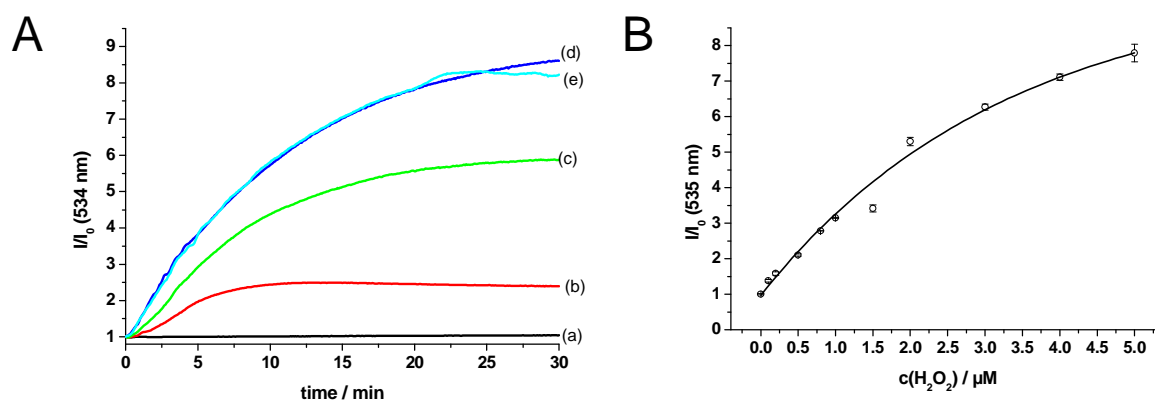
Figure 2.8. A: Time trace of the fluorescence of the system HP Green (10 µM) and HRP (0.1 U/mL) at pH 7.4 and 30 °C in presence of (a) 0, (b) 1, (c) 5, (d) 10 and (e) 20 µM of HP (final concentration, each). B: Calibration plot of I/I_0 (after 11 min) *vs*. the concentration of HP.

Calibration plots for the kinetic assay of HP were established using a microtiterplate (MTP) reader. All solutions and the MTP were stored at 30 °C before the assay was performed so to minimize the effects of temperature. HP Green (in a final concentration of 10 µM) and HP in various concentrations were placed in each well and diluted with PBS of pH 7.4. The reaction was started by addition of HRP (in a final activity of 0.1 U/mL) and incubating at 30 °C for 10 min under exclusion of light. A delay time of 1 minute was chosen for the time between sample preparation and start of measurement thus resulting in an overall incubation time of 11 min. The resulting calibration plot (Fig. 2.8B) shows the probe to have a dynamic range from 0.1 to 5 µM of HP. The limit of detection (LOD, defined as 3σ) is 64 nM, which equals 16 pmols of HP per well (250 µL). The calibration plot can be described by the equation $y = y_0 + A_1*exp(-x/t_1)$, with values of 9.70 ± 0.03, -8.73 ± 0.03 and 3.29 ± 0.03 for y_0, A_1 and t_1, respectively. The correlation coefficient (R^2) is 0.997.

2.4 Enzymatic Assay for D-Glucose

Most optical enzymatic detection schemes[44] for glucose are making use of glucose oxidase (GOx, E.C. 1.1.3.4), which is a stable, easy to handle and inexpensive enzyme. It catalyzes the conversion of β-D-glucose into D-glucono-1,5-lactone. Hydrogen peroxide is formed as a reaction product and its concentration can be measured and related to the

concentration of glucose. To prove the principle, glucose (in a final concentration of 100 µM) and GOx (1 U/mL) were added to a solution of HP Green (10 µM) and HRP (0.1 U/mL) in PBS of pH 7.4 at 30 °C. The concentrations of dye and HRP equal those of the experiments related to Fig. 2.8. Fluorescence increases immediately upon injection of glucose (Fig. 6.5B). The kinetics of the enzymatic reaction was investigated via time trace measurements (Fig. 2.9). The fluorescence of HP Green in the presence of HRP and GOx served as a blank signal. Its intensity was followed over 30 min (trace a). An increase by 22% is found, probably owing to photooxidation (see above). The addition of various concentrations of D-glucose induces a distinct increase of fluorescence intensity. The reaction is not completed after 30 min as saturation is not reached for any amount of D-glucose added except for 1 µM (trace b).
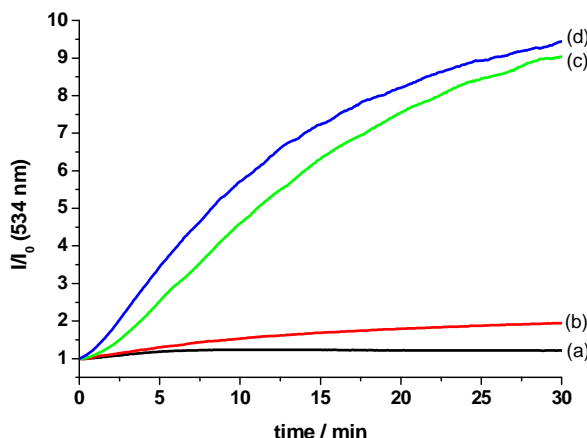
Figure 2.9. Time trace of the fluorescence of HP Green (10 µM), HRP at 0.1 U/mL and GOx at 1 U/mL at pH 7.4 and 30 °C in presence of (a) 0, (b) 1, (c) 20 and (d) 100 µM of D-glucose (final concentration, each).

A calibration plot was established under the same conditions as for the HP calibration (see above) after an 11 min incubation time and under exclusion of light in the plate reader. The resulting graph (Fig. 2.10) shows a dynamic range from 2 to 30 µM of glucose. The LOD (3σ) is 644 nM, which equals 161 pmol of glucose per well (250 µL). The calibration plot can be described by the equation $y = (A_1-A_2)/(1+\exp((x-x_0)/dx)) + A_2$, with values of -1.66 ± 1.12, 8.32 ± 0.18, 6.81 ± 1.50 and 6.5 ± 0.09 for A_1, A_2, x_0 and dx, respectively. The correlation coefficient (R^2) is 0.996.
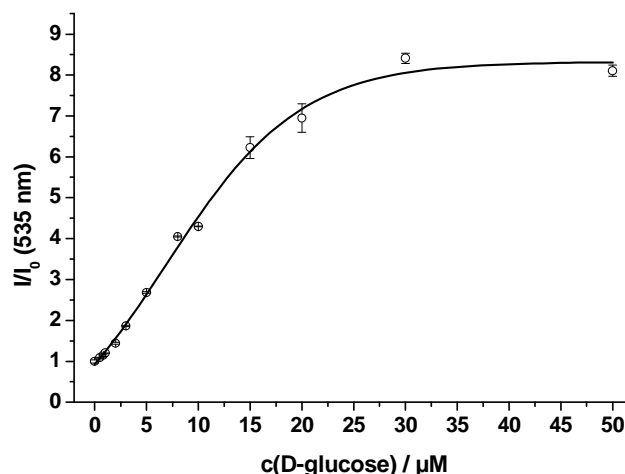
Figure 2.10. Calibration graph (including standard deviations for n = 8) obtained by plotting I/I_0 (after 11 min) *vs.* the concentration of D-glucose.

2.5 Enzymatic Assay for L-Lactate

An assay for L-lactate was developed to illustrate that HP Green is also suitable in combination with less stable oxidases like lactate oxidase (LOx; E.C. 1.13.12.4).[45] LOx is a flavine type enzyme that converts L-lactate into pyruvate and HP under aerobic conditions. It is much less stable than GOx. L-lactate (20 µM) and LOx (1 U/mL) were added to a solution of HP Green (10 µM) and HRP (0.1 U/mL) in PBS of pH 7.4 at 30 °C. The concentrations of dye and HRP equal those of the experiments related to Figs. 2.8 and 2.9. Fluorescence intensity increased immediately after injection and reached its maximum after 30 min (Fig. 6.5C). The kinetics of the enzymatic reaction was investigated *via* time trace measurements (Fig. 2.11). The intensity (I/I_0) of the blank (trace a) increased to reach an almost constant level after 15 min (I/I_0 = 1.8). Photooxidation of HP Green is probably the reason. The addition of various concentrations of L-lactate causes a distinct increase of fluorescence intensity, which reaches a constant level after 15 min for all quantities of L-lactate added, with the exception of 1 µM (trace b). Furthermore, the signal hardly increases further if lactate concentrations exceed 20 µM. Therefore, 20 µM of L-lactate may be interpreted as the upper limit of the dynamic range (traces c and d).
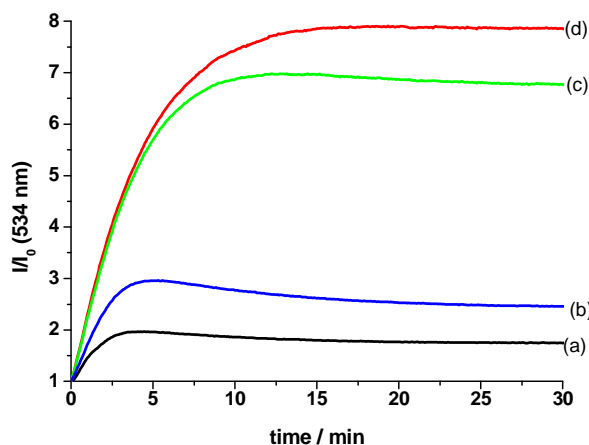
Figure 2.11. Time trace of the fluorescence of HP Green (10 µM), HRP at 0.1 U/mL and GOx at 1 U/mL at pH 7.4 and 30 °C in presence of (a) 0, (b) 1, (c) 20 and (d) 100 µM of D-glucose (final concentration, each).

A calibration plot was established in MTPs at the same conditions of probe, HRP and enzyme as in the case of the glucose assay. Fluorescence intensity was measured after incubation for 6 min in the dark at 30 °C. A plot of I/I_0 *vs.* concentration of L-lactate (Fig. 2.12) resulted in a dynamic range from 0.5 to 10 µM. The limit of detection (LOD, defined as 3σ) is 162 nM, which equals 41 pmol L-lactate per well (250 µL). The plot can be fit to the equation $y = y_0 + A_1*\exp(-x/t_1)$ with values of 5.54 ± 0.07, -4.50 ± 0.07 and 4.50 ± 0.14 for y_0, A_1 and t_1, respectively. The correlation coefficient (R^2) is 0.998.
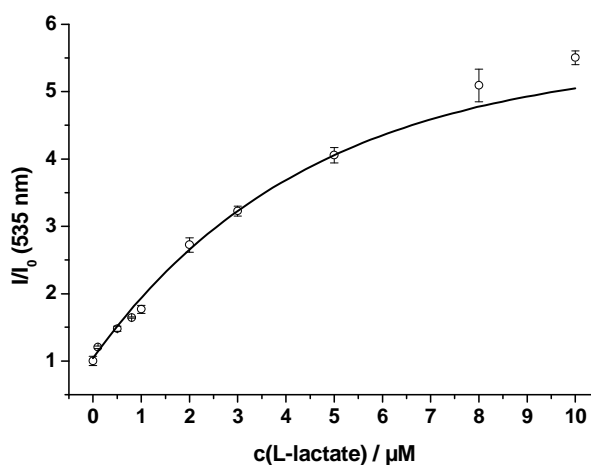
Figure 2.12. Calibration graph (including standard deviations for n = 8) obtained by plotting I/I_0 (after 6 min) *vs.* the concentration of L-lactate.

2.6 Effect of Oxygen Ingress

Fluorescence of HP Green displays certain sensitivity to oxygen that diffuses into the (aqueous) reaction mixtures from ambient air. This was observed for blank measurements of HP Green (10 µM) with HRP (0.1 U/mL) and oxidase (1 U/mL) in case of the D-glucose and L-lactate assays (Fig. 2.13). In all experiments, fluorescence increases due to autoxidation or photooxidation. The effect of oxygen ingress, however, can be reduced by the use of cuvettes closed with a stopcock. In case of the glucose assay after 10 min, the effect is reduced by 3.3% (I/I_0 1.20 *vs.* 1.16) (Fig 2.13A). The fluorescence of HP Green is even more affected in the L-lactate assay (Fig. 2.13B), where the ratio I/I_0 in closed cuvettes is reduced by almost 50% (I/I_0 3.61 *vs.* 1.86) after 10 min. Sealing minimizes further oxidation of HP Green by dissolved oxygen and allows a higher dynamic range. Despite of these effects the D-glucose and the L-lactate assay described in the previous sections can be successfully performed in MTPs without sealing.
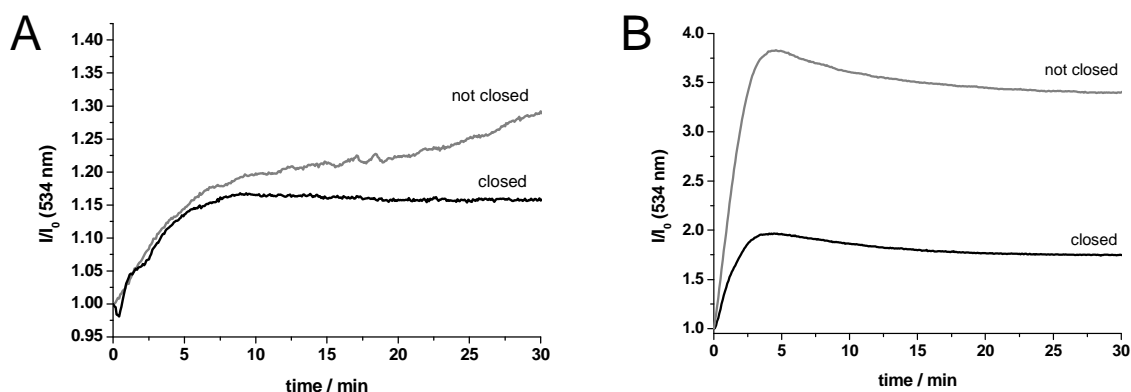
Figure 2.13. Time trace measurements of HP Green (10 µM), HRP (0.1 U/mL) and oxidase (1 U/mL) in PBS of pH 7.4 at 30 °C in either closed or not closed cuvettes. A: GOx; B: LOx.

2.7 In-vitro Imaging of Hydrogen Peroxide in NRK Cells

The ability of HP Green to act as an *in-vitro* probe for HP was examined by incubating NRK cells with a 50 µM solution of the probe for 30 min at 37 °C. Excess dye was then removed by washing the cells which afterwards were placed under a fluorescence microscope. Following photo-excitation with a mercury vapour lamp through a 465 to 495 nm bandpass filter, images were acquired over time. HP Green is easily internalized

and mainly located around the nucleus and its green fluorescence remains almost constant during recording. The presence of 100 µM concentrations of HP in the extracellular matrix causes a strong increase in brightness over time (Fig. 2.14A). The images at the beginning of the experiment reveal a homogenous distribution of the probe around the nuclei. Its brightness is low but increases by 35% after 75 min as a result of oxidation by HP according to the mean values of the histograms reflecting fluorescence intensity (Fig. 2.14B, plot b). These observations are supported by analyzing the histograms of the total images. They are shifted to higher values of tonal variations in the presence of HP (Fig. 6.6). The increase in signal is retarded with respect of the HP assay in solution, obviously because of slow transport of HP through the membrane and by partial decomposition of HP by intracellular catalase. No significant change is observed in case of the control experiment (Fig. 2.14B, plot a). Higher concentrations of HP Green are not recommended because it may be cytotoxic, whilst lower ones yield images of reduced contrast (Fig. 6.7). All fluorescence images are given in the experimental part (Figs. 6.8 and 6.9).
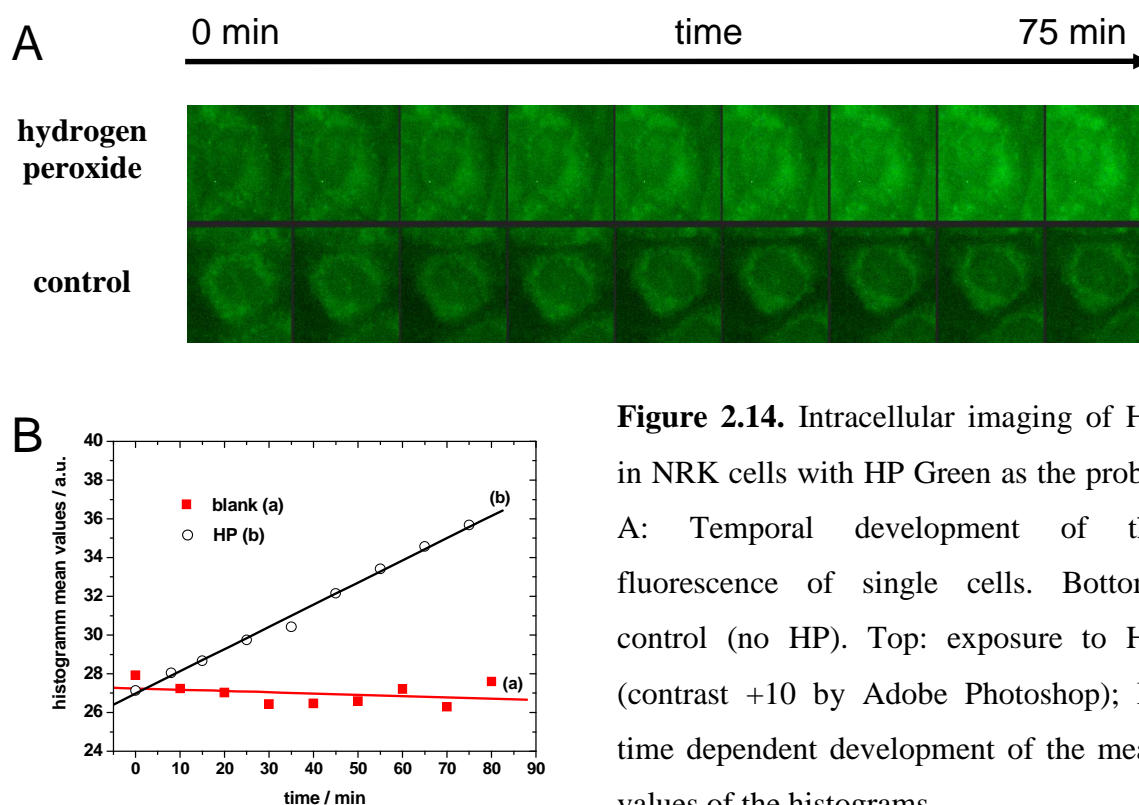
Figure 2.14. Intracellular imaging of HP in NRK cells with HP Green as the probe. A: Temporal development of the fluorescence of single cells. Bottom: control (no HP). Top: exposure to HP (contrast +10 by Adobe Photoshop); B: time dependent development of the mean values of the histograms.

2.8 Discussion and Conclusion

HP Green and probe **8** are based on the yellow fluorophore 4-amino-1,8-napththalimide. Their preparation is simple and their green fluorescence can be photoexcited with mercury and xenon lamps. (HP Green is mentioned further because of its use in the established assays.) They show emission maxima close to the one of fluorescein (534 nm *vs.* 514 nm) but a wider Stokes' shift (78 nm *vs.* 23 nm).[35] The low molar absorbance (7,600 L*mol^{-1}*cm^{-1}) is a drawback but is compensated by its good photostability (Fig. 2.5A, plot a). Photooxidation can be minimized by appropriate choice of instrumental settings such as the bandwidth of excitation shutters.

The addition of HP in the absence of the enzyme HRP causes a small increase of fluorescence, indicating suppression of the PET effect. The response to HP is much stronger in the presence of HRP, and this has resulted in fast and sensitive methods for the determination of HP, D-glucose and L-lactate. Using HRP, the LOD for HP is 64 nM, which is better by a factor of 28 than the one of the probe EuTc[18] (1.8 µM) and closely matches the one of the well established Amplex Red/HRP[23] (50 nM). The resorufin/HRP system is reported to have an LOD as low as 9 nM but is less often applied because of intrinsic limitations like nonlinearity of the response at high probe concentrations.[22] Recently reported terbium probes[46] or HRP-modified gold nanoclusters[47] display LODs of 3.7 nM and 30 nM, respectively. Commercially available assay kits (www.invitrogen.com) for D-glucose using Amplex Red/GOx/HRP show larger dynamic ranges but have a higher detection limit (3 µM). Optimized protocols even display a LOD of 2 µM[48], but the LOD of HP Green in the GOx/HRP scheme is 3-fold lower (0.64 µM). In case of L-lactate, the LOD of HP Green (162 nM) is more than 12-fold lower than that of standard NADH methods (2 µM).[49] Commercially available ready-to-use assay kits (www.biovision.com) show larger dynamic ranges (0.001-10 mM) but LOD values of 1 µM, only. The presence of a hexanoic acid also will enable immobilization of the probe on solid supports to end up with (bio)sensors for continuous monitoring of these species.

The use of HP Green to image HP inside cells is also demonstrated. However, the relative increase in fluorescence intensity will remain modest as long as HRP cannot be incorporated into the cells. Fluorescein derivatives with pinacol boronic acid esters possibly are more attractive alternatives because their (partly) quenched fluorescence recovers upon perhydrolysis and does not require the presence of an additional enzyme.[11]

In conclusion HP Green is a viable probe for HP and has very specific merits. It is likely to be generally applicable in combination with other oxidases.

2.9 Literature

1. J. S. Stamler, D. J. Singel, J. Loscalzo, Biochemistry of nitric oxide and its redox-activated forms. *Science*, **1992**, 258, 1898 – 1902.

2. K. Hensley, K. A. Robinson, S. P. Gabbita, S. Salsman, R. A. Floyd, Reactive oxygen species, cell signaling, and cell injury. *Free Radical Biol. Med.*, **2000**, 28, 1456 – 1462.

3. K. B. Beckman, B. N. Ames, The free radical theory of aging matures. *Physiol. Rev.*, **1998**, 78, 547 – 581.

4. W. J. Martin, Neutrophils kill pulmonary endothelial cells by a hydrogen-peroxide-dependent pathway. An in vitro model of neutrophil-mediated lung injury. *Am. Rev. Respir. Dis.*, **1984**, 130, 209 – 213.

5. K. M. Mohazzab-H., P. M. Kaminski, R. P. Fayngersh, M. S. Wolin, Oxygen-elicited responses in calf coronary arteries: role of H_2O_2 production via NADH-derived superoxide. *Am. J. Physiol. Heart Circ. Physiol.*, **1996**, 270, 1044 – 1053.

6. M. Giorgio, M. Trinel, E. Migliaccio, P. G. Pelicci, Hydrogen peroxide: a metabolic by-product or a common mediator of ageing signals? *Nat. Rev. Mol. Cell. Biol.*, **2007**, 8, 722 – 728.

7. S. G. Rhee, H_2O_2, a necessary evil for cell signaling. *Science*, **2006**, 312, 1882 – 1883.

8. B. D'Autreaux, M. B. Toledano, ROS as signalling molecules: mechanisms that generate specifity in ROS homeostasis. *Nat. Rev. Mol. Cell. Biol.*, **2007**, 8, 813 – 824.

9. Y. Shao, J. Wang, H. Wu, J. Liu, I. A. Aksay, Y. Lin, Graphene based electrochemical sensors and biosensors: a review. *Electroanalysis*, **2010**, 22, 1027 – 1036.

10. M. R. Guascito, E. Filippo, C. Malitesta, D. Manno, A. Serra, A. Turco, A new amperometric nanostructured sensor for the analytical determination of hydrogen peroxide. *Biosens. Bioelectron.*, **2008**, 24, 1057 – 1063.

11. B. C. Dickinson, C. J. Chang, A targetable fluorescent probe for imaging hydrogen peroxide in the mitochondira of living cells. *J. Am. Chem. Soc.*, **2008**, 130, 9638 – 9639.

12. Z. Lin, M. Wu, O. S. Wolfbeis, M. Schäferling, A novel method for time-resolved fluorimetric determination and imaging of the activity of peroxidase, and its

application to an enzyme-linked immunosorbent assay. *Chem. Eur. J.*, **2006**, 12, 2730 – 2738.

13. P. Trinder, Determination of blood glucose using an oxidase-peroxidase system with non-carcinogenic chromogen. *J. Clin. Path.*, **1969**, 22, 158 – 161.

14. H. Maeda, Y. Fukuyasu, S. Yoshida, M. Fukuda, K. Saeki, H. Matsuno, Y. Yamauchi, K. Yoshida, K. Hirata, K. Miyamoto, Fluorescent probes for hydrogen peroxide based on a non-oxidative mechanism. *Angew. Chem. Int. Ed.*, **2004**, 43, 2389 – 2391.

15. F. He, Y. Tang, M. Yu, S. Wang, Y. Li, D. Zhu, Fluorescence-amplifying detection of hydrogen peroxide with cationic conjugated polymers, and its application to glucose sensing. *Adv. Funct. Mater.*, **2006**, 16, 91 – 94.

16. D. Srikun, A. E. Albers, C. J. Chang, A dendrimer-based platform for simultaneous dual fluorescence imaging of hydrogen peroxide and pH gradients produced in living cells. *Chem. Sci.*, **2011**, 2, 1156 – 1165.

17. D. Srikun, A. E. Albers, C. I. Nam, A. T. Iavarone, C. J. Chang, Organelle-targetable fluorescent probes for imaging hydrogen peroxide in living cells via SNAP-tag protein labeling. *J. Am. Chem. Soc.*, **2010**, 132, 4455 – 4465.

18. O. S. Wolfbeis, A. Dürkop, M. Wu, Z. Lin, A europium-ion based luminescent sensing probe for hydrogen peroxide. *Angew. Chem. Int. Ed.*, **2002**, 41, 4495 – 4498.

19. O. S. Wolfbeis, M. Schäferling, A. Dürkop, Reversible optical sensor membrane for hydrogen peroxide using an immobilized fluorescent probe, and its application to a glucose biosensor. *Microchim. Acta*, **2003**, 143, 221 – 227.

20. A. Dürkop, O. S. Wolfbeis, Nonenzymatic direct assay of hydrogen peroxide at neutral pH using the Eu_3Tc fluorescent probe. *J. Fluoresc.*, **2005**, 15, 755 – 761.

21. A. Dürkop, M. Turel, A. Lobnik, O. S. Wolfbeis, Microtiter plate assay for phosphate using a europium-tetracycline complex as a sensitive luminescent probe. *Anal. Chim. Acta*, **2006**, 555, 292 – 298.

22. G. P. Brotea, R. J. Thibert, Fluorometric determination of hydrogen peroxide using resorufin and peroxidase. *Microchem. J.*, **1988**, 37, 368 – 376.

23. M. Zhou, Z. Diwu, N. Panchuk-Voloshina, R. P. Haugland, A stable nonfluorescent derivative of resorufin for the fluorometric determination of trace hydrogen peroxide: applications in detecting the activity of phagocyte NADPH oxidase and other oxidases. *Anal. Biochem.*, **1997**, 253, 162 – 168.

24. V. Towne, M. Will, B. Oswald, Q. Zhao, Complexities in horseradish peroxidase-catalyzed oxidation of dihydroxyphenoxazine derivatives: appropriate ranges for pH

values and hydrogen peroxide concentrations in quantitative analysis. *Anal. Biochem.*, **2004**, 334, 290 – 296.

25. www.invitrogen.com; The Molecular Probes® Handbook—A Guide to Fluorescent Probes and Labeling Technologies, 11th Edition.

26. A. P. de Silva, T. S. Moody, G. D. Wright, Fluorescent PET (photoinduced electron transfer) sensors as potent analytical tools. *Analyst*, **2009**, 134, 2385 – 2393.

27. N. Soh, O. Sakawaki, K. Makihara, Y. Odo, T. Fukaminato, T. Kawai, M. Irie, T. Imato, Design and development of a fluorescent probe for monitoring hydrogen peroxide using photoinduced electron transfer. *Bioorg. Med. Chem.*, **2005**, 13, 1131 – 1139.

28. M. Schäferling, D. B. M. Groegel, S. Schreml, Luminescent probes for detection and imaging of hydrogen peroxide. *Microchim. Acta*, **2011**, 174, 1 – 18.

29. K. Hanaoka, Y. Muramatsu, Y. Urano, T. Terai, T. Nagano, Design and synthesis of a highly sensitive off-on fluoresent chemosensor for zinc ions utilizing internal charge transfer. *Chem. Eur. J.*, **2010**, 16, 568 – 572.

30. H. He, M. A. Mortellaro, M. J. P. Leiner, S. T. Young, R. J. Fraatz, J. K. Tusa, A fluorescent chemosensor for sodium based on photoinduced electron transfer. *Anal. Chem.*, **2003**, 75, 549 – 555.

31. R. W. Sabins, in *Handbook of Biological Dyes and Stains: Synthesis and Industrial Applications*, WILEY-VCH, Weinheim, **2010**, pp. 266 – 274.

32. W. W. Stewart, Lucifer dyes – highly fluorescent dyes for biological tracing. *Nature*, **1981**, 292, 17 – 21.

33. J. Wegener, C. R. Keese, I. Giaver, Recovery of adherent cells after in situ electroporation monitored electrically. *BioTechniques*, **2002**, 33, 348 – 357.

34. S. M. Borisov, O. S. Wolfbeis, Optical Biosensors. *Chem. Rev.*, **2008**, 108, 423 – 461.

35. M. Link, New fluorescent labels and probes for biological applications. Dissertation, **2010**, Universität Regensburg.

36. A. Cul, A. Daïch, B. Decroix, G. Sanz, L. van Hijfte, Kinetic versus thermodynamic access to imidazoisoindolones. *Tetrahedron*, **2004**, 60, 11029 – 11039.

37. M. Link, P. Schulze, D. Belder, O. S. Wolfbeis, New diode laser-excitable green fluorescent label and its application to detection of bovine serum albumin via microchip electrophoresis. *Microchim. Acta*, **2009**, 166, 183 – 188.

38. R. Appel, Tertiary phosphane/tetrachloromethane, a versatile reagent for chlorination, dehydration, and P – N linkage. *Angew. Chem. Int. Ed.*, **1975**, 14, 801 – 811.

39. A. P. de Silva, H. Q. N. Gunaratne, J. Habib-Jiwan, C. P. McCoy, T. E. Rice, J. Soumillion, New fluorescent model compounds for the study of photoinduced electron transfer: the influence of a molecular electric field in the excited state. *Angew. Chem. Int. Ed.*, **1995**, 34, 1728 – 1731.

40. V. B. Bojinov, N. I. Georgiev, P. Bosch, Design and synthesis of highly photostable yellow-green emitting 1,8-naphthalimides as fluorescent sensors for metal cations and protons. *J. Fluoresc.*, **2009**, 19, 127 – 129.

41. P. Simon, G. Farsang, C. Amatore, Mechanistic investigation of the oxidation of p-anisidine in unbuffered DMF using fast scan rates at ultramicroelectrodes. *J. Electroanal. Chem.*, **1997**, 435, 165 – 171.

42. M. A. Gilabert, A. N. P. Hiner, P. A. García-Ruiz, J. Tudela, F. García-Molina, M. Acosta, F. García-Canovas, J. N. Rodríguez-López, Differential substrate behaviour of phenol and aniline derivatives during oxidation by horseradish peroxidase: kinetic evidence for a two-step mechanism. *Biochim. Biophys. Acta*, **2004**, 1699, 235 – 243.

43. A. Zhu, R. Romero, H. R. Petty, A sensitive fluorimetric assay for pyruvate. *Anal. Biochem.*, **2010**, 396, 146 – 151.

44. M.-S. Steiner, A. Duerkop, O. S. Wolfbeis, Optical methods for sensing glucose. *Chem. Soc. Rev.*, **2011**, DOI 10.1039/c1cs15063d.

45. B. Lillis, C. Grogan, H. Berney, W. A. Lane, Investigation into immobilization of lactate oxidase to improve stability. *Sens. Actuat. B*, **2000**, 68, 109 – 114.

46. Z. Ye, J. Chen, G. Wang, J. Yuan, Development of a terbium complex-based luminescent probe for imaging endogenous hydrogen peroxide generation in plant tissue. *Anal. Chem.*, **2011**, 83, 4163 – 4169.

47. F. Wen, Y. Dong, L. Feng, S. Wang, S. Zhang, X. Zhang, Horseradish peroxidase functionalized fluorescent gold nanoclusters for hydrogen peroxide sensing. *Anal. Chem.*, **2011**, 83, 1193 – 1195.

48. P. Mazura, R. Fohlerová, B. Brzobohatý, N. S. Kiran, L. Janda, A new, sensitive method for enzyme kinetic studies of scarce glucosides. *J. Biochem. Biophys. Methods*, **2006**, 68, 55 – 63.

49. J. Wangsa, M. A. Arnold, Fiber-optic biosensors based on the fluorometric detection of reduced nicotinamide adenine dinucleotide. *Anal. Chem.*, **1988**, 60, 1080 – 1082.

3. Conception of a Reusable Hydrogen Peroxide Chemosensor

3.1 Introduction

Detection schemes for hydrogen peroxide (HP) are not only limited to assays in solution, but can also be carried out by means of an optical sensor[1] or an electrochemical sensor[2]. In the former case, the probe is embedded into a polymer matrix and the sensing layer is spread on a polymeric support. The field of application pre-determines the properties of a sensor, for instance the use of a flexible or non flexible support or the type of hydrogel. Most HP sensors apply catalase that catalyzes the decomposition of HP to water and oxygen. Thus an oxygen sensitive probe can serve to quantify the amount of oxygen released by this reaction. The concept of sensing can be applied to continuously monitoring HP in a concentration range from 0.1 to 10 mM.[3] Alternatively, horseradish peroxidase (HRP) is used for the oxidation of substituted phenols (or its derivatives) to form a fluorescent compound. This approach most prominently features homovanillic acid[4] (4-hydroxy-3-methoxy-phenylacetic acid) or luminol[5] (5-amino-2,3-dihydrophthalazin-1,4-dione). The latter is immobilized with peroxidase in a nylon membrane to act as transducer in a flow-cell sensor with a limit of detection of 1 µM at a response time below 10 s.[6] The above mentioned chemosensors rely on the use of enzymes. However, europium tetracycline (EuTc) is one of the few alternatives that are applied as direct HP probe.[7] Changes in fluorescence intensity and in lifetime occur by substitution of water molecules from the coordination sites of Eu(III), thus being completely independent of oxidation. The fluorescent probe was embedded in a hydrogel and sensor devices for flow-through cells[7] and microtiterplates[8] were developed.

Here, a non-enzymatic approach similar to the EuTc sensor was developed using the oxidation of HP Green by HP. The choice of hydrogel and the utilization of particles, onto which HP Green is covalently conjugated, differs from the EuTc sensor. The response towards HP was investigated as well as the possibilities of reusing the sensor by regenerating HP Green with a reduction agent. The *p*-anisidine moiety is similar to the hydrochinone-chinone redox system. The number of reusable chemosensors for HP is low, however sensors based on the Prussian White-Prussian Blue redox pair can be regenerated by ascorbic acid.[9]

3.2 Particle Preparation and Choice of Materials
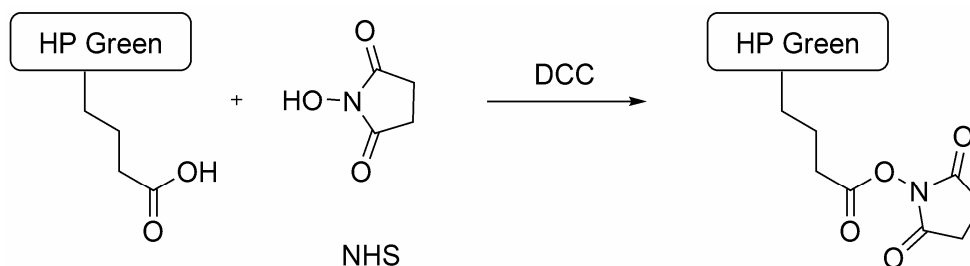
Figure 3.1. Generation of the NHS active ester of HP Green for particle labelling.

Three types of particles were labelled with HP Green in order to identify which polymeric support provides the highest fluorescence intensity. Therefore, the carboxylic acid of HP Green was activated by dicyclohexylcarbodiimide (DCC) and N-hydroxysuccinimide (NHS) *in situ* for 18 h at room temperature to yield the NHS ester (Fig. 3.1).[10] The solution was added to suspensions of poly(acrylonitrile) (PAN), polystyrene (PS) and cellulose (AC) particles in 10 mM phosphate buffer at pH 9, that were functionalized with amino groups on their surface thus forming an amide with HP Green. In addition, various amounts of HP Green were applied to receive a series of (theoretical) loadings of the dye on the particles. The concentration of HP Green is related to the weight of the particles. After 24 h, the labelling was terminated and the particles were extensively washed with water, ethanol and refluxing ethyl acetate to remove excess probe followed by drying at 75 °C. The dry particles were resuspended in phosphate buffered saline of pH 7.4 and their emission was measured from 475 to 600 nm after excitation at 450 nm (Fig. 6.10).
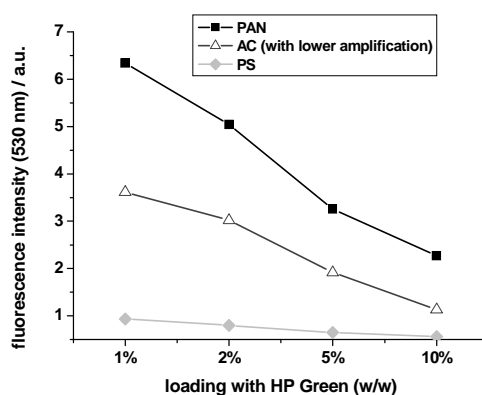
Figure 3.2. HP Green conjugated to aminomodified PAN-, PS- or AC-particles at different concentrations (w/w) of loading. Plot of fluorescence at 530 nm *vs.* loading.

The plot of fluorescence intensity at 530 nm *vs.* (theoretical) loading illustrates that emission was quenched at high loading for all particles (Fig. 3.2). PS exhibited the lowest intensity but higher luminescence was obtained for PAN particles. AC particles were measured at a lower detector voltage because their intensity was too high under conditions used for PAN and PS. Therefore, the choice was made in favour of the AC particles with a theoretical loading of 1% (w/w).

3.3 Kinetics and Calibration
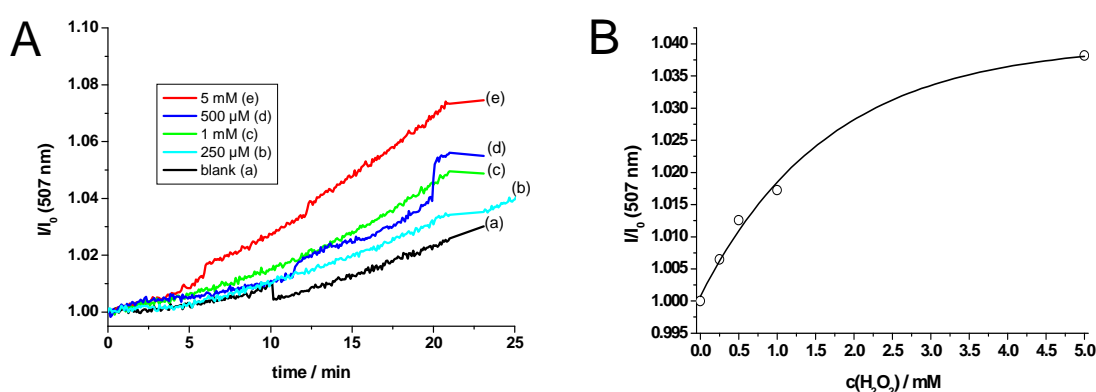
Figure 3.3. A: Time traces of fluorescence intensity of the chemosensor after flushing with (a) 0, (b) 0.25, (c) 1, (d) 0.5 and (e) 5 mM of HP in PBS of pH 7.4 at 25 °C. B: Relative signal change of the fluorescence intensity (I/I_0) of the sensor in the presence of 0, 0.25, 0.5, 1 and 5 mM of HP after 16 min 40 s (1000 s).

Initially, 6 mg of the dyed AC particles were suspended in 1 mL of a 1 M $Na_2S_2O_4$ solution (in PBS) and were shaken at 40 °C for another 24 h to completely reduce HP Green. Following work-up, the particles were added to a 2.5 % (w/w) D4 hydrogel solution in ethanol/water and spread on a poly(ethyleneglycol terephthalate) transparent support and dried at room temperature. Circular sensor spots were punched out and stored in 1 M $Na_2S_2O_4$ to prevent oxidation by oxygen from ambient air. The kinetics of the reaction of HP Green and HP in the sensor membrane was studied via time trace measurements and by referencing against the corresponding initial intensity (I/I_0). The wet sensor was fixed into a flow-through cell and flushed with solutions of hydrogen peroxide of different concentration (Fig. 3.3A). 507 nm was chosen as detection wavelength because the maximum of the emission spectra was blue-shifted by 27 nm in the hydrogel matrix

(compared to 534 nm for HP Green in solution). Fluorescence intensity increased over time (25 min) but the signal displayed high noise and other inconvenient features like abrupt increase of signal as depicted in trace (d) at around 20 min. The reaction of the sensor with HP (traces b to e) is slow because the extent in signal change is low. The response time was not determined as the signal increase of any of the samples was finished within 25 min. Trace (a) in Fig. 3.3A shows the signal of the sensor purged with buffer only. A weak but continuous increase in fluorescence intensity is observed ($I/I_0 = 1.02$ after 20 min), which is likely due to autoxidation or photooxidation. The behaviour of HP Green in the sensor membrane differs only slightly from that of HP Green and HP in solution in absence of horseradish peroxidase (Chapter 2.3.2). Traces (b) to (e) show that HP can be detected with sufficient sensitivity after 1000 s of reaction time. This yields a preliminary calibration plot for HP (Fig. 3.3B) over the concentration range from 0.25 to 5 mM. The plot can be described by the equation $y = y_0 + A_1*exp(-x/t_1)$, with values of 1.040 ± 0.002, -0.039 ± 0.002 and 1663 ± 293 for y_0, A_1 and t_1, respectively. The correlation coefficient (R^2) is 0.99. Efforts to reproduce the experiments failed. Therefore, no standard deviations could be calculated for the calibration plot.

3.4 Effect of Concentration of Labelled Particles
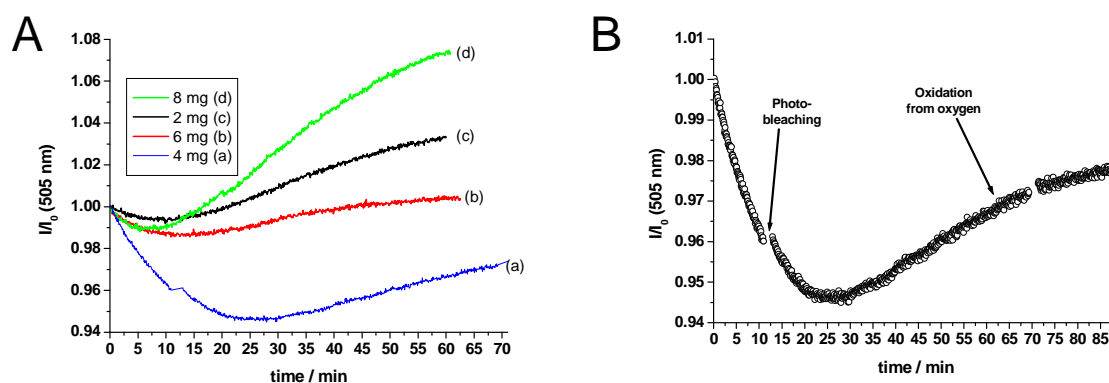
Figure 3.4. Effect of oxygen on the blank sensor. A: Time traces of the fluorescence at 505 nm after flushing with air saturated PBS of pH 7.4 at (a) 4, (b) 6, (c) 2 and (d) 8 mg including variation of the mass of the particles. B: Enlargement of trace (a).

As efforts of reproducing the results shown in section 3.3 failed, the fluorescence of the sensor was investigated with respect to the mass of the particles, which were embedded in 2.5% (w/w) D4 hydrogel. Therefore, four sensor membranes with varying amounts of

particles from 2 to 8 mg were prepared following the same protocol as described above. The fluorescence of the sensors was investigated over 70 min upon flushing with 10 mM PBS of pH 7.4 (Fig. 3.4A). The time traces revealed that emission initially decreases for a certain time, e.g. 11.5 min for 6 mg of particles in the sensor (trace b). After reaching a minimum, fluorescence increased constantly. Fig. 3.4B depicts an enlargement of time trace (a) of the sensor with 2 mg of particles. It is obvious that two processes occur simultaneously. First, HP Green was photobleached because the emission had the same intensity after closing the excitation shutter for 2 min before closing (at continuous buffer flow). In case of leaching, a lower intensity was to be expected. After 26 min, photobleaching is compensated by oxidation of HP Green from dissolved oxygen that (constantly) penetrates through the sensor membrane. Intensity increased although the excitation shutter was closed for 2 min, indicating that autoxidation or photooxidation likely had taken place. Furthermore, the emission spectra depicted a red-shift of the fluorescence maxima. In case of 2 mg of AC particles in the sensor foil, the initial maximum at 496 nm moved to 515 nm during 60 minutes of flushing with PBS (Fig. 3.5A). Emission spectra of a sensor with 15 mg particles (arbitrarily), however, had a maximum at 525 nm which did not shift during the experiment (Fig. 3.5B). Therefore, a mass of 15 mg of AC particles was chosen for the following investigations despite of the fact that high amounts of particles favoured photooxidation (Fig. 3.4, trace d). At this stage of sensor development it was important to reproduce results in order to draw reliable conclusions.
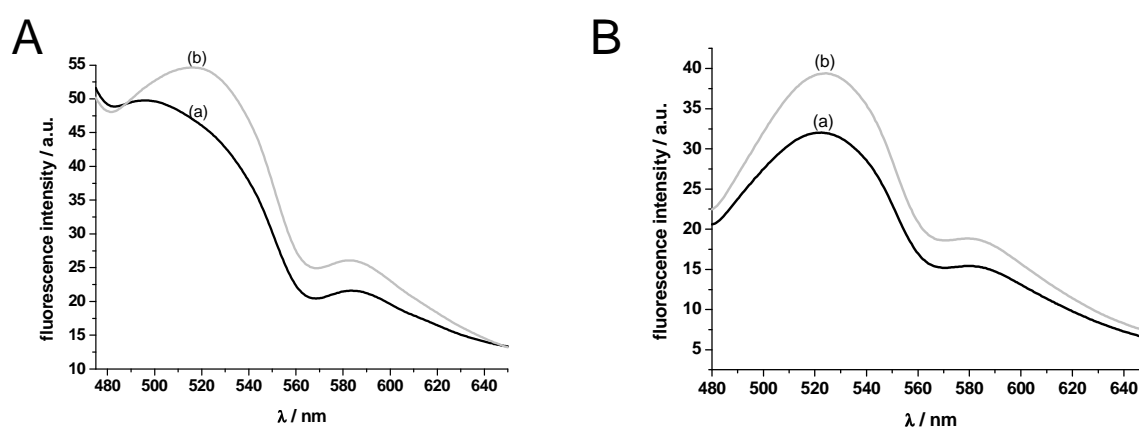
Figure 3.5. Fluorescence spectra of the sensor foil (a) before and (b) after 60 min of flushing with PBS of pH 7.4. A: 2 mg of AC in 2.5 % D4 hydrogel. B: 15 mg of AC in 2.5% D4 hydrogel.

3.5 Oxidation and Reduction

The ability to reuse the chemosensor was tested by purging the sensor with HP and a reductive agent in consecutive turns. Here, sodium dithionite ($Na_2S_2O_4$; 1 M in PBS of pH 7.4) was arbitrarily chosen and subjected to measurements of sensor spots, which consisted of 15 mg of dyed AC particles in 2.5 % (w/w) D4 hydrogel. First, the sensor was purged with $Na_2S_2O_4$ in order to reduce HP Green and to yield a baseline with low intensity. Fluorescence decreased immediately when $Na_2S_2O_4$ passed through the sensor layer indicating that HP Green is reduced (Fig. 3.6, trace a). Reduction was completed within 11 min and the fluorescence intensity was reduced by 23% from $I/I_0 = 1.04$ to 0.8. Then, $Na_2S_2O_4$ was replaced by a 100 µM solution of HP upon which emission started to rise by 38% from $I/I_0 = 0.8$ to 1.1. Consecutive turns of reduction and oxidation were repeated two times. The sensor shows a response time of 70 s (defined as t_{95}) for reduction. The one of oxidation is 8 min 15 s. This large difference in time is explained by the strongly different concentrations of $Na_2S_2O_4$ (1 M) and HP (100 µM). An important fact is that the baseline continuously shifted to higher values after every reduction step.
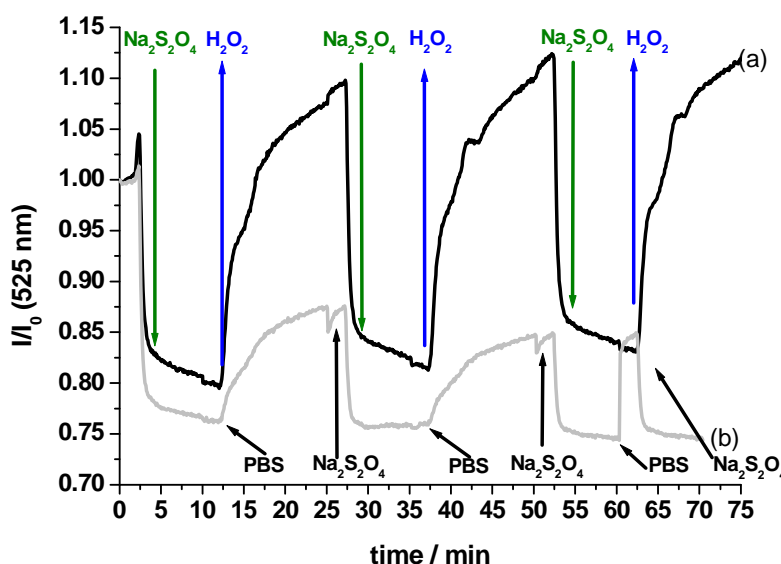
Figure 3.6. Time trace at 525 nm of the chemosensor displaying changes in fluorescence upon consecutive reduction and oxidation of HP Green.

Furthermore, HP was replaced by PBS to check whether or not dissolved oxygen in the buffer impacted the sensor. Solutions of $Na_2S_2O_4$ and PBS were added at the same time

as in the previous experiment with HP. First, HP Green was reduced with $Na_2S_2O_4$ as emission decreased by 25% from $I/I_0 = 1.01$ to 0.76 within 10.5 min. When buffer passed the sensor membrane, fluorescence increased by 15% (from $I/I_0 = 0.76$ to 0.87) within 14 min, which is due to dissolved oxygen. The response time (defined as t_{95}) for dissolved oxygen is 16 min 10 s. The one for reduction is 45 s. As a consequence, no stable baseline was obtained due to the sensor being oxidized to a certain extent by dissolved oxygen.

3.6 Discussion and Conclusion

A low number of particles entails to noise on the time traces. Furthermore, the emission maximum shifts to higher wavelengths during the measurement (Figs. 3.4A and 3.5A). Hence, it can be assumed that the recorded intensity did not exceed the instrument´s background noise substantially. Therefore, the data of kinetics and calibration of the HP Green sensor membrane are not reliable despite of the fact that distinct changes of emission could be ascribed to different concentrations of HP (Fig. 3.3B). Higher amounts of particles yielded a stable emission maximum and were not "falsified" by a shift. As a disadvantage, the sensor displayed a higher cross-sensitivity to oxygen in solution than membranes with lower content of particles.

The high fluorescence at the beginning of the sensor experiments (Fig. 3.6) could be reduced by $Na_2S_2O_4$, thus indicating that most of HP Green was present in its oxidized state. Hence, a preliminary use of $Na_2S_2O_4$ during sensor preparation can be avoided. Furthermore, $Na_2S_2O_4$ improved the response of the sensor for HP compared to the experiments in chapter 3.3. It was possible to oxidize and reduce HP Green in the polymer matrix, which illustrates that, in principle, the sensor can be recovered. Oxidation, however, took place in the presence of HP or dissolved oxygen, thus limiting the sensitivity of the sensor for HP. Chemosensors for HP that apply the redox pair Prussian White-Prussian Blue displayed similar time traces to HP (increasing intensity) and the reductive agent ascorbic acid (decreasing intensity) but showed no cross-reactivity to oxygen.[9] Furthermore, their response time for 100 µM of HP is around 3 min, which is 5 min shorter than the one of the HP Green chemosensor. No exact quantification can be found in reference 9 besides a plot of response time *vs.* concentration of HP. It has to be assumed that the authors used t_{95} as definition.

As conclusion, the chemosensor shows a fluorescence increase in presence of hydrogen peroxide but the effect of dissolved oxygen renders the device less practicable.

Improvements may be achieved if HRP is co-immobilized into the sensor membrane. This should yield much shorter response times and sensitivity at lower concentrations of HP. Furthermore, the effect of oxygen in the HP samples is probably negligible due to strongly enhanced fluorescence upon reaction with HP as found for the HP assay in solution (see chapter 2.3).

3.7 Literature

1. S. M. Borisov, O. S. Wolfbeis, Optical Biosensors. *Chem. Rev.*, **2008**, 108, 423 – 461.

2. I. Tiwari, M. Singh, Preparation and characterization of methylene blue-SDS-multiwalled carbon nanotubes nanocomposite for the detection of hydrogen peroxide. *Microchim. Acta*, **2011**, DOI: 10.1007/s00604-011-0620-5.

3. H. E. Posch, O. S. Wolfbeis, Optical sensor for hydrogen peroxide. *Microchim. Acta*, **1989**, I, 41 – 50.

4. F. Schubert, F. Wang, H. Rinneberg, Fibre optic fluorometric enzyme sensors for hydrogen peroxide and lactate, based on horseradish peroxidase and lactate oxidase. *Microchim. Acta*, **1995**, 121, 237 – 247.

5. T. M. Freeman, W. R. Seitz, Chemiluminescence fiber optic probe for hydrogen peroxide based on the luminol reaction. *Anal. Chem.*, **1978**, 50, 1242 – 1246.

6. F. Preuschoff, U. Spohn, D. Janasek, E. Weber, Photodiode-based chemiluminometric biosensors for hydrogen peroxide and L-lysine. *Biosens. Bioelectron.*, **1994**, 9, 543 – 549.

7. O. S. Wolfbeis, M. Schäferling, A. Dürkop, Reversible optical sensor membrane for hydrogen peroxide using an immobilized fluorescent probe, and its application to a glucose biosensor. *Microchim. Acta*, **2003**, 143, 221 – 227.

8. M. Schäferling, M. Wu, J. Enderlein, H. Bauer, O. S. Wolfbeis, Time-resolved luminescence imaging of hydrogen peroxide using sensor membranes in a microwell format. *Appl. Spectrosc.*, **2003**, 57, 1386 – 1392.

9. I. Del Villar, I. R. Matias, F. J. Arregui, J. Echeverría, F. J. Arregui, J. Echeverría, R. O. Claus, Strategies for fabrication of hydrogen peroxide sensors based on electrostatic self-assembly (ESA) method. *Sens. Actuat. B.*, **2005**, 108, 751 – 757.

10. Martin Link, New fluorescent labels and probes for biological applications. **2010**, Dissertation Universität Regensburg.

4. Optical Approach to the Detection of D/L-Lactate via Boronic Acids

4.1 Introduction

Lactate is the anion of lactic acid (α-hydroxypropionic acid; $pK_a = 3.86$) and contains an asymmetric carbon atom.[1] Two optically active isomers exist, and the L-(S) enantiomer is predominant in animal organism[2,3,4,5] and is produced under anaerobic conditions during the final steps of glycolysis.[6] The D-(R) form is mainly produced in the metabolism of microorganisms[7,8] and plants[9], however, few occurrences are known for mammals.[10,11] Lactate - and also lactic acid - is ubiquitous in everyday life. The latter acts as an additive (E270) in food[12] or as a disinfectant[13,14] in combination with detergents for dish-washing and cleaning. In both cases it serves as an acidifier by decreasing the pH value to 3-4 which will prevent most microorganisms or bacteria from growing. Furthermore, lactate is produced naturally by lactic acid bacteria during fermentation in food and beverages.[15] There are numerous substrates that can be found in e.g. dairy products, sourdough, wine or beer, that are metabolized into pyruvate following common metabolic pathways like glycolysis. In a final step, lactate dehydrogenase (LDH) transforms pyruvate to lactate depending on the specifity of the enzyme for the D- or L-enantiomer.

In the field of sports medicine, lactate concentrations in blood are monitored during exercise thus serving as an indicator for training status and fitness.[16] The concentration of lactate in blood gives information about the position of aerobic and anaerobic thresholds: a significant increase of lactate from 2 up to 4 mM under physical exhaustion can be observed.[17,18,19] Additionally, lactic acid is used as a monomer for poly(lactic acid), a biodegradable, aliphatic polyester that undergoes hydrolytic scission once imparted into the body. Its ester bonds are cleaved thus releasing non-toxic lactic acid, rendering it suitable for applications as a drug delivering system in biomedicals. Both enantiomers can be subjected to polycondensation whereas applying different ratios of these enantionmers controls the properties of poly(lactic acid) like melting temperature for instance. [20,21,22]

There is large interest in the detection of D- or L-lactate because this important analyte occurs in various media as stated above. Common detection schemes make use of lactate converting enzymes, namely lactate oxidase (LOx), D-lactate dehydrogenase (D-LDH) and L-lactate-dehydrogenase (L-LDH). All of them produce pyruvate under either aerobic

conditions (LOx) or anerobic conditions (D/L-LDH). LOx is a flavine type enzyme that requires oxygen, LDH however, depends on the oxidized nicotinamide adenine dinucleotide (NAD$^+$) as cofactor to catalyze the conversion of the substrate. Therefore, lactate concentrations are determined *via* oxygen consumption or NADH production. An alternative route is *via* hydrogen peroxide that is produced by LOx, as well.[16] Common amperometric biosensors use immobilized LOx as transducer and detect changes in the electric current following the reaction with L-lactate. They provide rapid, simple and direct measurements with low limits of detection (LOD) and a wide linear range. One such sensor reaches a LOD of 0.8 µM and has a linear range between 2 and 1000 µM of L-lactate.[23] In contrast, D-lactate sensing can only be realized with D-LDH biosensors because D-lactate is not converted by LOx. [24] Aside from a lactate biosensor that utilizes the intrinsic fluorescence of lactate monooxygenase,[25] common optical detection methods combine the above listed enzymes with fluorophores or probes. One biosensor applies an oxygen-sensitive ruthenium probe (Ru(ph$_2$phen)$_3^{2+}$), whose fluorescence is quenched by oxygen. Inside the sensor layer lactate reacts with LOx, the oxygen concentration in the microenvironment around Ru(ph$_2$phen)$_3^{2+}$ is decreased and this induces an increase in fluorescence intensity. The biosensor monitors lactate concentrations between 0 to 5 mM with a response time of 3 min.[26] Alternatively, LDH can be used as recognition system and the optical characteristics of its reduced cofactor NADH serve as transducer. Following the reaction with L-lactate, an increase in absorbance at 340 nm is obtained. The linear range is between 0.2 and 1 mM.[27] More sensitivity is achieved by measuring the fluorescence intensity of NADH that emits at 460 nm after photoexcitation at 360 nm. A recently developed fibre optical lactate sensor shows a linear response from 0.06 to 1 mM L-lactate with a LOD of 20 µM and a response time of 1 s. Furthermore, it was successfully applied to single cell lactate detection.[28] Classic cuvette tests provide another possibility to detect lactate, e.g. *via* LDH and NADH.[29] Commercially available colorimetric assay kits are widely applied in biochemistry or clinical chemistry due to the fact that they are easy to handle, enable up to 96 assays simultaneously and yield reliable results.[29]

All approaches mentioned above are well established and so-called indirect methods because the detection of lactate is carried out via another analyte. Hence, the need for a probe that binds lactate selectively is very high because this would enable new applications for lactate quantization. The most important task is imaging of lactate in cells as a non-invasive method, which could not be realized yet. Several receptors are discussed in the

literature. Guanidinium groups show a strong interaction with lactate[30] as guanidium-containing arginine is located in the active site[31] of LDH.

Boronic acids are widely known to bind diols in aqueous media which is primarily used for saccharide detection. Both receptors were combined in indicator-receptor displacement assays to determine the binding constants of some carboxylates and α-hydroxycarboxylates. These investigations[32] revealed that the receptors are not able to bind lactate selectively because malate, tartrate and citrate possess higher binding constants. The group of Parker developed a Eu(III) complex with a ligand consisting of a macrocyclic cyclen that carries two glutarate substituents and one azaxanthone moiety to facilitate the lanthanide emission (Fig. 4.1). A change in luminescence intensity is observed once lactate enters the coordination sphere of Eu(III). Citrate, however, causes minor interferences.[33] The use of lactate binding proteins like TTHA0766, a secondary transporter that was overexpressed from *Thermus thermophilus*[34] or of genetically modified glucose/galactose binding protein (GGBP) labelled with a fluorophore also was reported. [35]
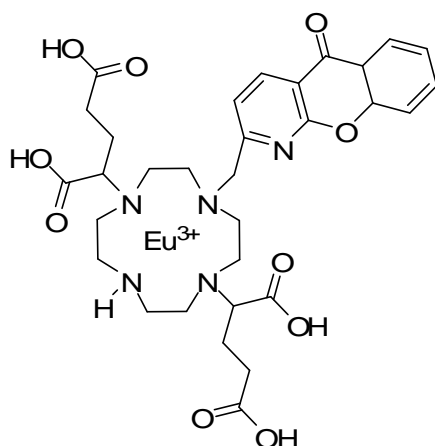
Figure 4.1. Chemical structure of the Eu(III)-chelate complex for detection of lactate and citrate.

Boronic acids form five- or six-membered cyclic esters with bidentate chelating ligands forming covalent bonds.[36] The reaction is fast, reversible, and occurs in aqueous media thus making them well suitable for applications in the field of synthetic receptors. Besides their widely investigated interactions with polyols, in particular saccharides and carbohydrates,[37, 38, 39] boronic acids also react with diols, carboxylates and α-hydroxy-carboxylates, including L-lactate.[32, 40] In case of phenylboronic acids, the trigonal (sp^2 hybridized) boronic acid species is in equilibrium with its cyclic boronate ester formed upon addition of lactate. These considerations do not take into account the existence of an

anionic tetrahedral (sp^3 hybridized) boronic acid species, whose concentration is low at neutral pH and which reacts with lactate at slow rate[41] (Fig. 4.2). A holographic lactate sensor based on this equilibrium was successfully developed by the group of Christopher Lowe[42] with low cross-reactivity towards pyruvate and glucose.
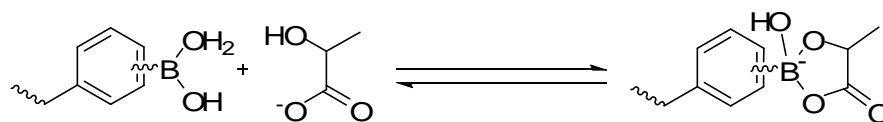
Figure 4.2. The equilibrium between a phenylboronic acid and its negatively charged boronate ester upon reaction with lactate at pH 7.

Our approach combines a phenylboronic acid as the receptor with the use of red light emitting fluorophores to obtain probes that are capable of the detection of lactate levels in the µM concentration range. The Ru(II)- and hemicyanine fluorophores were chosen owing to their easy preparation and well matching spectral characteristics for investigations on biological material (large Stokes´ shift; $\lambda_{abs} \approx 460$ nm, $\lambda_{em} \approx 610$ nm). Following syntheses, the response of the probes to both enantiomers of lactate was analyzed. The results are compared with the help of the following selectivity calculation: The increases of fluorescence intensity (in percent) for both lactate enantiomers are divided at a given concentration in order to easily compare the ratio I/I$_0$. The same equation is used to compare the ratios I/I$_0$ of fluorophores that carry either an *ortho-* or *meta*-phenylboronic acid group.

$$Selectivity_{D/L} = \frac{Increase(D)}{Increase(L)} \qquad\qquad Selectivity_{o/m} = \frac{Increase(ortho)}{Increase(meta)}$$

Finally, the cross-reactivity to sugars was investigated in order to gain information regarding their influence on the boronic acid-lactate interaction.

4.2 Hemicyanine (ICT) Probe

Hemicyanine dyes are of high interest as electrochromic probes for analysis of membrane potential. These molecules are amphiphilic because one end consists of a hydrophilic pyridinium salt that is spaced by methine groups from the lipophilic aniline end. Furthermore, both ends are modified to increase the amphiphilic character. The hydrophilic

component often carries sulfonic acids while medium-length carbon chains are attached to the aniline nitrogen.[43, 44] In case of saccharide sensing, a phenylboronic acid was attached to the polar end to create the pyridinium salt which entails to a photoinduced internal charge transfer (ICT) probe.[45] The formation of a boronic acid saccharide ester causes a shift from electron deficient R-B(OH)$_2$ to electron rich R-B$^-$(saccharide)(OH) thereby modifying the electron-donating ability of the boronic acid moiety.[46] This also results in an increase or decrease of fluorescence intensity, as expected.

4.2.1 Preparation
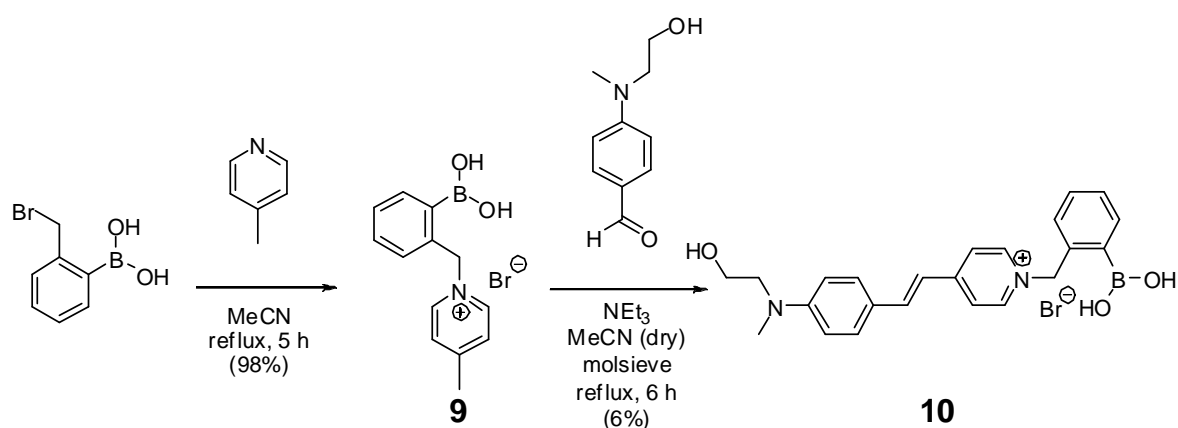
Figure 4.3. Synthesis of hemicyanine probe **5** with an *ortho*-phenylboronic acid.
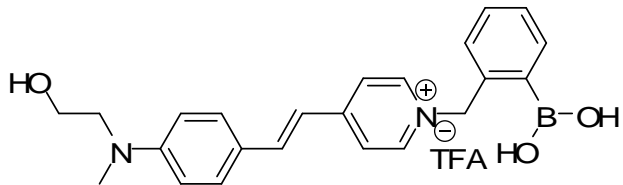
As reported[45] 2-(bromomethyl)phenylboronic acid reacted via a nucleophilic substitution with 4-picoline to the 1-(2-boronobenzyl)-4-methylpyridinium bromide **9**. In the final step, **9** was condensed with N-methyl-N-(2-hydroxyethyl)-4-aminobenzaldehyde to the desired hemicyanine dye (E)-1-(2-boronobenzyl)-4-(4-((2-hydroxyethyl)(methyl)amino)styryl)-pyridinium **10** (Fig. 4.3). The crude product was purified by preparative HPLC to obtain pure **10** due to the low yield (Fig. 6.2). Classic column chromatography on silica, basic alumina or Sephadex LH20, unfortunately, did not lead to the separation of unreacted precursor **9** from the desired end product.

4.2.2 Spectroscopic Characterization – UV, Fluorescence and Effect of pH

The probe shows an absorption maximum at 467 nm and an emission maximum at 610 nm in phosphate buffer of pH 7, resulting in a Stokes´ shift of 143 nm. The extinction

coefficient ε and quantum yield ϕ were determined to be 22,250 L*mol^{-1}*cm^{-1} and 0.022, respectively (Fig. 4.4A and Tab. 4.1). So its brightness (Bs) is rather weak (Bs = $\phi*\varepsilon \approx$ 500). Fluorescence depends on pH and increases under basic conditions (Fig. 4.4B).

Table 4.1. Structure, chemical and spectroscopic data of **10** in aqueous media unless noted otherwise. TFA: trifluoroacetate.

formula	$C_{25}H_{26}BF_3N_2O_5$
M.W. (g/mol)	502.29
λ_{abs} (nm)	469
λ_{em} (nm)	610
ε (L*mol^{-1}*cm^{-1})	22,250
ϕ	0.022[a]

a) Quantum yields (QY) were determined in aqueous solution with 0.5% (v/v) DMSO against the reference dye Ru(bpy)$_2$Cl$_2$ x 6 H$_2$O whose QY is reported to be 0.028 in air-saturated water.
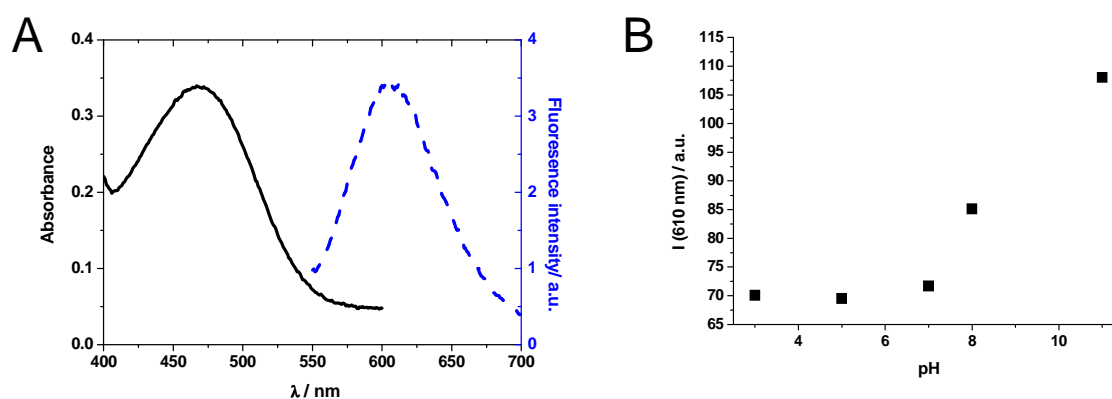
Figure 4.4. Compound **10** (100 µM) in phosphate buffered solutions (10 mM); left: absorption (A) and emission spectra (B) at pH 7; right: plot of pH *vs.* fluorescence intensity at 610 nm.

4.2.3 Response to D-Lactate and L-Lactate
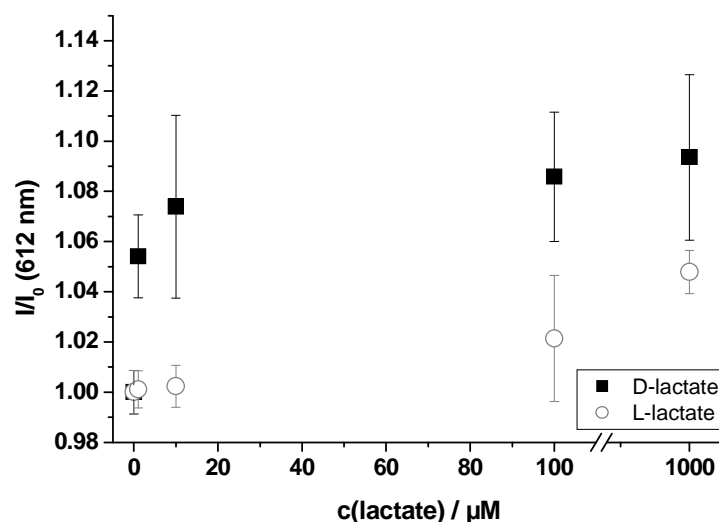
Figure 4.5. Effect of the addition of D-lactate and L-lactate to probe **10** (100 µM) in phosphate buffer of pH 7 (10 mM). All data are referenced to a blank sample containing **10** only.

Solutions with varying concentrations of D-lactate or L-lactate were added to probe **10** in phosphate buffer (pH 7, 10 mM) at room temperature (21 °C $\pm$ 1 °C) (Fig. 4.5). The fluorescence intensity at 612 nm of each sample was measured after 5 min and referenced against a blank containing **10** (100 µM) only in phosphate buffer (pH 7, 10 mM). This entails to an increase in intensity on all concentrations of analyte (1, 10, 100, 1000 µM) with the highest for 1000 µM for both lactate enantiomers. However, the interaction of the boronic acid receptor and the analyte is weak, the recognition of D-lactate occurs more readily than in the case of the L-enantiomer. This is emphasized by the selectivity of **10** for D/L-lactate (Tab. 4.2).

Table 4.2. Selectivity data of **10** towards D-lactate enantiomers.

c(lactate) / µM	1	10	100	1000
Selectivity	49	32	4	2

The selectivity in the low µM range reveals that probe **10** binds preferably to D-lactate to give an increase in fluorescence intensity, which is up to 49-fold higher than with L-lactate. The selectivity for the D-enantiomer becomes lower with increasing lactate

concentration. However, the ratio I/I_0 of **10** with 1000 µM D-lactate still doubled that of L-lactate (9.4% compared to 4.8%). Consequently, D-lactate appears to form a stronger bond although no binding constants were determined.

4.2.4 Interference by Saccharides
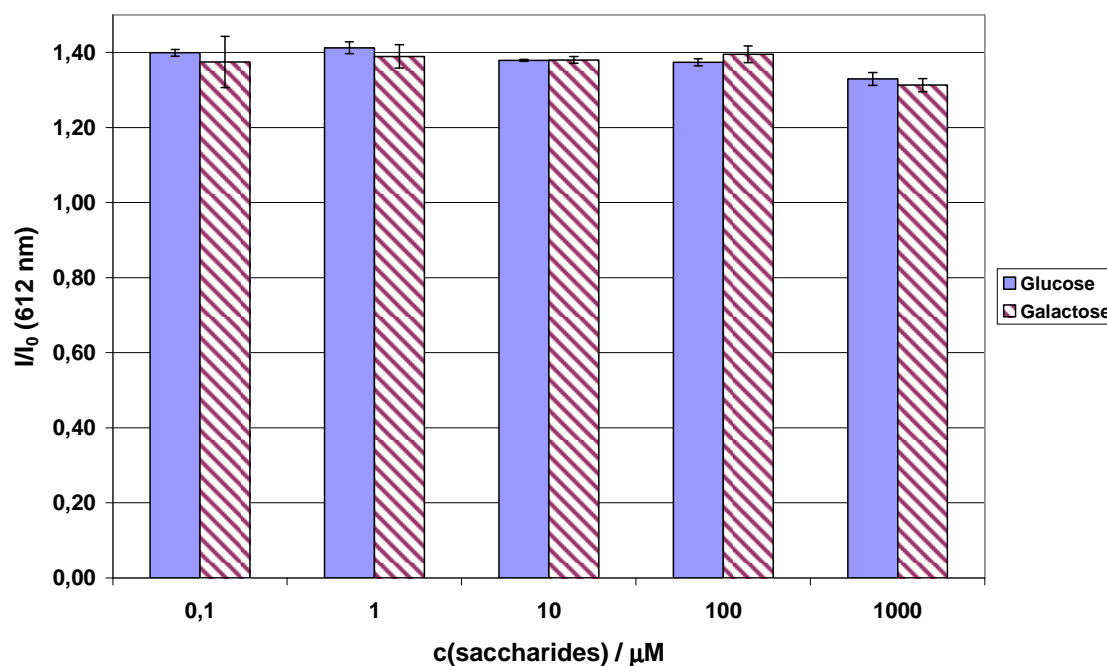
Figure 4.6. Effect of saccharides when added to a mixture of probe **10** (100 µM) and D-lactate (1000 µM) in phosphate buffer of pH 7 (10 mM). All data are referenced to a blank sample containing **10** only and D-lactate.

Boronic acids have been used as recognition units mainly for sugars because of their strong interaction. This has to be regarded as putative source of interference when **10** is applied to real samples like cell extracts, yoghurt or blood. Therefore, the fluorescence intensity of 100 µM of **10** saturated with 1000 µM of D-lactate was investigated upon addition of saccharides of varying concentration (Fig. 4.6). In all cases (0.1, 1, 10, 100, 1000 µM) the graph depicts an increase of luminescence up to 40% when either glucose or galactose was added. Even low concentrations of saccharides had a high impact on the signal. Furthermore, it was not possible to distinguish glucose from galactose with probe **10**. The same experiment with L-lactate was not performed because no different results were expected regarding the response of **10**. Hence, although probe **10** shows significant binding

preference for D-lactate in the µM range, its stronger binding to hexoses prevents its further use as an enantioselective probe for D-lactate.

4.3 Ruthenium (PET) Probes

The spectral properties of ruthenium complexes are governed by ligand-to-metal charge transfer (LMCT) processes between the HOMO of ruthenium(II) and the LUMO of the ligands. Complexes have different colours depending on the number of diimine ligands or halides coordinated. $Ru(bpy)_2Cl_2$ (bpy = 2,2´-bipyridine) and $[Ru(phen)_3]^{2+}$ display violet and orange colours, respectively, and have intense and broad absorption bands around 450 nm. Furthermore, they display an emission at 600 nm and beyond. Numerous compounds have been synthesized for applications such as sensing of oxygen, sugars and anions in general.[47] The latter require receptors that influence the LMCT upon reaction with the analyte. In case of sugars, phenylboronic acids are linked via an aminomethyl linker to a fluorophore. In the "analyte free" state, a dative bond is formed between the nitrogen to the boron atom because of Lewis acid/base interaction. The intensity of the excited fluorophore is decreased (PET ON). In the "analyte bound" state, the dative bond is cleaved upon reaction with a sugar. The PET effect is diminished and fluorescence intensity thus restored (PET OFF).[48,49] The same behaviour is expected to occur on binding of both enantiomers of lactate (Fig. 4.7).

PET ON   **PET OFF**
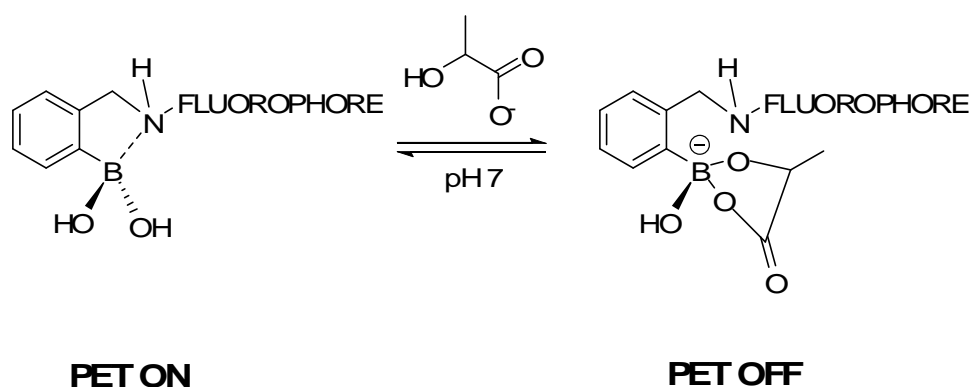
Figure 4.7. PET effect in aminomethyl-phenylboronic acids coupled to fluorophores.

4.3.1 Preparation
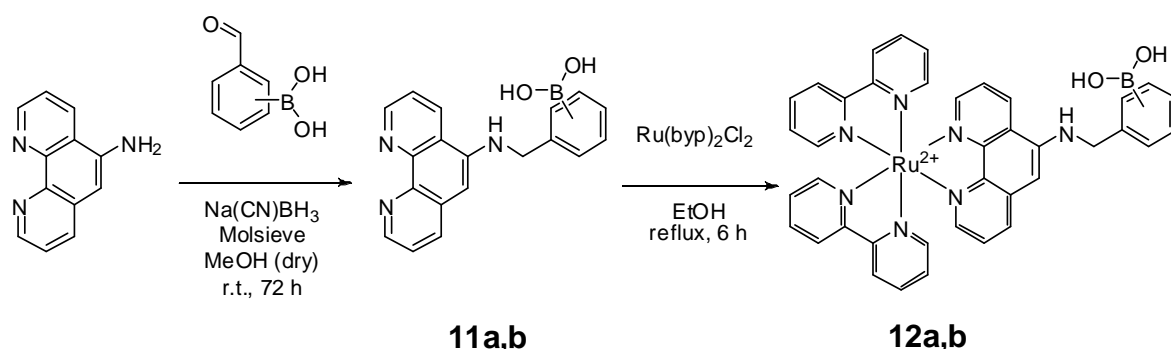
Figure 4.8. Synthesis of Ru(II) probes with *ortho-* (**12a**) and *meta*-phenylboronic acid (**12b**).

Compounds **11a** and **11b** were synthesized via reductive amination of 1,10-phenanthroline-5-amine with 2- or 3-formyl-phenylboronic acid. In a final step, the ligand was complexed with cis-dichlorobis(2,2`-bipyridine)ruthenium(II)-dihydrate to yield the fluorescent probes **12a** and **12b** with the boronic acid receptor group in *ortho* and *meta* position, respectively (Fig. 4.8). Compound **12a** was obtained as dichloride in contrast to **12b**, which was yielded as trifluoroacetate because of purification via preparative HPLC in order to remove impurities.

4.3.2 Spectroscopic Characterization – UV, Fluorescence and Effect of pH

The absorption and emission spectra show maxima at wavelengths that are typical for Ru(II)-complexes, with a Stokes´ shift of 155 nm. The lifetime τ is similar for both probes as well as the quantum yield ϕ and the extinction coefficient ε (Tab. 4.3). Only a weak pH-dependence of the emission is detectable, which is constant for both probes within the physiological pH-range (Fig. 4.9).

Table 4.3. Structure, chemical and spectroscopic data of **12a** and **12b**, respectively, in phosphate buffer of pH 7 (10 mM) unless noted otherwise.

	12a (*ortho*)	**12b** (*meta*)
formula	$[C_{39}H_{32}BN_7O_2Ru](X)_2$	
M.W. (g/mol)	813.50	968.63
	X = Cl[a]	X = TFA[b]
λ_{abs} (nm)	457	458
λ_{em} (nm)	613	614
ε (L*mol^{-1}*cm^{-1})	8,600	7,900
ϕ[c]	0.027	0.025
τ (ns)[d]	406	395

a) Cl: chloride. b) TFA: trifluoroacetate. c) Quantum yields (QY) were determined in aqueous solution with 0.5% (v/v) DMSO against the reference dye $Ru(bpy)_2Cl_2$ x 6 H_2O whose QY is reported to be 0.028 in air-saturated water. d) Luminescence lifetimes (τ) were measured in 0.1 M NaOH solution with fluorescein as the reference.
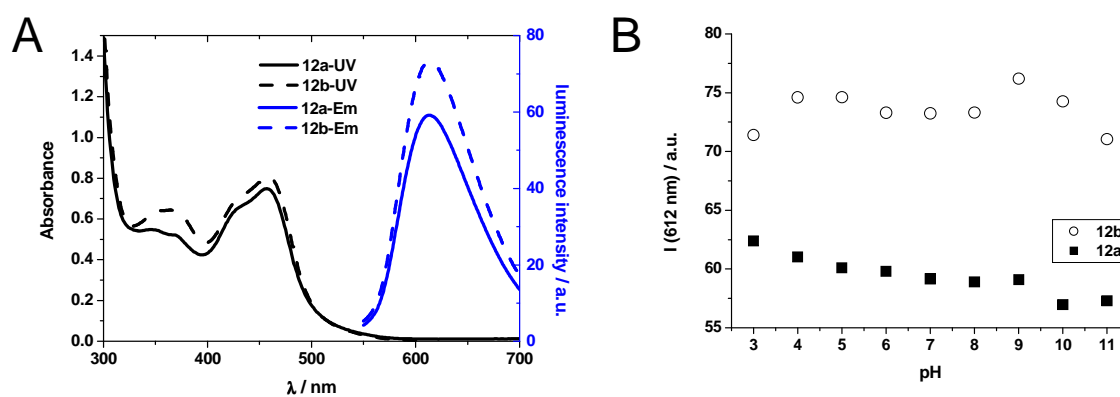
Figure 4.9. Compounds **12a** and **12b** (100 μM), respectively, in phosphate buffered solutions (10 mM); A: absorption (left) and emission spectra (right) at pH 7; B: plot of pH *vs.* luminescence intensity (610 nm).

4.3.3 Response to D-Lactate and L-Lactate

A

B
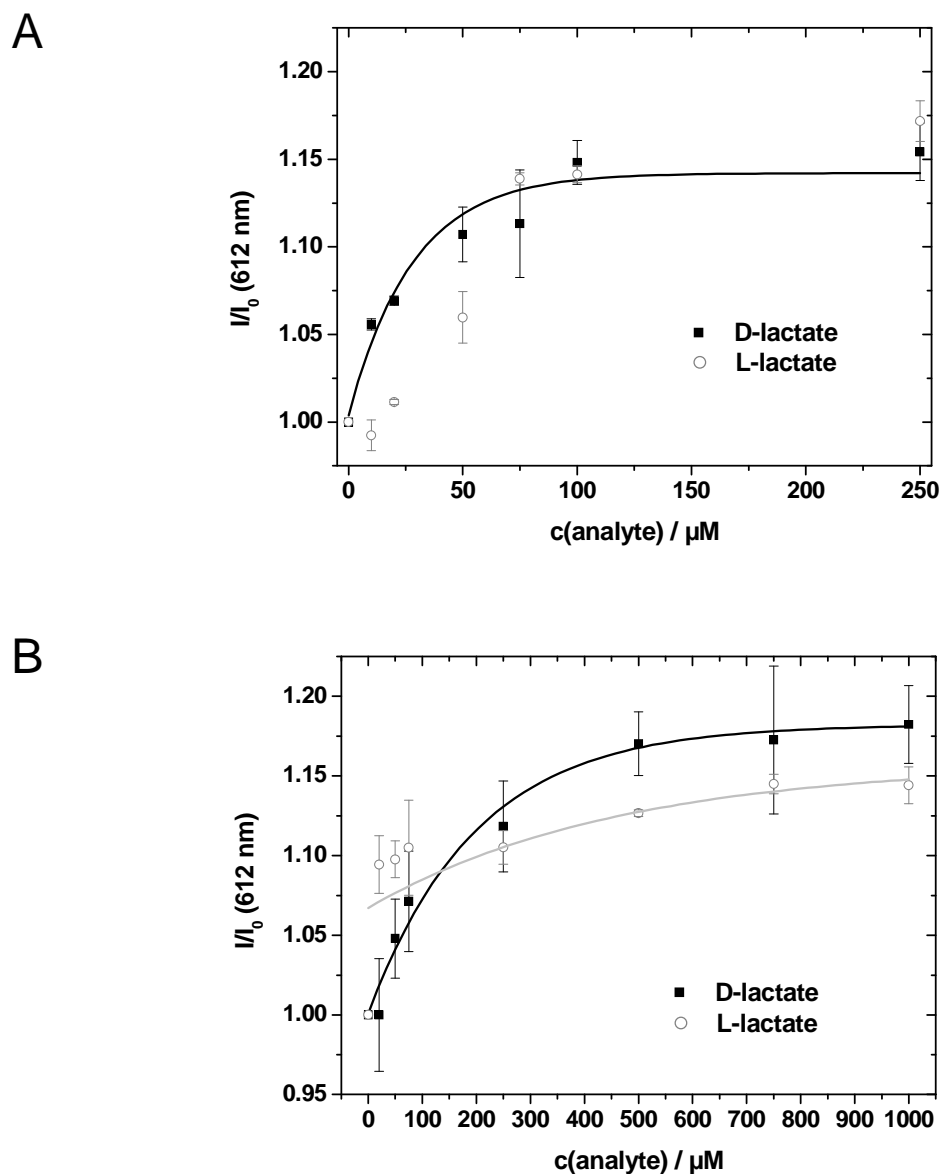
Figure 4.10. Effect of the addition of D-lactate and L-lactate to probes **12a** (A) and **12b** (B) (5 µM), respectively, in phosphate buffer of pH 7 (10 mM).

Solutions with varying D- or L-lactate concentrations were added to either probe **12a** or **12b** dissolved in phosphate buffer (pH 7, 10 mM) at room temperature (29 °C ± 1 °C) (Fig. 4.10). The luminescence intensity at 612 nm of each sample was measured after 5 min and referenced against a blank containing either **12a** or **12b** (5 µM) only, in phosphate buffer (pH 7, 10 mM). An increase in intensity was obtained for all concentrations of analyte with exception of **12a** and 10 µM L-lactate (presumably an

outliner). The titration of D-lactate with both probes reveals an exponential character although saturation is reached already for 250 µM lactate in case of **12a** and not at 1000 µM lactate. The reaction of **12b** with L-lactate gave signals exhibiting linearity in contrast to the sigmoid character of the other titration with **12a** (Fig. 4.10). The calculation of selectivity values reveals that **12a** and **12b** differentiate both lactate enantiomers, especially in the low µM concentration range (Tab. 4.4). The two enantiomers can be distinguished with probe **12a** only at 20 and 50 µM of lactate. Higher concentrations show similar selectivity values in contrast to probe **10** although both carried an *ortho*-phenylboronic acid. Compound **12b** differentiated both lactate enantiomers at any concentration present. However, it shows no preference for one enantiomer over the whole concentration range added. Here, L-lactate is strongly preferred at concentrations from 20 to 50 µM (similar to **12a**), but D-lactate seems to be bound better in concentrations from 500 to 1000 µM.

Table 4.4. Selectivity data of **12a** and **12b** towards D-lactate.

c(lactate) / µM	20	50	75	100	250	500	750	1000
Selectivity **12a**	6.1	1.8	0.8	1.0	0.9			
Selectivity **12b**	3.3E-4	0.5	0.7		1.1	1.3	1.2	1.3

It was expected that the receptor group with the *ortho*-phenylboronic acid binds the analyte stronger than the *meta*-compound which was already proven in titrations of glucose to *ortho*-, *meta*- and *para*-derivatives of sugar probes.[50] Selectivity values (see Section 4.1) were calculated to reveal the possible preference of D- and L-lactate, respectively for either the *ortho*- (**12a**) or *meta*- (**12b**) phenylboronic acid receptor (Tab. 4.5). In case of D-lactate, the selectivity values are all higher than 1 suggesting that the *ortho*-derivative binds the analyte stronger than the *meta*-derivative. For example, the ratio I/I$_0$ of **12a** with 50 µM D-lactate doubled that of **12b** (2.2 compared to 0.6). Finally, one can assume that L-lactate shows similar behaviour only for concentrations higher than 75 µM because, here, the selectivity values are higher than one.

Table 4.5. Selectivity data (*ortho*/*meta*) towards D- or L-lactate, respectively.

c(lactate) / µM	20	50	75	250
Selectivity **D**	2,234	2.2	1.6	1.3
Selectivity **L**	0.12	0.6	1.3	1.6

4.3.4 Interference by Saccharides
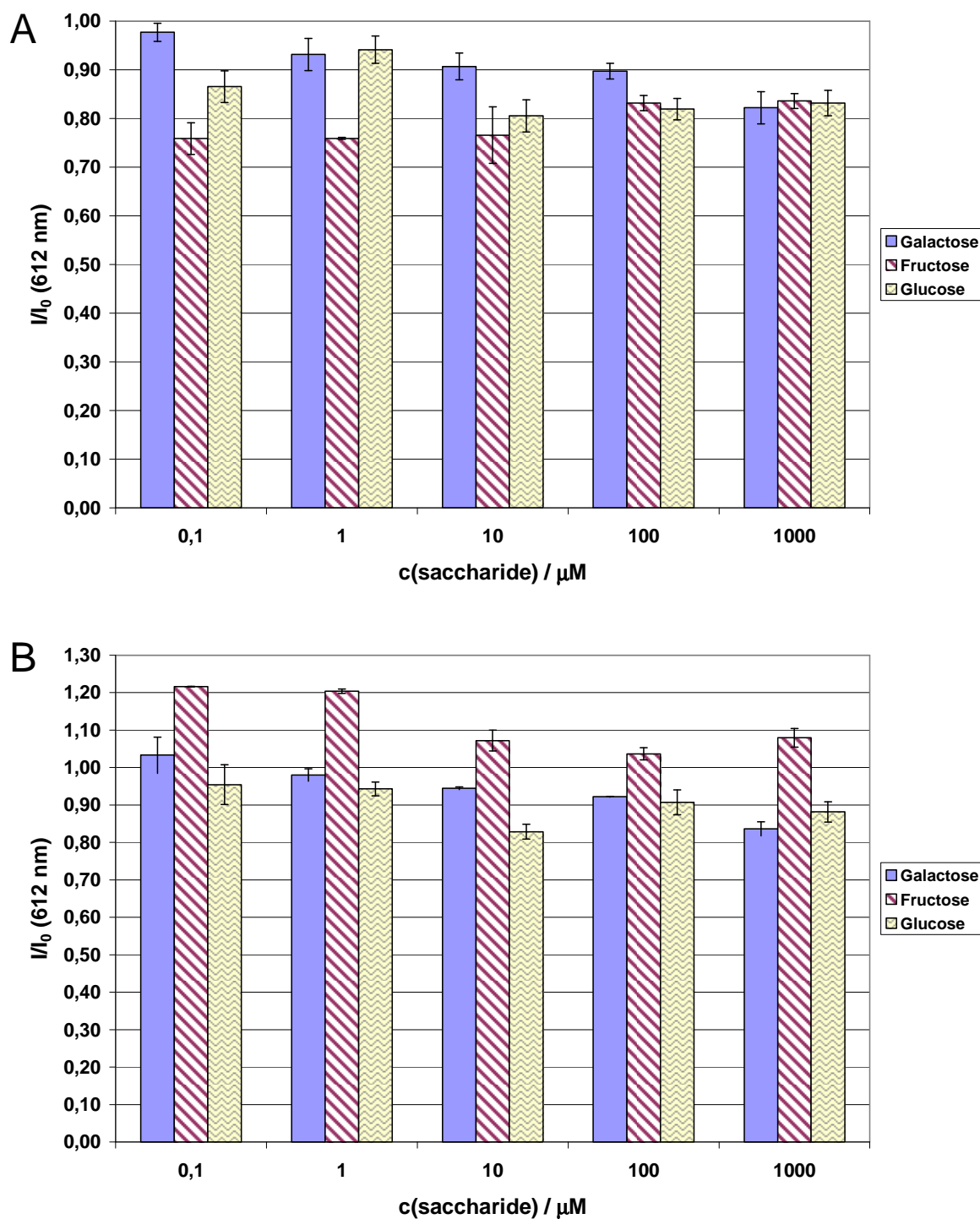
Figure 4.11. Effect of saccharides when added to a mixture of probe **12a** (10 µM) and 1000 µM of either D- (A) or L-lactate (B) in phosphate buffer of pH 7 (10 mM). All data are referenced to a blank sample containing **12a** and either D- or L-lactate only.

Probe **12a** was chosen for the following experiments due to its more pronounced response towards both lactate enantiomers. D-glucose, D-fructose or D-galactose (0.1, 1, 10, 100, 1000 µM), respectively, were added to a solution of **12a** (10 µM) saturated with D- or L-lactate (1000 µM) to test the interference of saccharides on the probe-lactate-interaction. A blank sample containing **12a** (10 µM) and D-or L-lactate (1000 µM) served as reference whereas signal changes of 10% were tolerated (Fig. 4.11). In all cases, D-fructose strongly interfered the lactate-boronic acid interaction, which is typical for probes sensing saccharides with D-fructose binding strongest.[50,51] Surprisingly, the luminescence intensity was quenched in the presence of D-lactate up to 25% (Fig. 4.11A) but increased with the L-enantiomer up to 21% (Fig. 4.11B). Even small amounts of D-glucose already changed the starting signal by decreasing its intensity. D-galactose, however, interferes only at high concentrations.

4.4 A Cyanine Probe for Lactate

The cyanines represent one big group of dyes primarily (but not exclusively) used for near infrared (NIR) fluorescence spectroscopy. Their absorption lies in the near infrared region of the electromagnetic spectrum and they display weakly red shifted emission. NIR fluorescence spectroscopy has the advantage that background emission from biological material is strongly reduced which is of high relevance in e.g. cellular imaging. There is a large number of dyes commercially available (Cy5, Cy7) that can be used in laser applications[52] or bioanalysis[53]. The most popular one is Indocyanine Green which is widely used in medicine as an optical indicator in diagnostics.[54] Cyanines with amino-reactive chloro groups are used as biolabels for proteins (e.g. IR806) and change their colour from green to blue when conjugated to primary amino groups.[55] Due to their easy preparation, a phenylboronic acid moiety was linked to an amino reactive cyanine label. The interaction with lactate and glucose was investigated regarding its influence on the photoinduced charge transfer of the probe.

4.4.1 Preparation

The commercially available near-infrared dye S0378 is selective for compounds containing a primary amino group. It has been applied as a clickable fluorophore when conjugated to azidopropylamine.[56] Here, the cyanine dye was reacted with 3-aminophenylboronic acid in a nucleophilic substitution to yield the boronic acid carrying dye **13** (Fig. 4.12).
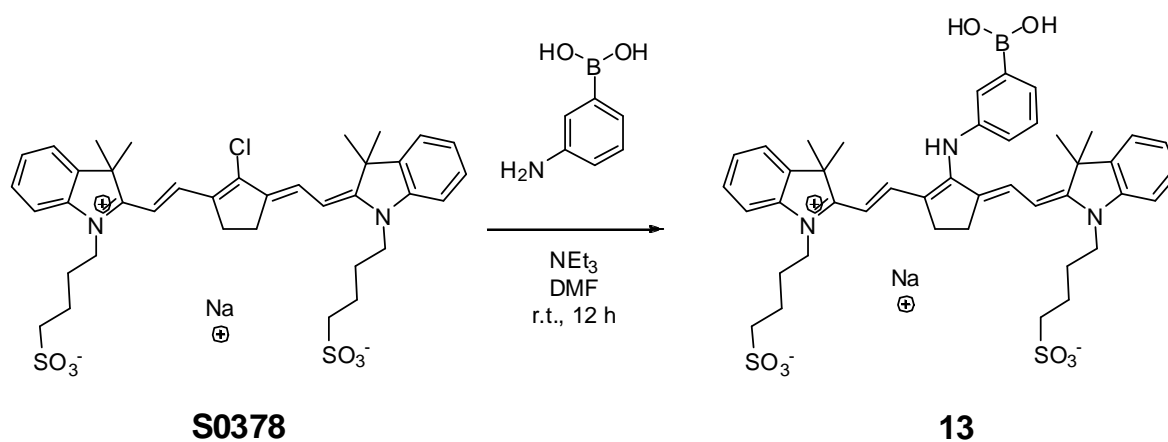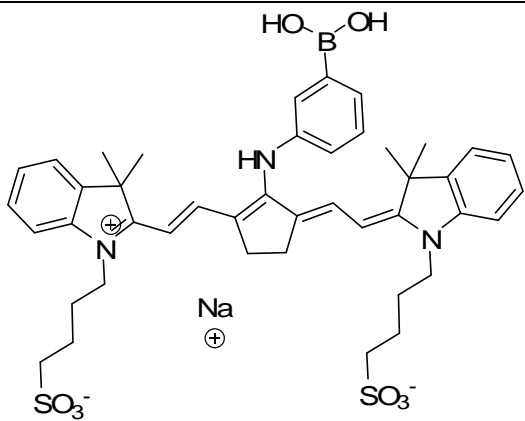
Figure 4.12. Synthesis of cyanine probe **13** with *meta*-phenylboronic acid.

4.4.2 Spectroscopic Characterization – UV, Fluorescence and Effect of pH

Compound **13** shows an absorption maximum at 690 nm and the emission maximum at 784 nm in the near infrared (NIR) resulting in a Stokes´ shift of 94 nm. The extinction coefficient is 95,400 L*mol^{-1}*cm^{-1} in phosphate buffer of pH 7, and as high as 150,000 L*mol^{-1}*cm^{-1} in dry methanol (Fig. 4.13A and Tab. 4.6).

Table 4.6. Structure, chemical and spectroscopic data of **13** in phosphate buffer of pH 7 (10 mM) unless noted otherwise.

formula	$C_{43}H_{51}BN_3NaO_8S_2$
M.W. (g/mol)	835.31
λ_{abs} (nm)	690
λ_{em} (nm)	784
ε (L*mol^{-1}*cm^{-1})	95,400 (buffer)
	150,000 (MeOH)
τ (ps)[a]	265

a) Fluorescence lifetime τ was determined in aqueous solution against glycogen (β = 25 mg/mL) as scatterer.
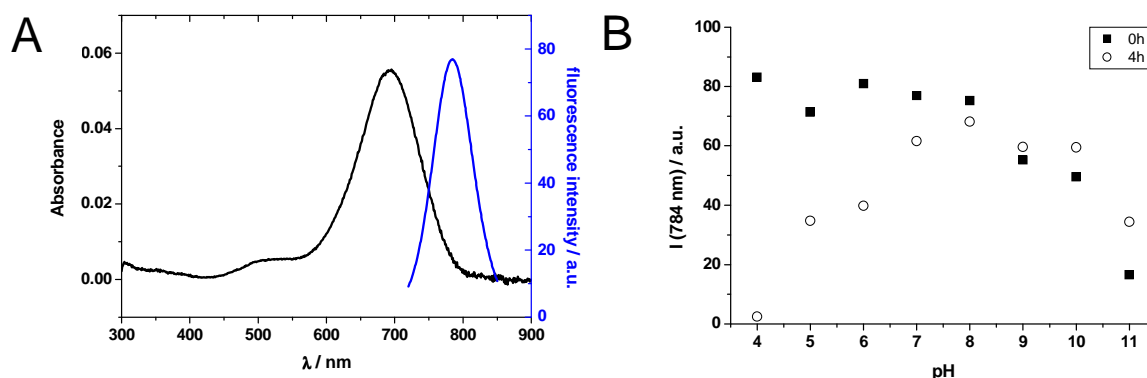
Figure 4.13. Compound **13** (10 µM) in phosphate buffered solutions (10 mM); A: absorption (left) and emission spectra (right) at pH 7; B: plot of pH *vs.* fluorescence intensity (784 nm) at 0 and 4 h.

The fluorimetric pH titration of a freshly prepared sample of **13** in phosphate buffer (10 mM) displayed an emission maximum around 780 nm, whose intensity was increasing with acidic pH. The signal was nearly constant over a wide region from pH 4 to 8. After 4 hours, however, a loss of intensity was detectable from the acidic to neutral pH region whereas slightly basic conditions values caused no significant change (Fig. 4.13B). The appearance of a second, blue-shifted band, in both absorption (527 nm) and emission (594 nm) spectra were reason for the changes observed (Fig. 4.14). The emission around 594 nm ($\lambda_{exc.}$ = 527 nm) was of low intensity. The isosbestic points around 570 nm (UV)

and at 710 nm (emission) indicated the presence of a dual system of a blue and a purple chromophore, which are transformed into one another. It has been published[57], that the blue shifted bands are formed upon protonation of the *meso*-nitrogen atom resulting in an equilibrium of two protonated forms. The addition of base, however, could neither stop the reaction nor shift the equilibrium back to the blue chromophore which hints at the reaction being irreversible. This is further supported by the fact that the new absorption band at 527 nm appears (to a lesser extent) even at slightly alkaline pH. The observations led to the suggestion that a hydrolysis, that is catalyzed by protons is taking place instead of an equilibrium between two protonated forms.
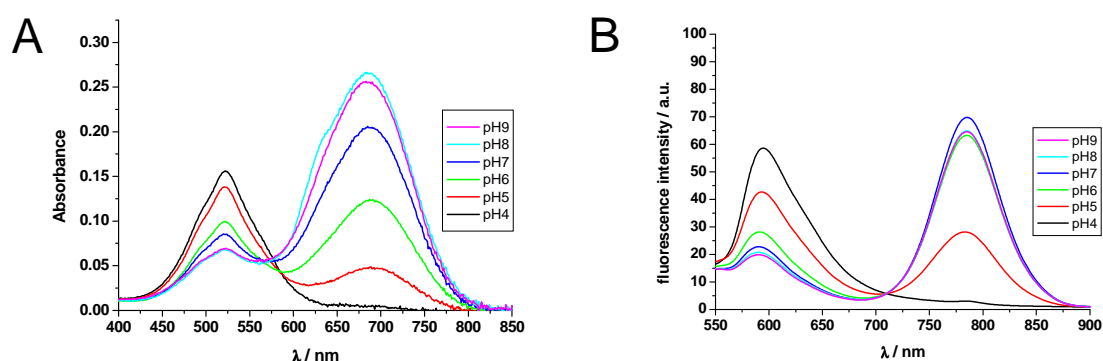
Figure 4.14. Effect of pH on absorption (A) and emission (B) spectra of **13** (10 µM) after 4 h in phosphate buffered (10 mM) solutions from pH 4 to 9 upon excitation at 527 nm.

4.4.3 Response to D-Lactate and L-Lactate

The effects of aqueous media and pH value were investigated to determine the most suitable conditions for the reaction of probe **13** with D- and L-lactate. The emission of **13** (1 µM) in phosphate buffered solution was measured over 60 min. A pH of 7, 9 and 11 was chosen to minimize the rate of hydrolysis. A continuous decrease in fluorescence intensity is obtained for all blank samples, which is supposed to be the slowest at pH 11 at first glance (Fig. 4.15). Referencing all intensities against the corresponding starting value (I/I_0), however, reveals that the loss of intensity is similar at all pH values regarding measurement uncertainty. Neither the addition of D- nor L-lactate influenced the signal significantly. The addition of 100 µM D-lactate at pH 9 shows different behaviour but the effects also may be caused by measurement uncertainty (Tab. 4.7).
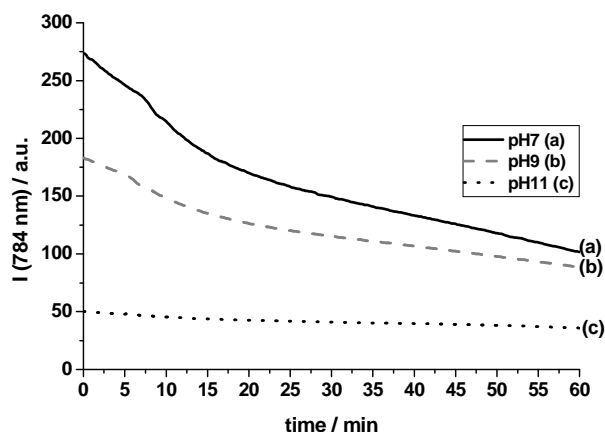
Figure 4.15. Time trace measurements of the decomposition of **13** (1 µM) in phosphate buffered solutions (10 mM) at pH 7, 9 and 11 over 60 min.

Table 4.7. Loss of fluorescence intensity at 784 nm over time. Data were referenced against the starting value at t = 0 min. Spectra are given in Experimental Part, Fig. 6.11.

time/min	I/I_0 at pH 7			I/I_0 at pH 9			I/I_0 at pH 11		
	blank	D	L	blank	D	L	blank	D	L
0	1	1	1	1	1	1	1	1	1
1	0.97	0.95	0.94	0.98	1.02	0.93	0.95	0.94	0.94
10	0.93	0.86	0.90	0.93	0.98	0.89	0.89	0.91	0.90
30	0.77	0.82	0.86	0.86	0.92	0.83	0.78	0.85	0.84

4.4.4 Reaction with D-Glucose

The interaction of the boronic acid receptor and glucose was investigated because a significant change of signal was expected due to the strong binding. The reaction was carried out in phosphate buffer of pH 11 to reduce media influence on the emission maximum to a certain extent. Furthermore, the strong basic pH provided optimal conditions to form the boronic acid-saccharide ester.[58] Surprisingly, the addition of 1 mM D-glucose to 1 µM **13** did not significantly alter the signal. Contrarily, a continuous decrease was detected, which also occurs with a blank sample at this pH. Finally, the reaction was performed in dry DMSO, however, no different observations, could be made (Fig. 4.16).
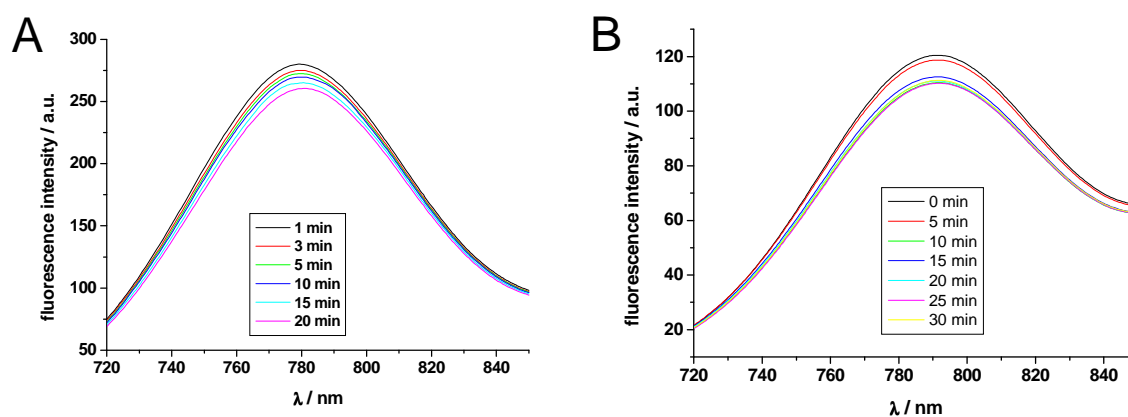
Figure 4.16. Emission spectra of probe **13** after addition of D-glucose over time upon excitation at 690 nm; A: 1 µM **13** and 1 mM glucose in phosphate buffer of pH 11; B: 10 µM **13** and 500 µM glucose in dry DMSO. Excitation was performed at 690 nm.

4.5 Discussion and Conclusion

The experiments prove that all fluorophores - with the exception of cyanine dye **13** - are capable of binding lactates via their phenylboronic acid moiety. A preference for the non-physiological D-enantiomer was observed for all compounds as higher changes in fluorescence intensity were detected. Furthermore, the position of the receptor group proved to be ambitious for the detection. Compound **12a** (with an *ortho*-phenylboronic acid) displayed a higher response to low concentrations of D-lactate as the *meta*-derivative **12b** although the latter can be used for a larger range up to 1000 µM (Tab. 4.5). In general, high values of selectivity were obtained for low µM concentrations of both lactate enantiomers (Tab. 4.4).

The calibration plots revealed a linear, sigmoidal or exponential behaviour of the fluorescence signal with an increase of up to 18% after the addition of 1 mM D-lactate to **12b** (Fig. 4.10B). Although the interaction between receptor and target was weak, different fluorescence intensities were obtained in a concentration range for D-lactate between 0 to 250 µM. All probes, [Ru(II) (**12a** and **12b**); hemicyanine (**10**)] display comparable responses to D-lactate but very different ones for L-lactate. Compound **12a**, with an *ortho*-phenylboronic acid, differed at distinguishing the two enantiomers, although it carried the same receptor group as **10**. The influence of water and pH value must be taken into consideration for the cyanine dye **13**. Its decomposition commenced immediately in

aqueous media even at neutral pH. Therefore it could not be used as a reliable NIR probe, but was successfully applied in a disposable sensor for acidic gases (see Chapter 5).

Finally, the effect of saccharides as major interfering agents was investigated. In general high concentrations of D-fructose, D-glucose and D-galactose strongly interfered with the signal of the probe, in presence of either D- or L-lactate. The most significant alterations (up to 40%) were obtained for **10** and both galactose and glucose. The Ru(II)-probe **12a** differed in its response towards the sugars added. Quenching (up to - 25%) occurred in all five cases for **12a** saturated with D-lactate. In the presence of L-lactate, however, the addition of D-glucose and D-galactose quenched the luminescence intensity whereas D-fructose increased it for all concentrations.

In conclusion, the experiments hint at boronic acids being suitable for the detection of lactate levels by fluorescence spectroscopy. A differentiation between the two enantiomers is possible at concentrations from 20 µM to 75 µM and 500 µM to 1000 µM for probes **12a** and **12b** (Tab. 4.4), and 1 µM to 1000 µM for probe **10** (Tab. 4.2). The presence of sugars should be avoided owing to their strong interference. This problem cannot be solved easily, but requires the design of a more specific receptor for D- or L-lactate, respectively. Boronic acids with sterically hindered groups like chiral N-heterocycles were introduced by the group of Anslyn.[59,60] The response of several α-hydroxycarboxylic acids towards various receptors were investigated in indicator displacement assays with a preference for citrate, malate and tartrate.[32] The use of chiral N-heterocycles in combination with phenylboronic acids may offer a possibility to detect lactate, however their incorporation to hemicyanine or phenanthroline moieties is not trivial. Switching the fluorophore scaffold (e.g. naphthalimides) may enable a successful preparation.

4.6 Literature

1. A. Burger, H. Wachter, Hunnius Pharmazeutisches Wörterbuch, 8. Edition, Berlin – New York, de Gruyter, **1998**.

2. F. Weigang, M. Reiter, A. Jungbauer, H. Katinger, High-performance liquid chromatographic determination of metabolic products for fermentation control of mammalian cell culture: Analysis of carbohydrates, organic acids and orthophosphate using refractive index and ultraviolet detectors. *J. Chromatogr.*, **1989**, 497, 59 – 68.

3. Q. Xue, E. S. Yeung, Indirect fluorescence determination of lactate and pyruvate in single erythrocytes by capillary electrophoresis. *J. Chromatogr. A*, **1994**, 661, 287 – 295.

4. J. Gleitz, C. Tosch, T. Peters, Continuous enzyme-linked fluorometric detection of L-(+)-lactate released from brain vesicles under anoxic conditions. *J. Neurosc. M.*, **1996**, 67, 97 – 102.

5. S. Passarella, L. de Bari, D. Valenti, R. Pizzuto, G. Paventi, A. Atlante, Mitochondria and L-lactate metabolism. *FEBS Letters*, **2008**, 582, 3569 – 3576.

6. D. Voet, J. G. Voet, C. W. Pratt, Lehrbuch der Biochemie, 1. Edition, Weinheim – Wiley-VCH, **2002**.

7. T. N. Darling, J. J. Blum, D-lactate production by Leishmania braziliensis through the glyoxalase pathway. *Mol. Biochem. Parasitol.*, **1988**, 28, 121 – 128.

8. D. L Vander Jagt, L. A. Hunsaker, N. M. Campos, B. R. Baack, D-lactate production in erythrocytes infected with Plasmodium falciparum. *Mol. Biochem. Parasitol.*, **1990**, 42, 277 – 284.

9. A. Atlante, L. de Bari, D. Valenti, R. Pizzuto, G. Paventi, S. Passarella, Transport and metabolism of D-lactate in Jerusalem artichoke mitochondria. *Biochim. Biophys. Acta*, **2005**, 1708, 13 – 22.

10. D. Giesecke, A. Fabritius, P. v. Wallenberg, A quantitative study on the metabolism of D(-)-lactic acid in the rat and the rabbit. *Comp. Biochem. Physiol.*, **1981**, 69B, 85 – 89.

11. R. B. Brandt, S. A. Siegel, M. G. Waters, M. H. Bloch, Spectrophotometric assay for D(-)-lactate in plasma. *Anal. Biochem.*, **1980**, 102, 39 – 46.

12. H. Ishiwata, T. Yamada, N. Yoshiike, M. Nishijima, A. Kawamoto, Y. Uyama, Daily intake of food additives in japan in five groups estimated by the market basket method. *Eur. Food. Res. Technol.*, **2002**, 215, 367 – 374.

13. S. Zhang, J. M. Farber, The effects of various disinfectants against *Listeria monocytogenes* on fresh-cut vegetables. *Food Microbiol.*, **1996**, 13, 311 – 321.

14. E. Mbandi, L. A. Shelef, Automated measurements of antilisterial activities of lactate and diacetate in ready-to-eat meat. *J. Microbiol. Meth.*, **2002**, 49, 307 – 314.

15. S.-Q. Liu, Practical implications of lactate and pyruvate metabolism by lactic acid bacteria in food and beverage fermentations. *Int. J. Food Microbiol.*, **2003**, 83, 115 – 131.

16. N. Nikolaus, B. Strehlitz, Amperometric lactate biosensors and their application in (sports) medicine, for life quality and wellbeing. *Microchim. Acta*, **2008**, 160, 15 – 55.

17. H. Stegmann, W. Kindermann, A. Schnabel, Lactate kinetics and individual anaerobic threshold. *Int. J. Sports Med.*, **1981**, 2, 160 – 165.

18. H. Rusko, P. Luhtanen, P. Rahkila, J. Viitasalo, S. Rehunen, M. Härkönen, Muscle metabolism, blood lactate and oxygen uptake in steady state exercise at aerobic and anaerobic thresholds. *Eur. J. Appl. Physiol.*, **1986**, 55, 181 – 186.

19. P. Mognoni, M. D. Sirtori, F. Lorenzelli, P. Cerretelli, Physiological responses during prolonged exercise at the power output corresponding to the blood lactate threshold. *Eur. J. Appl. Physiol.*, **1990**, 60, 239 – 243.

20. R. K. Kulkarni, E. G. Moore, A. F. Hegyeli, F. Leonard, Biodegradable poly(lactic acid) polymers. *J. Biomed. Mater. Res.*, **1971**, 5, 169 – 181.

21. O. Martin, L. Avérous, Poly(lactic acid): plasticization and properties of biodegradable multiphase systems. *Polymer*, **2001**, 42, 6209 – 6219.

22. L. Nobs, F. Buchegger, R. Gurny, E. Allémann, Poly(lactic acid) nanoparticles labelled with biologically active NeutravidinTM for active targeting. *Eur. J. Pharm. Biopharm.*, **2004**, 58, 483 – 490.

23. M. R. Romero, F. Ahumada, F. Garay, A. M. Baruzzi, Amperometric biosensor for direct blood lactate detection. *Anal. Chem.*, **2010**, 82, 5568 – 5572.

24. A.-M. Gué, H. Tap, P. Gros, F. Maury, A miniaturised silicon based enzymatic biosensor: towards a generic structure and technology for multi-analytes assays. *Sensor. Actuat. B*, **2002**, 82, 227 – 232.

25. W. Trettnak, O. S. Wolfbeis, A fully reversible optic lactate biosensor based on the intrinsic fluorescence of lactate monooxygenase. *Fresenius Z. Anal. Chem.*, **1989**, 334, 427 – 430.

26. S. G. Ignatov, J. A. Ferguson, D. R. Walt, A fiber-optic lactate sensor based in bacterial cytoplasmic membranes. *Biosens. Bioelectron.*, **2001**, 16, 109 – 113.

27. C.-I. Li, Y.-H. Lin, C.-L. Shih, J.-P. Tsaur, L.-K. Chau, Sol-gel encapsulation of lactate dehydrogenase for optical sensing of L-lactate. *Biosens. Bioelectron.*, **2002**, 17, 323 – 330.

28. X. T. Zheng, H. B. Yang, C. M. Li, Optical detection of single cell lactate release for cancer metabolic analysis. *Anal. Chem.*, **2010**, 82, 5082 – 5087.

29. Abcam-Lactate Colorimetric Assay Kit for Lactate (www.abcam.com); EnzyChrom™ Lactate Assay Kit (www.gentaur.com); Lactate Assay Kit (www.biovision.com).

30. P. Horváth, A. Gergely, B. Noszál, Characterization of lactate-guanidinium and lactate-lactate interactions in aqueous solution by spectropolarimetry. *J. Chem. Soc., Perkin Trans. 2*, **1996**, 1419 – 1422.

31. J. R. Exequiel T. Pineda, R. Callender, S. D. Schwartz, Ligand binding and protein dynamics in lactate dehydrogenase. *Biophys. J.*, **2007**, 93, 1474 – 1483.

32. S. L. Wiskur, J. J. Lavigne, A. Metzger, S. L. Tobey, V. Lynch, E. V. Anslyn, Thermodynamic analysis of receptors based on guanidinium/boronic acid groups for the complexation of carboxylates, α-hydroxycarboxylates and diols: driving force for binding and cooperativity. *Chem. Eur. J.*, **2004**, 10, 3792 – 3804.

33. R. Pal, D. Parker, L. C. Costello, A europium luminescence assay of lactate and citrate in biological fluids. *Org. Biomol. Chem.*, **2009**, 7, 1525 – 1528.

34. N. Akiyama, K. Takeda, K. Miki, Crystal structure of a periplasmic substrate-binding protein in complex with calcium lactate. *J. Mol. Biol.*, **2009**, 392, 559 – 565.

35. A. Sriram, X. Ge, P. Brothers, H. Lam, G. Rao, L. Tolosa, Optical sensing of lactate using a fluorescently labelled lactate binding protein. *Abstract of Papers, 238th ACS National Meeting, Washington, DC, United States*, **2009**.

36. J. P. Lorand, J. O. Edwards, Polyol complexes and structure of the benzeneboronate ion. *J. Org. Chem.*, **1959**, 24, 769 – 774.

37. J. Yoon, A. W. Czarnik, Fluorescent chemosensors of carbohydrates. A means of chemically communicating the binding of polyols in water based on chelation-enhanced quenching. *J. Am. Chem. Soc.*, **1992**, 114, 5874 – 5875.

38. T. D. James, K. R. A. S. Sandanayake, S. Shinkai, Saccharide sensing with molecular receptors based on boronic acid. *Angew. Chem. Int. Ed.*, **1996**, 35, 1910 – 1922.

39. H. S. Mader, O. S. Wolfbeis, Boronic acid based probes for microdetermination of saccharides and glycosylated biomolecules. *Microchim. Acta*, **2008**, 162, 1 – 34.

40. R. Pizer, R. Selzer, The boric/lactic acid system. Equilibria and reaction mechanism. *Inorg. Chem.*, **1984**, 23, 3023 – 3026.

41. L. Babcock, R. Pizer, Dynamics of boron acid complexation reactions. Formation of 1:1 boron acid-ligand complexes. *Inorg. Chem.*, **1980**, 19, 56 – 61.

42. F. K. Sartain, X. Yang, C. R. Lowe, Holographic lactate sensor. *Anal. Chem.*, **2006**, 78, 5664 – 5670.

43. A. Hassner, D. Birnbaum, L. M. Loew, Charge-shift probes of membrane potential. Synthesis. *J. Org. Chem.*, **1984**, 49, 2546 – 2551.

44. P. Fromherz, C. O. Müller, Voltage-sensitive fluorescence of amphiphilic hemicyanine dyes in neuron membrane. *Biochim. Biophys. Acta*, **1993**, 1150, 111 – 122.

45. S. Trupp, A. Schweitzer, G. J. Mohr, Fluororeactands for the detection of saccharides based on hemicyanine dyes with a boronic acid receptor. *Microchim. Acta*, **2006**, 153, 127 – 131.

46. R. Badugu, J. R. Lakowicz, C. D. Geddes, Enhanced fluorescence cyanide detection at physiologically lethal levels: Reduced ICT-based signal transduction. *J. Am. Chem. Soc.*, **2005**, 127, 3635 – 3641.

47. O. S. Wolfbeis, I. Klimant, T. Werner, C. Huber, U. Kosch, C. Krause, G. Neurauter, A. Dürkop, Set of luminescence decay time based chemical sensors for clinical applications. *Sens. Actuat. B*, **1998**, 51, 17 – 24.

48. L. Zhu, S. H. Shabbir, M. Gray, V. M. Lynch, S. Sorey, E. V. Anslyn, A structural investigation of the N-B interaction in an *o*-(*N,N*-Dialkylaminomethyl)arylboronate system. *J. Am. Chem. Soc.*, **2006**, 128, 1222 – 1232.

49. H. Fang, G. Kaur, B. Wang, Progress in boronic acid – based fluorescent glucose sensors. *J. Fluoresc.*, **2004**, 14, 481 – 489.

50. M. D. Phillips, T. D. James, Boronic acid based modular fluorescent sensors for glucose. *J. Fluoresc.*, **2004**, 14, 549 – 559.

51. W. Tan, D. Zhang, Z. Wang, C. Liu, D. Zhu, 4-(*N,N*-Dimethylamine)benzonitrile (DMABN) derivatives with boronic acid and boronate groups: new fluorescent sensors for sacchardies and fluoride ion. *J. Mater. Chem.*, **2007**, 17, 1964 – 1968.

52. V. Sundström, T. Gillbro, Viscosity dependent radiationless relaxation rate of cyanine dyes. A picosecond laser spectroscopy study. *Chem. Phys.*, **1981**, 61, 257 – 269.

53. K. A. Mesce, K. A. Klukas, T. Clark Brelje, Improvements for the anatomical characterization of insect neurons in whole mount: the use of cyanine-derived fluorophores and laser scanning confocal microscopy. *Cell Tissue Res.*, **1993**, 271, 381 – 397.

54. V. I. Kochubey, T. V. Kulyabina, V. V. Tuchin, G. B. Altshuler, Spectral characteristics of indocyanine green upon its interaction with biological tissues. *Opt. Spectrosc.*, **2005**, 99, 560 – 566.

55. D. Oushiki, H. Kojima, T. Terai, M. Arita, K. Hanaoka, Y. Urano, T. Nagano, Development and application of a near-infrared fluorescence probe for oxidative stress based on differential reactivity of linked cyanine dyes. *J. Am. Chem. Soc.*, **2010**, 132, 2795 – 2801.

56. P. Kele, X. Li, M. Link, K. Nagy, A. Herner, K. Lörincz, S. Bèni, O. S. Wolfbeis, Clickable fluorophores for biological labelling – with or without copper. *Org. Biomol. Chem.*, **2009**, 7, 3486 – 3490.

57. A. B. Descalzo, K. Rurack, On the signalling pathways and Cu[II]-mediated anion indication of *N-meso*-substituted heptamethine cyanine dyes. *Chem. Eur. J.*, **2009**, 15, 3173 – 3185.

58. D. G. Hall, Boronic Acids-Preparation, Applications in Organic Synthesis and Medicine. 1. Edition, Weinheim – Wiley-VCH, **2005**.

59. L. Zhu, E. V. Anslyn, Facile quantification of enantiomeric excess and concentration with indicator-displacement assays: an example in the analyses of α-hydroxyacids. *J. Am. Chem. Soc.*, **2004**, 126, 3676 – 3677.

60. L. Zhu, Z. Zhong, E. V. Anslyn, Guidelines in implementing enantioselective indicator-displacement assays for α-hydroxycarboxylates and diols. *J. Am. Chem. Soc.*, **2005**, 127, 4260 – 4269.

5. Aminocyanines as Blue to Purple Probes in Irreversible Sensors for Acidic Gases

5.1 Introduction

Cyanines[1] constitute one group of fluorophores that belong to the class of longwave dyes besides porphyrin, squaraine and BODIPY derivatives. They absorb and emit light in the VIS to near-infrared (NIR) region and have high molar absorbance and photostability. These characteristics render them suitable fluorescent probes and labels for biomedical applications[2] and bioimaging schemes[3] because background emission from biological material is prevented. Some of them perfectly match the NIR "diagnostic window", ranging from 700-900 nm. Here, light can deeply penetrate tissue because endogenous absorbers like oxy- and deoxyhaemoglobin exhibit a minimum of absorbance.[4] In this context, Indocyanine Green (absorption around 800 nm[5]) is most prominently applied as it is clinically approved for photodynamic therapy and ophthalmology. Moreover, it is used in fluorescent studies of enzymes and proteins.[6, 7, 8] Next in line are the so-called Cy dyes. These consist, e.g. of two indole or benzoxazol derivatives which are linked *via* a polymethine bridge to create a symmetric fluorophore. Each heterocyclic aromatic N-atom is bound to an alkyl chain, which results in a positively charged, quaternized N-atom. The charge is delocalized along the polymethine chain creating a conjugated system. (General building blocks of cyanines are displayed in the structure of S0378 in Fig. 5.1). Numerous Cy fluorochromes are derived from this scaffold, for instance Cy5 and Cy7. Here, five and seven C-atoms, respectively, condense both indol moieties. This entails to a red shift on the absorption maximum from 647 nm (Cy5) to 753 nm (Cy7).[9] Furthermore, the type of condensed heteroaromatic moieties determines the spectral properties.[10] Synthetic modifications increase the functionality of cyanines[11, 12] rendering them suitable for laser[13, 14] and imaging[15] applications or as NIR probes for pH[16] and reactive oxygen/nitrogen species such as hydroxyl radical, hydrogen peroxide or hypochlorite.[17]

A large number of functionalized cyanines are used as fluorescent labels for biomolecules.[18] One example illustrates the conjugation of cyanine oxysuccinimidyl esters to oligonucleotides, whose hybridization was studied *via* FRET afterwards.[19] Other functionalized cyanines display alterations in the centre of their conjugated π-electron system containing a reactive (chloro) group and a four- to six-membered aliphatic/aromatic

ring with the latter facilitating the substitution of the (chloro) leaving group (www.licor.com).[20,] The labels preferably react *via* S_N1 type mechanism with the sterically hindered ring preventing nucleophilic attack *via* S_N2. The temporary carbocation is stabilized by the carbon double bonds of the cyclopentenyl or -hexenyl moiety.[21] Upon conjugation to amines (or thiols), the probes undergo blue shifts in absorption and emission because the electron withdrawing chloro atom is substituted by an electron donating amine.[22] The hypsochromic shift is more pronounced for the absorption maximum than for the emission resulting in Stokes´ shifts of more than 100 nm. So-called aminocyanines are characterized by broad absorption bands, high molar absorbance and strong fluorescence between 750 and 800 nm. Protonation of the fluorophore in aqueous media switches off one part of the chromophoric system. This results in a further blue shift of both absorption and emission.[23] It has been proposed that the protonation of the *meso*-nitrogen atom yields an equilibrium of two protonated forms thus resulting in the blue shifted band.[24] The addition of a small volume of aminocyanine in phosphate buffer of pH 4.3 to a buffer of pH 9.4 had no influence on the intensity of the NIR emission which indicates that the protonation is irreversible.[25] Recent studies of the Nagano group, however, illustrate, that these effects are mostly be given in presence of monoamine moieties and can be suppressed by the attachment of diamine groups. For instance, mono-N-protected piperazine was conjugated to the NIR probe IR-786, which then displays stable NIR fluorescence at 789 nm under acidic conditions. Several NIR fluorescent aminocyanine pH probes were prepared based on this principle.[26] Stable NIR fluorescence of aminocyanines is also demonstrated by the Weck group.[27] Their novel optical NIR imaging strategy combines aminocyanines with polyamide dendrons.

A detailed account on the spectral changes of monoamine conjungated cyanines are yet to be published in literature. Therefore, the kinetics of the reaction of aminocyanines with protons was examined here more closely. The rate was investigated at different pH (4 to 9) for two types of monoamine substituents. Ethanolamine and 3-aminophenylboronic acid (compound **13** from Chapter 4.4) were each reacted with dye S0378 and the temporal development of their spectral characteristics were investigated and compared. Despite of the fact that aminocyanines cannot act as reversible pH indicators, a different application was found. They can be employed as colorimetric dyes in a disposable, irreversible sensor for acidic gases when embedded in a hydrogel matrix. Colorimetric gas sensors are known, e.g. for hydrochloric[28] and acetic acid[29], ammonia[30] and oxygen[31] but only HCl was investigated in the present work.

5.2 Synthesis and Characterization of NIR Probes for HCl Gas

5.2.1 Preparation
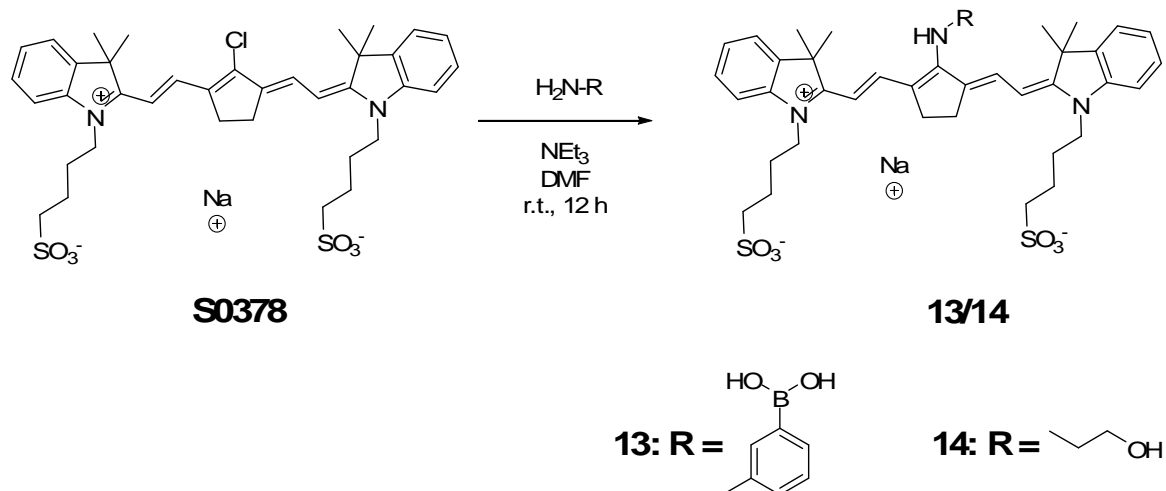
Figure 5.1. Synthesis of aminocyanine dyes **13** and **14** with either 3-aminophenylboronic acid or ethanolamine groups.
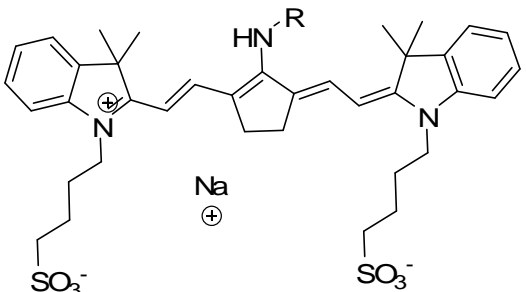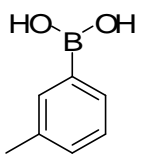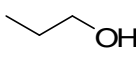
The preparation of each of the two dyes was performed in one step and by a simple protocol[32] using affordable starting materials. Cyanine dye S0378, which undergoes specific reactions with primary amines[22] was reacted with 3-aminophenylboronic acid or ethanolamine. The precursors were dissolved in DMF and excess triethylamine (NEt$_3$) was added, which acts as scavenger for hydrochloric acid and deprotonates the amine (Fig. 5.1). The colour of the solution changed from green to blue and the end of the reaction was monitored *via* thin layer chromatography. The products precipitated from tert.-butylmethyl ether (TBME) in high yield (> 90%) and purity. Both aminocyanine dyes **13** and **14** are blue and black solids, respectively and display blue colour in solution.

5.2.2 Spectroscopic Characterization – UV and Fluorescence

The absorption of **13** in phosphate buffered solution at pH 7 displays peaks at 690 nm and at 527 nm (weak). The spectrum of **14** is characterized by two peaks as well, which are blue-shifted to 652 nm and 512 nm. The extinction coefficients of 95,000 and 109,000 L*mol^{-1}*cm^{-1} are characteristic for aminocyanines. Following excitation at 690 nm and 652 nm, respectively, both dyes emit near-infrared light with maxima at 784 nm and

778 nm and with a very short decay time (Tab. 5.1 and Fig. 5.2). All data were obtained after immediate measurements of freshly prepared samples. The spectral characteristics change dramatically when exposed to aqueous media over time (see below).

Table 5.1. Structure, chemical and spectroscopic data of **13** and **14** in phosphate buffer of pH 7 (10 mM) unless noted otherwise.

		13	**14**
R		HO–B–OH (3-methylphenyl)	⌒OH (propanol)
λ_{abs} (nm)		690	652
λ_{em} (nm)		784	778
ε (L*mol^{-1}*cm^{-1})		95,000	109,000
τ (ps)		265[a]	n.d.

a) Fluorescence lifetime τ was determined in aqueous solution against glycogen ($\beta = 25$ mg/mL) as scattering sample.
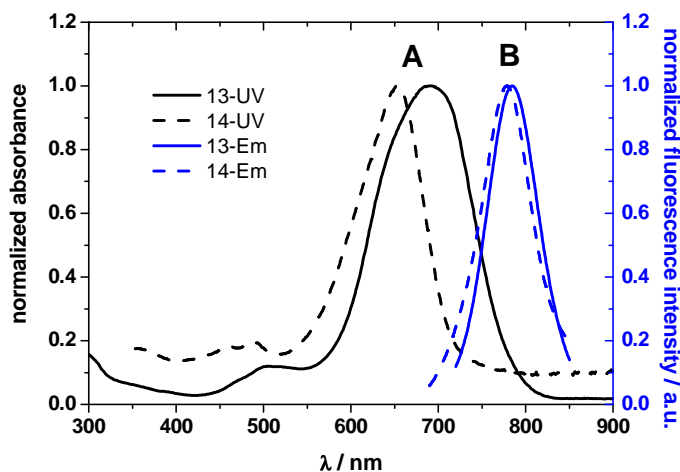
Figure 5.2. Absorption (A) and emission (B) spectra of compound **13** and **14** (10 µM) in phosphate buffered solution (10 mM) at pH 7.

5.3 Effect of pH

5.3.1 General Observation
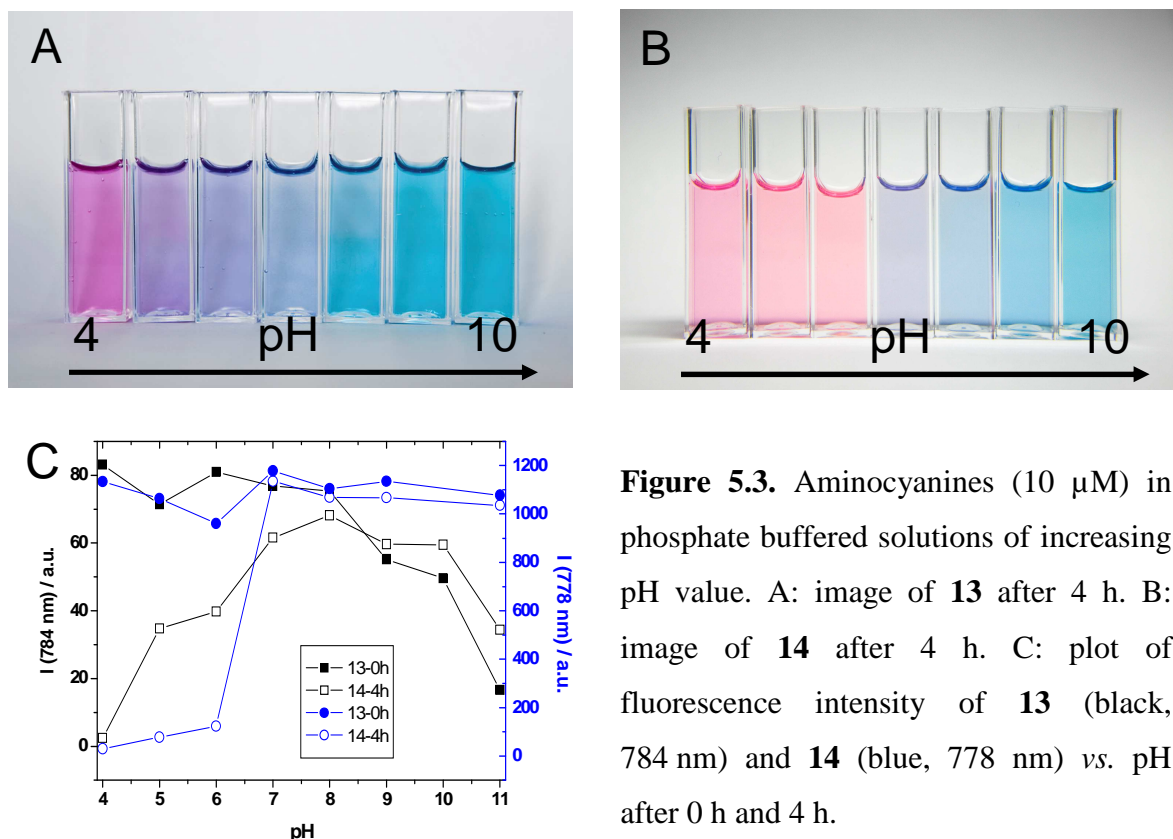
Figure 5.3. Aminocyanines (10 µM) in phosphate buffered solutions of increasing pH value. A: image of **13** after 4 h. B: image of **14** after 4 h. C: plot of fluorescence intensity of **13** (black, 784 nm) and **14** (blue, 778 nm) *vs.* pH after 0 h and 4 h.

Freshly prepared solutions of both dyes display fluorescence around 780 nm. The intensity of **13** and **14** differs slightly from pH 4 to 11 (Fig. 5.3C). Changes in the chromogenic system occur upon exposure to aqueous media which can easily be seen by eye vision. Images of both dyes were taken after 4 h (arbitrary) with a common digital camera. In general, the colour of the solution remains blue for basic pH values whereas it becomes purple in the acidic to neutral pH region. In case of compound **13**, mixed colours of purple and blue between pH 5 and 7 indicate, that the conversion of the fluorophore has not been completed yet (Fig. 5.3A). Contrarily, it seems that compound **14** was transferred into its purple counterpart within 4 h completely at acidic pH (Fig. 5.3B). Fluorescence spectra of **13** and **14** at 784 nm and 778 nm respectively, reflect these observations, too. A loss in intensity occurs for both probes at almost all pH values, however, it is higher pronounced in the acidic region (Fig. 5.3C). In case of compound **14**, a plot of fluorescence intensity

vs. pH has a sigmoidal shape with low luminescence at acidic pH values, but high luminescence in the basic region. Additionally, both dyes were subjected to cyclic voltammetry measurements against a silver/silver chloride electrode (Ag/AgCl) in phosphate buffer of pH 9.5. Potentials were determined to be 336 mV for probe **13** and 400 mV for probe **14**, respectively (Fig. 6.1). No changes in absorbance took place during oxidation at 400 mV over 10 min. Therefore, all spectral changes are induced by the aqueous environment and do not originate from oxidation processes.

5.3.2 Characterization of Probe 13 in Aqueous Solution

A more detailed investigation aimed at the time- and pH-dependence of the colour change. Compound **13** was dissolved in aqueous solution with pH values from 4 to 9, and absorption spectra were recorded from 350 to 850 nm after 4 h. Again, the UV spectrum exhibited two characteristic peaks at 690 nm and 527 nm, but their intensities changed with respect to their starting levels (Fig. 5.4A). At pH 4, the absorption peak at 690 nm vanished completely and only the peak at 527 nm remained. Similar observations were made for pH 5 and 6, however, some absorbance at around 690 nm was still detected, which explained the colour on the respective samples (Fig. 5.3A). Contrarily, low changes of absorption occurred under neutral and basic conditions. The effect of pH further influenced the emission characteristics. Following photoexcitation at 527 nm, a second emission at 595 nm was detected besides the one at 784 nm (Fig. 5.4B).
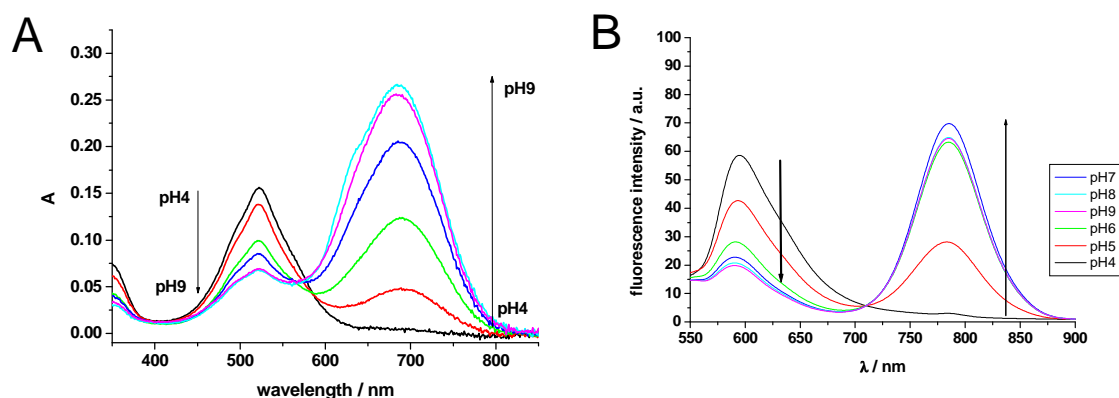
Figure 5.4. Compound **13** (10 µM) in phosphate buffered solution (10 mM) from pH 4 to 9. A: Absorption spectra after 4 h. B: Emission spectra after 4 h following excitation at 527 nm.

The acidic conditions caused an increase of fluorescence intensity at 595 nm comparable to the characteristics of the absorption spectra. The fluorescence at 784 nm disappeared almost completely at pH 4 but not in a neutral and basic environment. Isosbestic points in both absorption and emission spectra at 577 nm and 708 nm, respectively, indicate that a two component system exists, which consists of the blue starting chromophore **13** and its purple counterpart.

Compound **13** was subjected to kinetic studies in phosphate buffered solutions at pH 4 and 9 and both emissions (at 784 nm and 595 nm) were traced over time. All emission spectra at pH 4 exhibited changes in fluorescence intensity that occurred continuously until the conversion was completed (Fig. 5.5A). The emission at 784 nm almost fully vanished after 4 h and only the red emission at 595 nm remained. The overlap of all spectra revealed an isosbestic point around 710 nm that occurred for other acidic pH values, too (Fig. 6.12). Changes of fluorescence intensity within 4 h were also depicted for emission spectra at pH 9. However, these were restricted to the emission at 784 nm only (Fig. 5.5B). Furthermore, no isosbestic point was obtained, which indicated that the conversion proceeded primarily under acidic conditions.
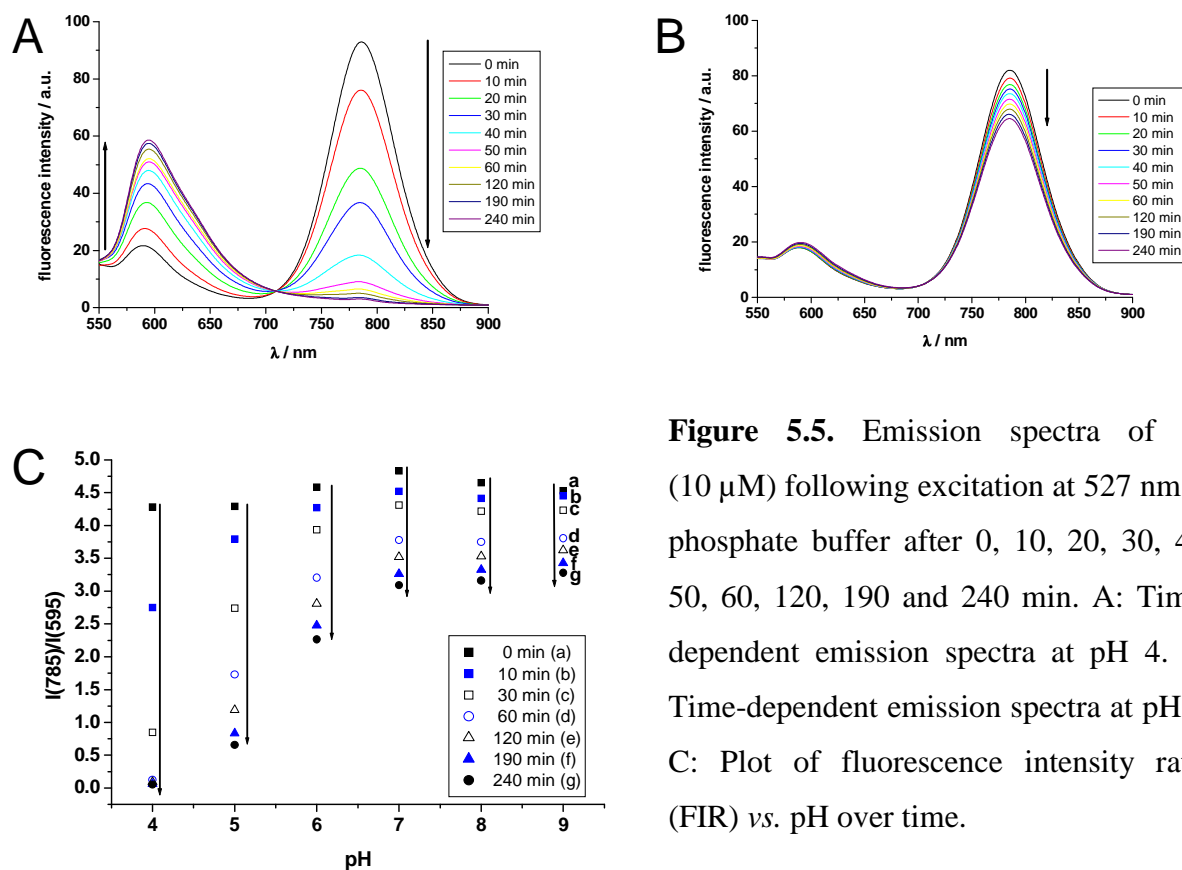
Figure 5.5. Emission spectra of **13** (10 µM) following excitation at 527 nm in phosphate buffer after 0, 10, 20, 30, 40, 50, 60, 120, 190 and 240 min. A: Time-dependent emission spectra at pH 4. B: Time-dependent emission spectra at pH 9. C: Plot of fluorescence intensity ratio (FIR) *vs.* pH over time.

Additionally, the kinetics of the conversion of **13** was studied for each pH value using the fluorescence intensity ratio (FIR) of both intensities at 784 nm and 595 nm, respectively.

$$FIR = \frac{I_{784}}{I_{595}}$$

The dual-wavelength emission of the system enables an intrinsically referenced fluorimetric evaluation, thereby minimizing interferences that may originate from sample preparation or the instrumental set up.[33] Ratiometric analysis of all spectra showed that the FIR decreased in general over time. The ratio is primarily influenced by an acidic environment in analogy to the emission spectra (Fig. 5.4C). A less pronounced decrease is obtained for pH values from 7 to 9. Both observations indicate that the rate of conversion is high in acidic environment and low under basic conditions.

5.3.3 Characterization of Probe 14 in Aqueous Solution
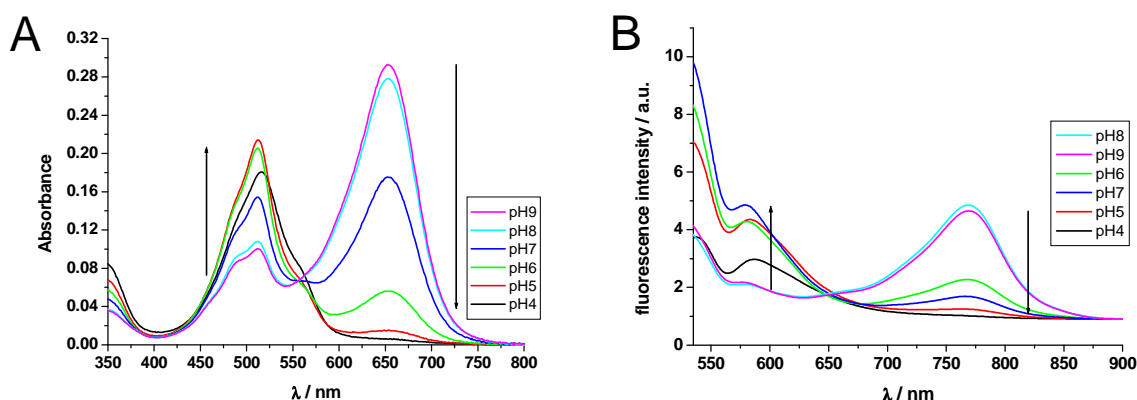
Figure 5.6. Spectra of compound **14** (10 µM) in phosphate buffered solution (10 mM) from pH 4 to 9. A: Absorption spectra after 4 h. B: Emission spectra after 4 h following excitation at 512 nm.

The same experiments were performed for compound **14** as described for compound **13**. First, **14** was dissolved in phosphate buffered solutions with pH varying from 4 to 9, and absorption spectra were then recorded from 350 to 800 nm after 4 h of incubation. The most significant changes, again, occurred at pH 4 and 5. Here, the absorption band at 652 nm disappeared completely and the one at 512 nm increased. At pH 7, however, a

relatively high absorption at 652 nm remained. Low changes were obtained in basic environment (Fig. 5.6A). The effect of pH on the fluorescence intensity was examined after 4 h (Fig. 5.6 B). Following photoexcitation at 512 nm, all spectra showed behaviour similar to those of compound **13**. The emission at 778 nm decreased in intensity whereas a blue-shifted band below 600 nm appeared which gained intensity at low pH values. It has to be noticed that the extent of increase below 600 nm obviously does not follow the scheme pH 4>5>6>7. Although isosbestic points were detected around 560 nm (absorption) and 660 nm (fluorescence), respectively, it could not be concluded that a dual system of two chromophores is present after 4 h. It is rather likely that further processes caused decomposition of the purple counterpart especially at pH 4.

Finally, compound **13** was subjected to kinetic studies in aqueous solutions at pH values from 4 to 9 (Fig. 5.7 and Fig. 6.13). Both fluorescence intensities around 600 nm and at 778 nm were followed over 4 h.
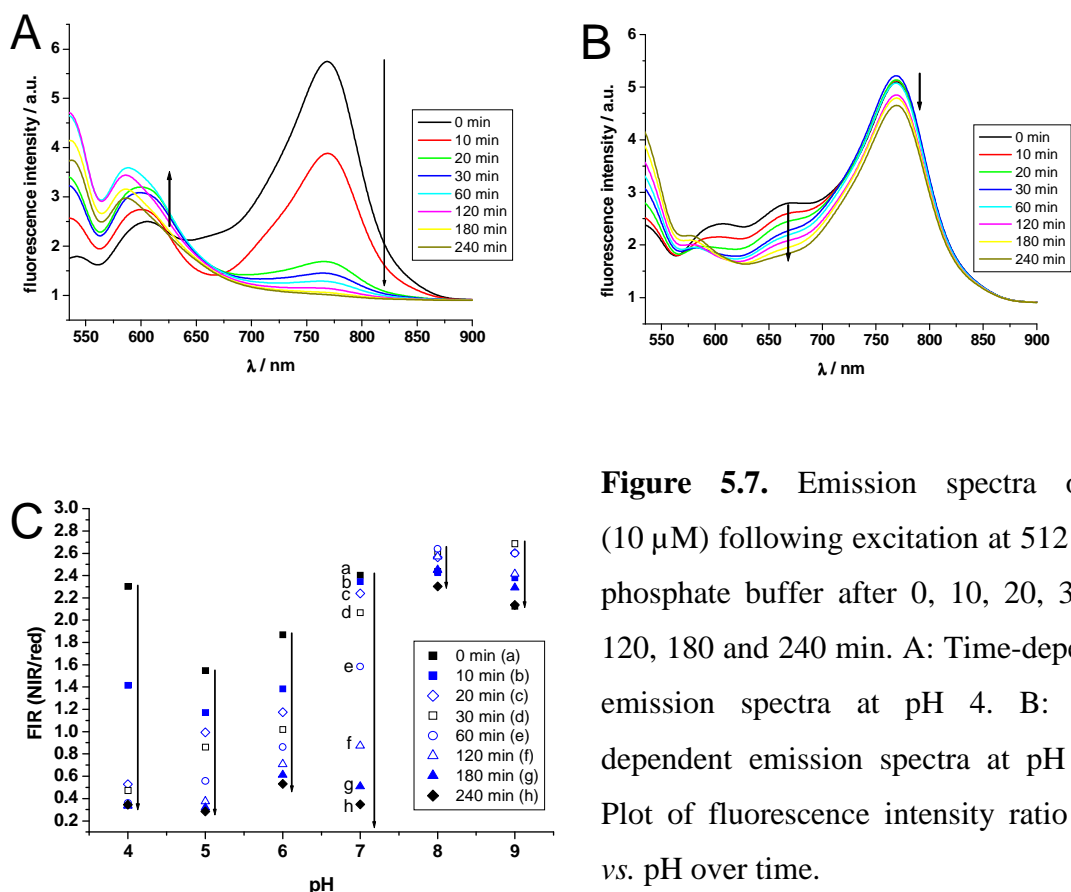
Figure 5.7. Emission spectra of **14** (10 µM) following excitation at 512 nm in phosphate buffer after 0, 10, 20, 30, 60, 120, 180 and 240 min. A: Time-dependent emission spectra at pH 4. B: Time-dependent emission spectra at pH 9. C: Plot of fluorescence intensity ratio (FIR) *vs.* pH over time.

All emission spectra at pH 4 display changes in fluorescence intensity that occurred continuously until the conversion was finished (Fig. 5.7A). The emission at 778 nm vanished completely after 4 h and only the red one around 600 nm was detectable. Its maximum, however, did not stay on a fixed wavelength; it was slightly blue shifted during the measurements thus preventing the determination of an isosbestic point. Changes of fluorescence intensity within 4 h were depicted for emission spectra at pH 9, however, these were not restricted to the emission at 778 nm. A weak additional band between 650 to 700 nm decreases, as well (Fig. 5.7B). The kinetics was studied for each pH value using the fluorescence intensity ratio (FIR) of both intensities at 778 nm and around 600 nm, respectively (Fig. 5.7C). Ratiometric analysis of all spectra showed that the FIR decreased in general over time. The ratio is primarily influenced by acidic environment in analogy to compound **13**. A less pronounced decrease was obtained for pH 8 and 9. Again, both observations indicate that the rate of conversion is high in acidic environment and low under basic conditions.

5.4 Isolation and Attempted Characterization of the Purple Product

Decomposition of aminocyanines has been reported[23-25] but no exact chemical structure of a decomposition product has been determined yet. To identify the product, compound **14** was stirred in aqueous HCl for 6 hours and the crude product was subjected to HPLC/MS analysis (Fig. 6.4). The choice was made in favour of compound **14** as boronic acids (compound **13**) are more difficult to analyze *via* mass spectrometry. The chromatogram reveals the presence of several components. However, only the one with a retention time of 10.3 min displays the desired absorbance at 534 nm. The product was isolated by preparative HPLC but yields were very low after every run, rendering an exact structural characterization almost impossible. The spectroscopic properties and the mass to charge ratio (m/z), however, were determined (Tab. 5.2). The m/z value of the purple product is 754.319, which is an increase of 16 compared to compound **14**. The absorption peaks at 534 nm instead of formerly 512 nm and features a molar extinction coefficient ε of 47,200 $L*mol^{-1}*cm^{-1}$. Upon excitation at 530 nm, two emission bands are detected at 547 and 588 nm, respectively (Fig. 5.8A). The fluorescence quantum yield ϕ is 1.4%. Furthermore, both emissions are affected by pH. The intensity at 547 nm follows a sigmoid curve with high fluorescence intensity at low pH (Fig. 5.8B). A pK_a of 7.3 was determined when the data were fit. Furthermore, IR spectroscopy of the purple decomposition product displayed

an additional band at 1,673 cm^{-1} compared to the IR spectrum of compound **14**. This wave number is characteristic for α-β-unsaturated ketones and it could not be assigned to any other functional group.
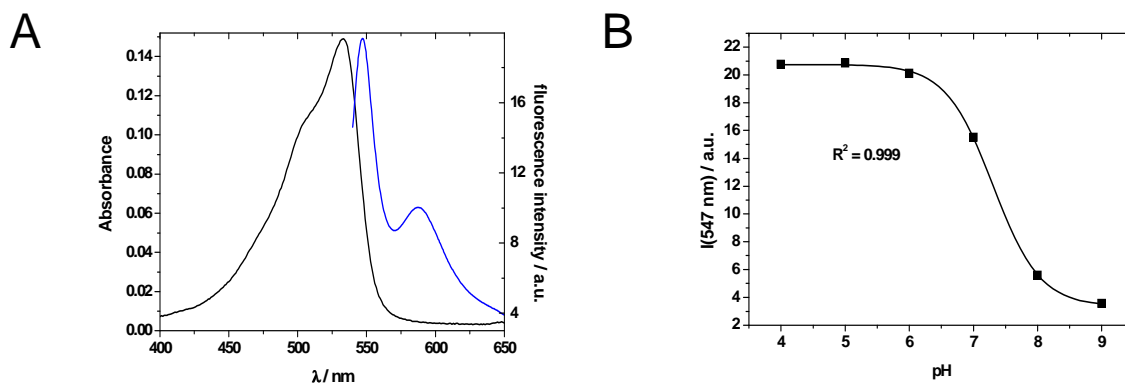
Figure 5.8. The purple product (3 µM). A: Absorption and emission spectra in phosphate buffer of pH 7; B: Effect of pH on the fluorescence intensity in phosphate buffered solutions of pH 4 to 9.

Table 5.2. Chemical and spectroscopic data of the purple product in phosphate buffer of pH 7 (10 mM) except noted otherwise.

m/z	λ_{abs} (nm)	ε (L*mol^{-1}*cm^{-1})	λ_{em} (nm)	ϕ^a
754.319	534	47,200	547 and 588	1.4%

a) determined in air-saturated ethanol against the reference Rhodamine 6G, whose quantum yield is reported to be 0.95 in air-saturated ethanol[34].

5.5 A Colorimetric Sensor Membrane for Acidic Gases

As the blue to purple switch of **13** and **14** is catalyzed by protons, the dyes are well suited for sensing acidic gases. They cannot be used as pH indicators in solution because the reaction time is by far too slow compared to classic indicators like phenolphthalein or congo red, which change their colour instantaneously at different pH. In accordance with earlier publications[25], the decrease in the NIR absorption of **13** and **14** is irreversible which enables the detection of the presence of acidic gases in a certain closed environment. Upon embedding into a cocktail and deposition on a transparent support, the sensor foil can display clear information whether acidic gases have occurred or not. Hence, an irreversible, disposable sensor layer may be used as an indicator for inappropriate storage

conditions and to detect exposure to acidic gases inside packaging or in context with occupational health.

5.5.1 Choice of Materials and Experimental Setup

Aminocyanine **14** was chosen for the sensor preparation because the decrease of its FIR in buffered solution at pH 4 remains almost the same after 30 min instead of 45 min for probe **13** (Fig. 5.9A). The next step requires the dye to be embedded in an appropriate polymer, which is permeable to gases but blocks humidity from air. The use of water must be avoided already at the stage of sensor preparation because a cocktail of hydrogel and dye in water/alcohol mixtures causes colour changes before submitting the sensor to application. Polystyrene (PS) was found to be inappropriate for sensor preparation because aminocyanine **14** precipitated from dissolved PS in many organic solvents. Therefore, PS is used as top layer of the sensor but another polymer for embedding the probe is needed. Various hydrogels have been described[35, 36], but most of them have to be dissolved in water/ethanol mixtures in order to be processed. Hypan hydrogel, a block-copolymer consisting of hard and lipophilic domains of polyacrylonitrile as well as soft and hydrophilic blocks of polyacrylamide, is insoluble in water and many other organic solvents except for dimethylsulfoxide (DMSO).[37] Covalent attachment of compound **14** is not needed because the sensor is not supposed to be exposed to water.
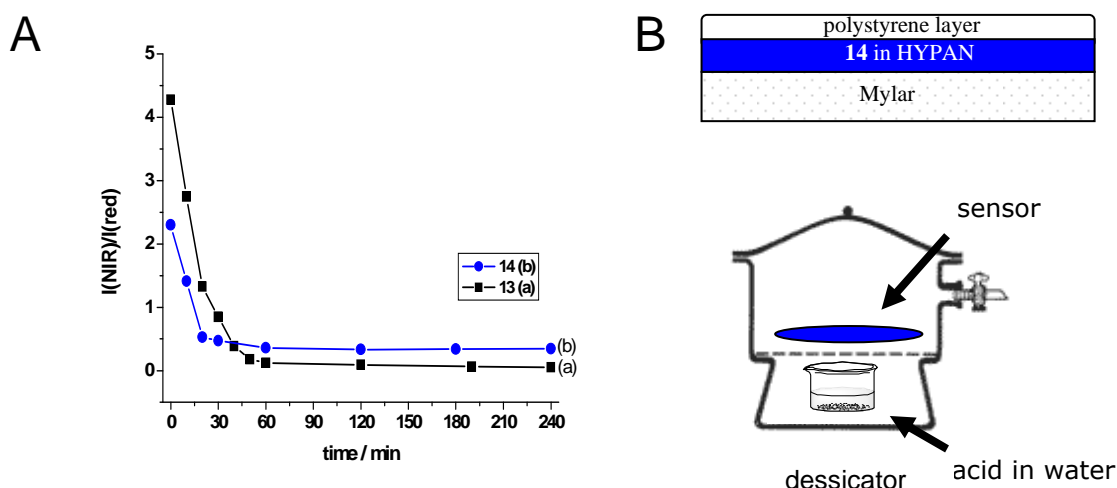
Figure 5.9. A: Plot of FIR *vs.* time for compound **13** and **14** in buffered solution at pH 4; B: Sensor composition and experimental setup.

The sensor consists of two membranes, which are spread layer by layer with a knife-coating device on an optically transparent support (Mylar[TM], ethyleneglycol-terephthalate polyester). The sensor foil is placed in a desiccator above acid/water mixtures of various concentrations. Once the equilibrium is reached between liquid and gas phase, the resulting vapour pressure of acid can be related to a certain concentration of gas at constant temperature (Fig. 5.9B).[38]

5.5.2 Response to Gaseous Hydrochloric Acid

The high molar absorbance of the cyanine dye **14** along with the use of a transparent polyester support (Mylar) enables photographing of the sensor foils so to quantify the changes caused by acidic gases (Fig. 5.10). The sensor was fixed with Tesa stripes on the inner side of a desiccator and its reactive membrane was exposed to the vapour of a 24% (w/w) water/hydrochloric acid mixture, resulting in a partial pressure of 1.3 mbar of HCl. Hydrochloric acid was chosen arbitrarily as a representative for acids with appropriate vapour pressure. Images were taken over time through the glass of the desiccator with a digital camera in order to give sharp-contrast images (Fig. 5.10). Desiccator and camera were placed in a room with only artificial light and a temperature kept at 20 °C.
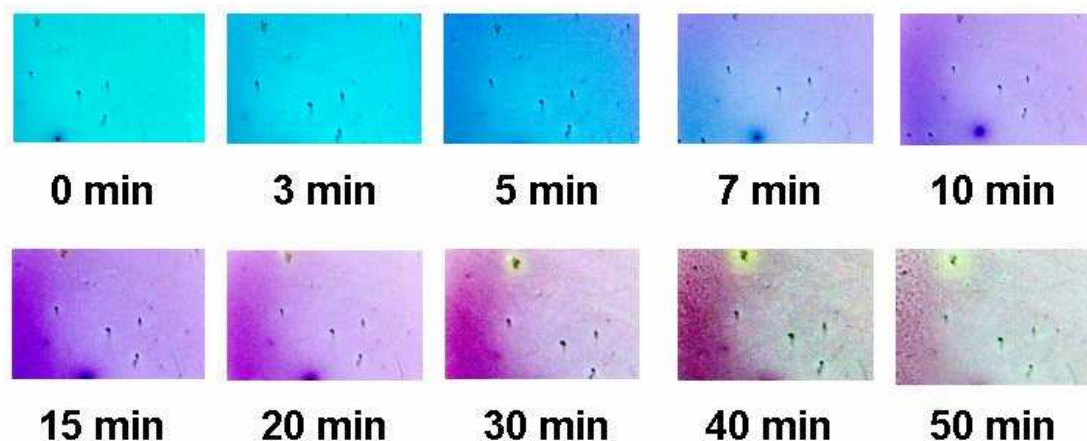
Figure 5.10. Images displaying the temporal development of the colour of the sensor in presence of 24% (w/w) HCl in water at 20 °C. This corresponds to a vapour pressure of HCl of 1.3 mbar.

The initial image revealed a heterogeneous distribution of the probe because dark blue dots were sprinkled over the turquoise sensor. Within twenty minutes of exposition, the

sensor changed its colour from turquoise over blue to purple, which was similar to the observations in water. Longer reaction times revealed bleaching of the sensor as the pale purple background vanished on the right part of the images. The temporal development of the colour of the sensor was also followed *via* photometry. In this case, the sensor spots were put onto the removable platform above mixtures of hydrochloric acid/water. Repetitive fixing and removing of the sensor from the inner wall of the desiccator over more than four hours would cause damages on the sensor membrane and therefore was not chosen for this experiment. The sensors were placed in quartz cuvettes (d = 2 mm) and the absorbance was measured from 400 to 800 nm (Fig. 5.11).
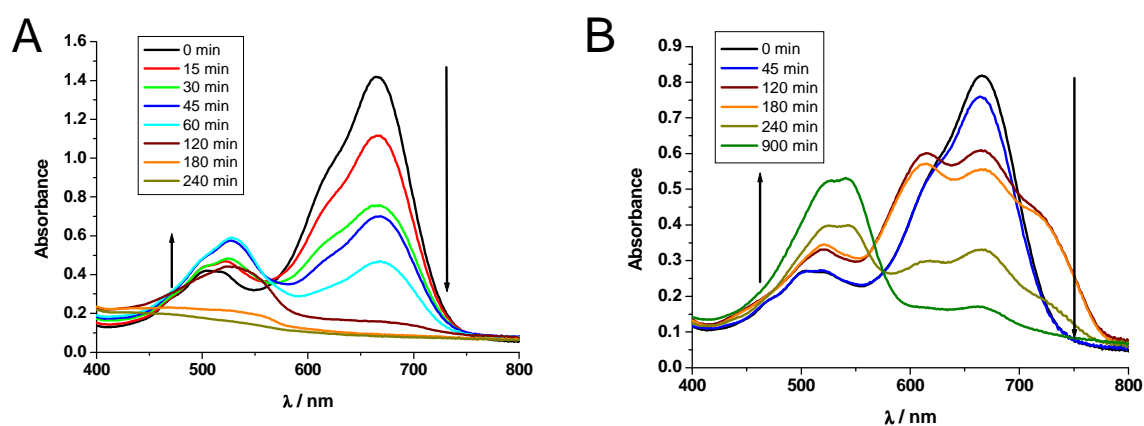
Figure 5.11. Absorption spectra illustrating the temporal development of the sensor in presence of (A) 32% (w/w) and (B) 2% (w/w) HCl in water at 25 °C, which corresponds to a vapour pressure of 43 mbar and 0.1 µbar of HCl.

At the beginning of the experiment, the UV spectra of the sensor in presence of 43 mbar HCl (32% (w/w) mixture) were characterized by two maxima at 665 and 505 nm (Fig. 5.11A). Both values differ from the ones of probe **14** in solution. The red absorption band was red shifted (665 nm *vs.* 652 nm) and the green one was blue shifted (505 nm *vs.* 534 nm). After exposition to HCl gas for 60 min, the band at 665 nm decreased and the absorption at 505 nm increased. Both absorption maxima were red shifted to 668 and 527 nm, respectively. The change from blue to purple also revealed the presence of an isosbestic point around 565 nm. After two hours, the red absorption band vanished completely and only the one at 527 nm remained. Upon further exposition to the acidic environment, almost no absorption was measured which is in accordance with the expected bleaching of the sensor. The sensor`s reactivity towards 0.1 µbar HCl (2%, w/w) was also

investigated, but changes in colour occurred more slowly (Fig. 5.11B). The absorption spectrum after 45 min of exposition was nearly the same as compared to the start. The absorption at 668 nm decreased slightly, but the one at 505 nm remained unchanged. After two hours, the red absorption band split and two maxima at 667 and 615 nm were detected. Both bands lost intensity over time and nearly disappeared after fifteen hours. The absorption at 505 nm increased over time and two local maxima appeared at 528 and 540 nm, respectively. Isosbestic points are located around 567 and 575 nm, respectively.
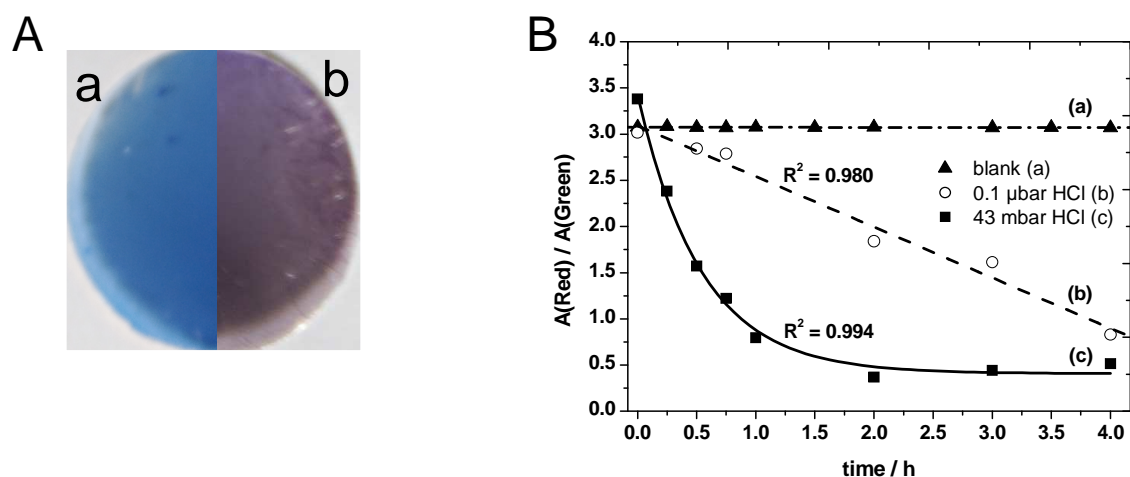
Figure 5.12. A: sensor membrane before (a) and after (b) reaction with HCl gas. B: Sensor membrane in presence of (a) no, (b) 0.1 µbar and (c) 43 mbar HCl at 25 °C. Plot of the ratio of the red and the green absorbance *vs.* time. Each curve is illustrated with its fit.

The spectral changes of both sensors were analyzed by dividing the absorbances of the maxima of the red (around 660 nm) and green (around 515 nm) band (Fig. 5.12B). A high ratio displayed high absorbance around 660 nm and low one around 515 nm, which is typical for the beginning of the experiment. In absence of HCl gas, the sensor did not change its ratio thus displaying a stable baseline (trace a). Upon exposition to HCl gas, the ratio decreased in both cases over time because the red absorbance became lower and the green one increased. The sensors had comparable starting ratios, but the presence of 43 mbar HCl altered the ratio more rapidly. Here, the ratio decay followed an exponential curve and stopped after two hours, which indicates that the sensor had fully reacted with the gas (trace c). In case of 0.1 µbar HCl (trace b), changes occurred more slowly and the ratio decreased linearly. After four hours, the ratio is comparable to that at 43 mbar HCl. According to the decay curves, the sensor foil is suitable to follow long-time processes and

ingress of an acidic gas. Therefore, it is suitable as colorimetric indicator for inappropriate storage conditions (e.g. for corrosive materials). A rapid determination method of acidic gases is feasible at high concentration within a 30 min incubation time.

5.6 Discussion and Conclusion

The preparation of both aminocyanines followed a previously published protocol[32] with comparable yields and purity. The absorption maximum of probe **13** is red shifted compared to probe **14** (690 *vs.* 652 nm) which can only be explained by a different mesomeric (M) effect induced on the groups attached to the amino group. The aromatic amine has a –M-effect due to its boronic acid whereas the aliphatic amine possesses a +M-effect causing a hypsochromic shift on the fluorophore. Upon protonation, the colour of the aminocyanines changes from blue to purple. These spectroscopic changes of aminocyanines have already been described in the literature for similar compounds.[23-25] Ratiometric analysis of the kinetics, however, was not performed for pH from 4 to 9 by other working groups. Furthermore, the effects on fluorescence of an aliphatic and an aromatic amine moiety were not compared. The fluorescence intensity ratio (FIR) at pH 4 (Fig. 5.9A) illustrates that the rate of transformation is similar for both probes within the first 30 min. The FIR after 10 min is around 60% of its starting value (63% *vs.* 61% for probes **13** and **14**) and decreases further to 20% (19% *vs.* 20% for probes **13** and **14**) after 30 min. Longer reaction times do not reduce the FIR of probe **14** further, however, the one of probe **13** has only 16% after 1 h. This may explain the fact that more nuances in colour can be detected.

The starting chromophore **14** reacted irreversibly to give a purple product, whose molecular weight increased by 16 g/mol according to mass spectrometry (MS). Although the molecular mass of the decomposition product of **13** could not be determined, it can be concluded that transformation of **13** yields the same purple fluorophore. Changes are likely to occur along the polymethine chain of the chromophore and not on the amine moiety. Probably, an α-β-unsaturated ketone has formed according to IR spectroscopy. Therefore, a structure for the purple product is proposed (Fig. 5.13), which contains a keto group at C7 of the polymethine chain, thus shortening the chromophoric system. A sum formula of $C_{39}H_{52}N_3O_8S_2^+$ was calculated from the HR-MS software, whose molecular weight conforms the experimentally obtained by 97%. It is expected that the transformation of **13** results in the same chromophore.

Figure 5.13. Suggested structure of the purple decomposition product of compound **14**.
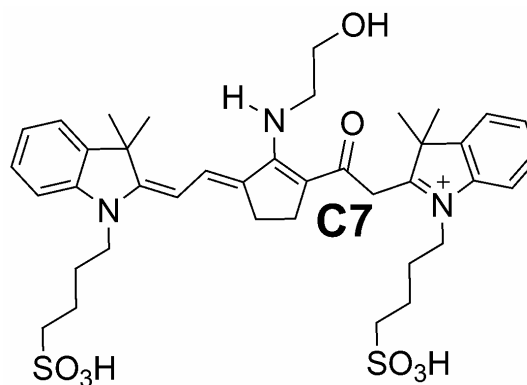
Aminocyanines can act as irreversible indicators for acidic gases when embedded into a polymer. The disposable sensor prepared makes use of the blue to purple switch of **14** in order to detect different partial pressures of hydrochloric acid. The sensor changes its colour from turquoise to purple but bleaches upon further exposition to gas. The rate of the transition from blue to purple depends on the partial pressure of HCl gas. As a disadvantage, the probe is distributed heterogeneously in the sensor membrane. Furthermore, DMSO as solvent for the Hypan hydrogel affords a long drying time. The utilization of aminocyanines without sulfonic acids will increase solubility in more volatile organic solvents (e.g. ethanol, THF) and may enable the use of humidity blocking polymers like polystyrene or poly(vinylalcohol).[39]

The spectral properties of aminocyanines can be applied to the detection of acidic environments. The irreversible, disposable sensor layer is intended for use as an indicator for inappropriate storage conditions and to detect exposure to acidic gases in the context of occupational health. Up to now, no structure or mechanism has been determined that would help to explain the transformation of the dyes into their purple counterparts. It is only reported that this problem can be solved by attaching diamines to the centre of the polymethine chain.[26] The development of the sensor is not complete at this stage. A homogeneous distribution of the dye in the sensor membrane has to be achieved, and the experiments have to be performed with other gaseous acids, such as acetic acid. Then, a complete evaluation may tell if the sensor can be used for acids in general or is restricted to hydrochloric acid, only.

5.7 Literature

1. A. Mishra, R. K. Behera, P. K. Behera, B. K. Mishra, G. P. Behera, Cyanines during the 1990s: A review. *Chem. Rev.*, **2000**, 100, 1973 – 2011.

2. L. Patsenker, A. Tatarets, O. Kolosova, O. Obukhova, Y. Povrozin, I. Fedyunyayeva, I. Yermolenko, E. Terpetschnig, Fluorescent probes and labels for biomedical applications. *Ann. N.Y. Acad. Sci.*, **2008**, 1130, 179 – 187.

3. J. O. Escobedo, O. R. Rusin, S. Lim, R. M. Strongin, NIR dyes for bioimaging applications. *Curr. Opin. Chem. Biol.*, **2010**, 14, 64 – 70.

4. J. Klohs, A. Wunder, K. Licha, Near-infrared fluorescent probes for imaging vascular pathophysiology. *Basic Res. Cardiol.*, **2008**, 103, 144 – 151.

5. R. Philip, A. Penzkofer, W. Bäumler, R. M. Szeimies, C. Abels, Absorption and fluorescence spectroscopic investigation of indocyanine green. *J. Photochem. Photobiol. A.*, **1996**, 96, 137 – 148.

6. V. I. Kochubey, T. V. Kulyabina, V. V. Tuchin, G. B. Altshuber, Spectral characteristics of indocyanine green upon its interaction with biological tissues. *Opt. Spectroscop.*, **2005**, 99, 560 – 566.

7. E. Delaey, F. van Laar, D. De Vos, A. Kamuhabwa, P. Jacobs, P. de Witte, A comparative study of the photosensitizing characteristics of some cyanine dyes. *J. Photochem. Photobiol. B*, **2000**, 55, 27 – 36.

8. B. Wetzl, M. Gruber, B. Oswald, A. Dürkop, B. Weidgans, M. Probst, O. S. Wolfbeis, Set of fluorochromophores in the wavelength range from 450 to 700 nm and suitable for labeling proteins and amino-modified DNA. *J. Chromatogr. B*, **2003**, 793, 83 – 92.

9. www.fluorophores.org

10. R. C. Benson, H. A. Kues, Absorption and fluorescence properties of cyanine dyes. *J. Chem. Eng. Data*, **1977**, 22, 379 – 383.

11. K. Kiyose, H. Kojima, T. Nagano, Functional near-infrared fluorescent probes. *Chem. Asian J.*, **2008**, 3, 506 – 515.

12. J. Pączkowski, J. Kabatc, B. Jędrzejewska, Polymethine dyes as fluorescent probes and visible-light photoinitiators for free radical polymerization. *Top. Heterocycl. Chem.*, **2008**, 14, 183 – 220.

13. K. A. Mesce, K. A. Klukas, T. Clark Brelje, Improvements for the anatomical characterization of insect neurons in whole mount: the use of cyanine-derived fluorophores and laser scanning confocal microscopy. *Cell Tissue Res.*, **1993**, 271, 381 – 397.

14. V. Sundström, T. Gillbro, Viscosity dependent radiationless relaxation rate of cyanine dyes. A picosecond laser spectroscopy study. *Chem. Phys.*, **1981**, 61, 257 – 269.

15. S. A. Hilderbrand, K. A. Kelly, R. Weissleder, C-H. Tung, Monofunctional near-infrared fluorochromes for imaging applications. *Bioconjugate Chem.*, **2005**, 16, 1275 – 1281.

16. Z. Zhang, S. Achilefu, Design, synthesis and evaluation of near-infrared fluorescent pH indicators in a physiologically relevant range. *Chem. Commun.*, **2005**, 5887 – 5889.

17. D. Oushiki, H. Kojima, T. Terai, M. Arita, K. Hanaoka, Y. Urano, T. Nagano, Development and application of a near-infrared fluorescence probe for oxidative stress based on differential reactivity of linked cyanine dyes. *J. Am. Chem. Soc.*, **2010**, 132, 2795 – 2801.

18. R. B. Mujumdar, L. A. Ernst, S. R. Mujumdar, C. J. Lewis, A. S. Waggoner, Cyanine dye labeling reagents: Sulfoindocyanine succinimidyl esters. *Bioconjugate Chem.*, **1993**, 4, 105 – 111.

19. M. Gruber, B. Wetzl, B. Oswald, J. Enderlein, O. S. Wolfbeis, A new fluorescence resonance energy transfer pair and its application to oligonucleotide labeling and fluorescence resonance energy transfer hybridization studies. *J. Fluoresc.*, **2005**, 15, 207 – 214.

20. G. Patonay, J. Salon, J. Sowell, L. Strekowski, Noncovalent labelling of biomolecules with red and near-infrared dyes. *Molecules*, **2004**, 9, 40 – 49.

21. H. C. Brown, C. Gundu Rao, M. Ravindranathan, Structural effects in solvolytic reactions. 29. Solvolysis of tertiary allylic p-nitrobenzoates. Effect of the allylic double bond on the rates of solvolysis of representative tertiary p-nitrobenzoates. *J. Org. Chem.*, **1978**, 43, 4939 – 4943.

22. H. H. Gorris, S. M. Saleh, D. B. M. Groegel, S. Ernst, K. Reiner, H. Mustroph, O. S. Wolfbeis, Long-wavelength absorbing and fluorescent chameleon labels for proteins, peptides and amines. *Bioconjugate Chem.*, **2011**, DOI: 10.1021/bc200192k.

23. X. Peng, F. Song, E. Lu, Y. Wang, W. Zhou, J. Fan, Y. Gao, Heptamethine cyanine dyes with a large Stokes´ shift and strong fluorescence: A paradigm for excited-state intramolecular charge transfer. *J. Am. Chem. Soc.*, **2005**, 127, 4170 – 4171.

24. A. B. Descalzo, K. Rurack, On the signalling pathways and Cu[II]-mediated anion indication of *N-meso*-substituted heptamethine cyanine dyes. *Chem. Eur. J.*, **2009**, 15, 3173 – 3185.

25. K. Kiyose, S. Aizawa, E. Sasaki, H. Kojima, K. Hanaoka, T. Terai, Y. Urano, T. Nagano, Molecular design strategies for near-infrared ratiometric fluorescent probes based on the unique spectral properties of aminocyanines. *Chem. Eur. J.*, **2009**, 15, 9191 – 9200.

26. T. Myochin, K. Kiyose, K. Hanaoka, H. Kojima, T. Terai, T. Nagano, Rational design of ratiometric near-infrared fluorescent pH probes with various pK_a values, based on aminocyanine. *J. Am. Chem. Soc.*, **2011**, 133, 3401 – 3409.

27. C. Ornelas, R. Lodescar, A. Durandin, J. W. Canary, R. Pennell, L. F. Liebes, M. Weck, Combining aminocyanine dyes with polyamide dendrons: A promising strategy for imaging in the near-infrared region. *Chem. Eur. J.*, **2011**, 17, 3619 – 3629.

28. K. Nakagawa, K. Tanaka, T. Kitagawa, Y. Sadaoka, Optochemical HCl gas sensor using substituted tetraphenylporphine-ethylcellulose composite films. *J. Mater. Chem.*, **1998**, 8, 1199 – 1204.

29. M. O´Toole, R. Shepherd, G. G. Wallace, D. Diamond, Inkjet printed LED based pH chemical sensor for gas sensing. *Anal. Chim. Acta*, **2009**, 652, 308 – 314.

30. J. Courbat, D. Briand, J. Damon-Lacoste, J. Wöllenstein, N. F. de Rooji, Evaluation of pH indicator-based colorimetric films for ammonia detection. *Sens. Actuat. B*, **2009**, 143, 62 – 70.

31. S. Wilhelm, O. S. Wolfbeis, Opto-chemical micro-capillary clocks. *Microchim. Acta*, **2010**, 171, 211 – 216.

32. P. Kele, X. Li, M. Link, K. Nagy, A. Herner, K. Lörincz, S. Bèni, O. S. Wolfbeis, Clickable fluorophores for biological labelling – with or without copper. *Org. Biomol. Chem.*, **2009**, 7, 3486 – 3490.

33. M. Schaeferling, A. Duerkop, Intrinsically referenced fluorimetric sensing and detection schemes: Methods, Advantages and Applications. *Springer Ser. Fluoresc.*, **2008**, 5, 373 – 414.

34. R. F. Rubin, A. N. Fletcher, Fluorescence quantum yields of some rhodamine dyes. *J. Luminesc.*, **1982**, 27, 455 – 462.

35. A. M. Mathur, S. K. Moorjani, A. B. Scranton, Methods for synthesis of hydrogel networks: a review. *Polym. Rev.*, **1996**, 36, 405 – 430.

36. O. S. Wolfbeis, Materials for fluorescence-based optical chemical sensors. *J. Mater. Chem.*, **2005**, 15, 2657 – 2669.

37. V. A. Stoy, New type of hydrogel for controlled drug delivery. *J. Biomater. Appl.*, **1988**, 3, 552 – 604.

38. E. V. Washburn, International critical tables of numerical data, physics, chemistry and technology, 3rd edition. **1928**, Volume XIII; McGraw-Hill Book Company Inc, New York and London.

39. L. V. Cancio, G. W. Miller, P.-C. Wu, Polyester compositions for gas and moisture barrier materials. **1982**, *U.S. Pat.* 4,284,671.

6. Experimental Part

6.1 General

Chemicals, enzymes and solvents were purchased from Sigma-Aldrich/Fluka (www.sigma-aldrich.com), Merck (www.merckchemicals.com), FEW (www.few.de) and ABCR (www.abcr.de). All were of analytical grade and used without further purification. Commercially available O-(2-aminoethyl)-cellulose, amino-modified polyacrylonitrile (PreSens GmbH, www.presens.de) and aqueous suspensions of amino-modified polystyrene beads with diameters of 500 nm (Polysciences, www.polysciences.com) were used for polymer labelling with HP Green. The pH of phosphate buffer solutions was adjusted on a CG 842 pH meter (Schott, www.schott.com). Deuterated solvents were obtained from Deutero GmbH (www.deutero.de). Spectroscopic measurements were performed in cuvettes made from quartz glass (Hellma, www.helma-analytics.com) or PMMA (Brand, www.brand.de). UV spectra were recorded on a Cary 50 biophotometer (Varian, www.varianinc.com). Fluorescence excitation and emission spectra were acquired on a FP-6300 spectrofluorometer (Jasco, www.jasco.de) or on an Aminco Bowman AB2 luminescence spectrometer (SLM Spectronic Unicam, www.spectronic.co.uk). Fluorescence lifetime was determined on a K2 multifrequency phase fluorometer (ISS, www.iss.com). pH was measured with a CG 842 pH-meter (Schott, www.schottinstruments.de). NMR spectra were recorded on an Avance 300 MHz spectrometer (Bruker, www.bruker-biospin.com). Chemical shifts (δ) are given in parts per million (ppm) using solvent signals as the reference. Coupling constants (J) are reported in Hertz (Hz). Splitting patterns are designated as s (singlet), d (doublet), t (triplet), m (multiplet). IR data were collected with an Excalibur FTS 3000 spectrometer (Biorad, www.bio-rad.com) equipped with a Golden Gate Diamond Single Reflection attenuated total reflection (ATR) system (Specac, www.specac.com). Mass spectra were acquired with a Thermoquest Finnigan TSQ (LC-ESI), a Finnigan MAT 95 (HR-EI), Finnigan Mat SSQ 710 (CI-EI) mass spectrometer (Finnigan Mat, Bremen, Germany) as well as on an Agilent 6540 (HR-ESI) mass spectrometer (Agilent, www.agilent.com). Curve fitting was done with Origin 6.1 from OriginLab Corporation (www.originlab.de). Centrifugation of the particles in 1.5 or 2 mL cups (Eppendorf, www.eppendorf.de) with a speed of 8000 rpm for 10 min was performed on an EBA 12 centrifuge (Hettich, www.hettich-zentrifugen.de). The particles were suspended in a polyurethane hydrogel Hydromed D4

(Cardiotech, www.cardiotech-inc.com) and spread with a knife coating device on the polyester support Mylar (product number 124-098-60, Goodfellow, www.goodfellow.de). Hypan (HN80) hydrogel was purchased from Hymedix (www.hymedix.com).

Phosphate buffer was prepared by dissolving 6.8995 g of NaH_2PO_4 x H_2O in 4.99 L of bidistilled water. The pH was adjusted with hydrochloric acid (0.1 M or 1 M) and sodium hydroxide solutions (0.1 M or 1 M), respectively. The buffer was filled up with bidistilled water up to a volume of 5 L. In case of phosphate buffered saline (PBS), 37.497 g of NaCl was added.

6.2 Synthesis and Sensor Preparation

6.2.1 Synthesis and Characterization of (1)
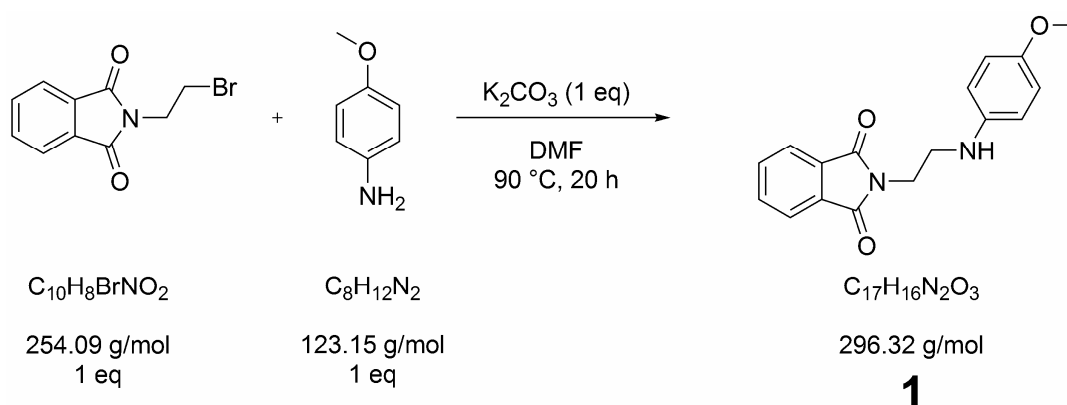
4 g (32 mmol) of *p*-anisidine, 8.26 g (32 mmol) of N-(2-bromoethyl)phthalimide and 4.48 g (32 mmol) of K_2CO_3 in 24 mL of DMF were heated at 90 °C for 20 h. The reaction mixture was poured into 350 mL of ice water. The brown-white precipitate was filtered off after 2 h, washed with cold water and dried over $CaCl_2$ in vacuum. The crude product was recrystallized from ethanol. Yield: 1.4 g (4.7 mmol, 15 %), off-white crystals, $C_{17}H_{16}N_2O_3$, melting point 101 °C. ESI-MS: m/z (M-H$^+$, cation) for $C_{17}H_{17}N_2O_3$, calculated 296.1, found 297.0. ^{1}H-NMR (300 MHz, CDCl$_3$): δ (ppm) 3.4 (t, 2H, J = 6.32 Hz), 3.7 (s, 3H), 3.94 (t, 2H, J = 6.31 Hz), 6.6 (dd, 2H, J = 6.58 Hz, 2.2 Hz), 6.75 (dd, 2H, J = 6.59 Hz, 2.2 Hz), 7.7 (dd, 2H, J = 5.49 Hz, 3.02 Hz), 7.85 (dd, 2H, J = 5.49 Hz, 3.02 Hz). ^{13}C-NMR (300 MHz, CDCl$_3$): δ (ppm) 37.62, 43.76, 55.80, 113.96, 114.93, 123.20, 123.33, 132.01,

134.05, 141.81, 152.21, 168.66. The compound was synthesized according to the literature and all NMR data are analogue.

6.2.2 Synthesis and Characterization of (2)
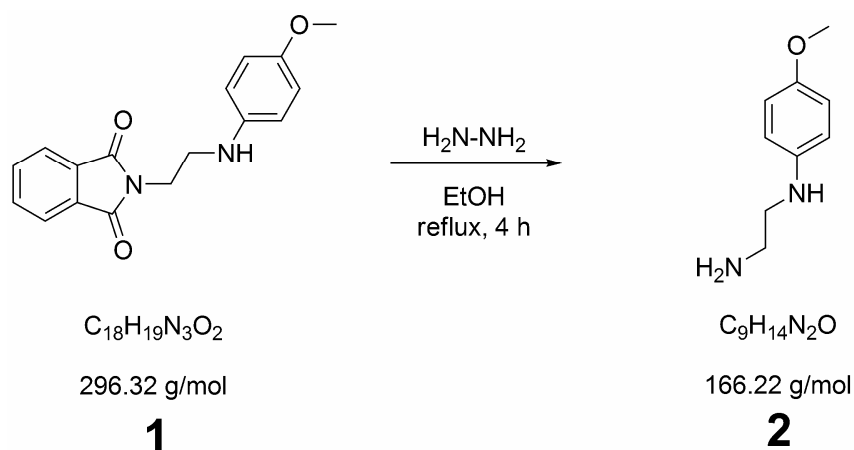
2 g (6.7 mmol) of **1** were dissolved in 40 mL of boiling ethanol and 426 µL (8.8 mmol) of hydrazine monohydrate were added to the brown solution in one portion. The mixture was refluxed for 4 h upon which a white solid precipitated. The mixture was cooled to room temperature and 10 mL of concentrated hydrochloric acid (37 %) were added. After 1 h, the precipitate was filtered off, the filtrate concentrated half to its volume and the pH adjusted to around 10 with aqueous NaOH. The solution was extracted with diethyl ether five times, the combined extracts dried over Na_2SO_4, the solvent removed, and the remaining brown oil left for crystallization in the refrigerator over night. The brown solid was used without further purification. Yield: 407 mg (2.45 mmol, 36%), brown solid, $C_9H_{14}N_2O$. ^{1}H-NMR (CDCl$_3$): δ (ppm) 2.95 (t, 2H, J = 5.22 Hz), 3.15 (t, 2H, J = 5.22 Hz), 3.75 (s, 3H), 6.61 (d, 2H, J = 2.2 Hz), 6.78 (d, 2H, J = 2.2 Hz). ^{13}C-NM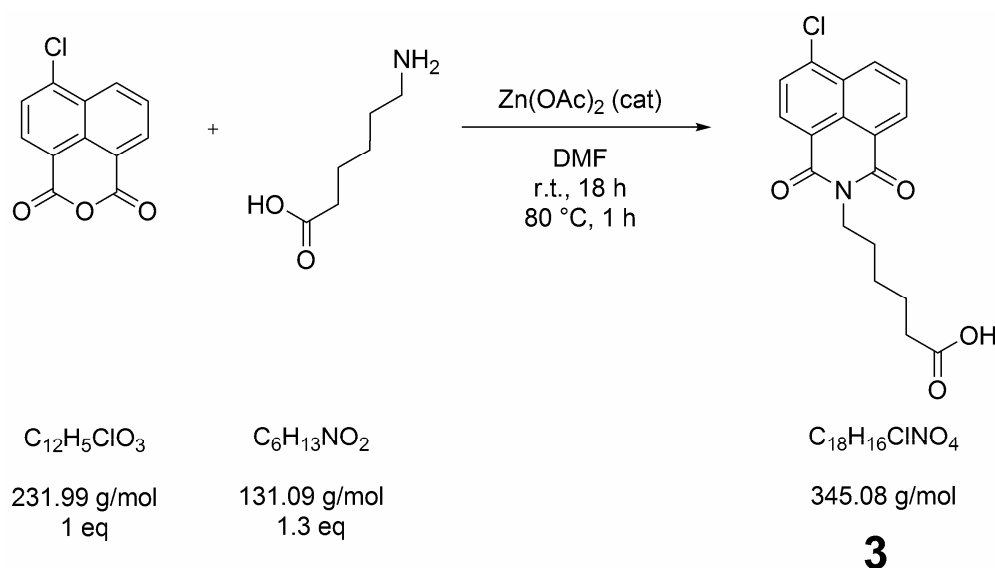R (300 MHz, CDCl$_3$): δ (ppm) 41.32, 47.59, 55.84, 114.32, 114.92, 142.67, 152.17. The compound was synthesized according to the literature and all NMR data are analogue.
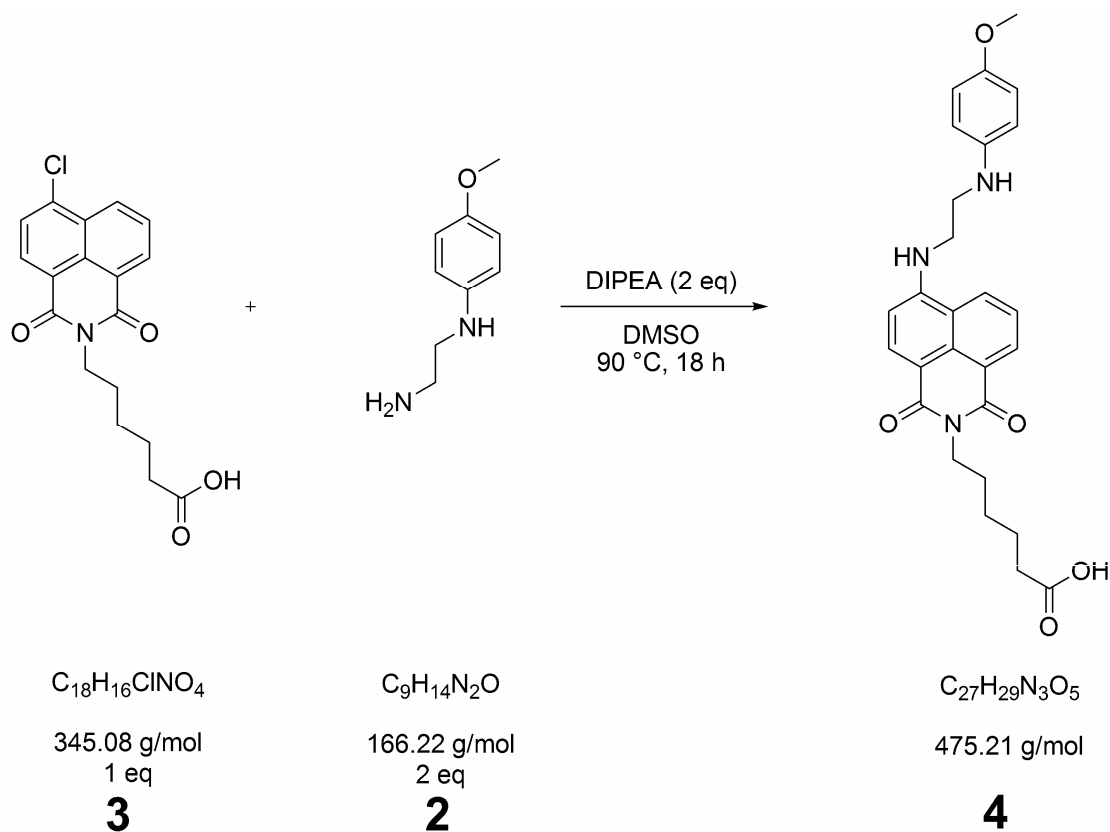
6.2.3 Synthesis and Characterization of (3)

$C_{12}H_5ClO_3$

231.99 g/mol
1 eq

$C_6H_{13}NO_2$

131.09 g/mol
1.3 eq

$C_{18}H_{16}ClNO_4$

345.08 g/mol

3

2.2 g (9.5 mmol) of 4-chloro-1,8-naphthalic anhydride, 1.62 g (12.3 mmol) of 6-aminocaproic acid and a catalytic quantity of zinc acetate were dissolved in 70 mL of DMF. After stirring at room temperature for 18 h, the yellow suspension was heated to 80 °C for 1 h and then poured into 350 mL of cold water. After 2 h, the resulting pale yellow precipitate was filtered off and washed with cold water. The crude product was dissolved in 100 mL of boiling ethanol and filtered hot. The yellow crystals were filtered off the filtrate solution, washed three times with cold ethanol and dried in a desiccator over solid KOH. Yield: 2.1 g (6.2 mmol, 64 %), pale yellow solid, $C_{18}H_{16}ClNO_4$. ESI-MS: m/z (M-H$^+$, cation) for $C_{18}H_{17}ClNO_4^+$, calculated 346.1, found 346.0. ^{1}H-NMR (300 MHz, DMSO-d6) δ (ppm) 12.0 (s, 1H), 8.46 (s, 1H), 8.42 (d, 1H, J = 1.65 Hz), 8.28 (d, 1H, J = 7.96 Hz), 7.9 (d, 2H, J = 7.95 Hz), 3.9 (t, 2H, J = 7.14 Hz), 2.2 (t, 2H, J = 7.41 Hz), 1.55 (m, 4H), 1.3 (m, 2H). ^{13}C-NMR (300 MHz, DMSO-d6) δ (ppm) 24.1, 25.9, 27.0, 33.4, 39.5, 121.1, 122.4, 127.4, 128.0, 128.1, 128.3, 129.7, 130.6, 131.3, 137.2, 162.4, 162.7, 174.3. The compound was synthesized according to the literature and all NMR data are analogue.

6.2.4 Synthesis and Characterization of (4; "HP Green")

$C_{18}H_{16}ClNO_4$

345.08 g/mol
1 eq

3

$C_9H_{14}N_2O$

166.22 g/mol
2 eq

2

$C_{27}H_{29}N_3O_5$

475.21 g/mol

4

438 mg (1.27 mmol) of **3** and 423 mg (2.54 mmol) of **2** were dissolved in 10 ml of DMSO and 432 µL (2 mmol) of diisopropylethylamine (DIEA) was added as a base. The mixture was stirred at 90 °C for 18 h and poured into 50 mL of ice water. The emulsion was centrifuged and the oil collected, dissolved in ethyl acetate, washed two times with water and dried over Na_2SO_4. The solvent was evaporated to obtain a tawny oil which was purified by column chromatography on silica with n-hexane/DCM mixtures (gradient from 2:8 to 1:99, v/v), DCM and DCM/MeOH mixtures (gradient from 98:2 to 9:1, v/v). Yield: 100 mg (0.21 mmol, 17 %), ochre solid, $C_{27}H_{29}N_3O_5$. ESI-MS: m/z [M-H$^+$, cation] for $C_{27}H_{30}N_3O_5^+$, calculated 476.22, found 476.1. ^{1}H-NMR (300 MHz, Acetone-d6): δ (ppm) 1.45 (m, 2H), 1.7 (m, 4H), 2.3 (t, 2H, J = 7.41 Hz), 3.55 (t, 2H, J = 6.04 Hz), 3.75 (m, 2H), 4.3 (t, 2H, J = 7.41), 6.65 (d, 2H, J = 9.06 Hz), 6.75 (d, 2H, J = 8.78 Hz), 6.9 (d, 1H, J = 8.51 Hz), 7.05 (m, 1H), 7.65 (t, 1H, J = 8.23 Hz), 8.35 (d, 1H, J = 8.51 Hz), 8.38 (d, 1H, J = 7.41 Hz), 8.55 (d, 1H, J = 8.51 Hz). ^{13}C-NMR (600 MHz, Acetone-d6): δ = 25.38, 27.28, 28.61, 30.30, 30.43, 30.55, 34.01, 40.09, 43.48, 43.54, 43.56, 43.61, 55.80, 104.77, 104.81, 110.32, 114.62, 115.56, 121.47, 121.52, 123.76, 125.22, 128.27, 130.71, 131.39, 134.86, 143.65, 151.17, 151.25, 152.83, 164.11, 164.82, 174.46 ppm. The compound was

synthesized according to the literature with the exception of the workup with column chromatography. All NMR data are analogue.

6.2.5 Synthesis and Characterization of (5)

$C_{18}H_{16}ClNO_4$

345.08 g/mol

3

$C_{20}H_{20}ClNO_4$

373.11 g/mol

5
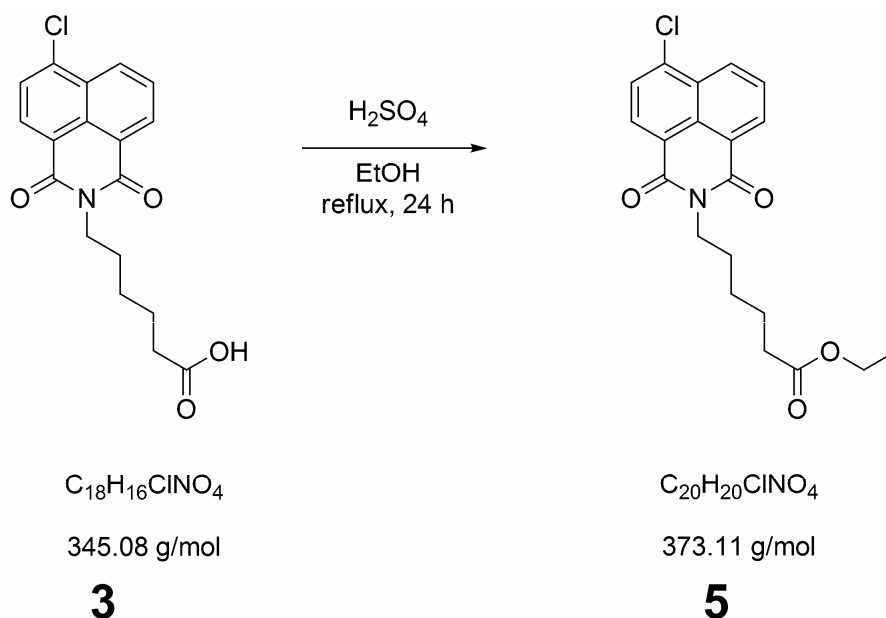
4 mL of concentrated sulfuric acid was dropped to a pale yellow suspension of 3.77 mg (10.9 mmol) of **3** in 200 mL of dry EtOH. The suspension was refluxed for 24 hours, cooled to room temperature and the volume was reduced to 20 mL. 50 ml of ethyl acetate are added and the organic layer was washed two times with 50 mL of water, 50 mL of brine, dried over Na_2SO_4 and reduced to dryness. The remaining oil solidified in the refrigerator over night and was then recrystallized from MeOH and dried over solid KOH in the desiccator. Yield: 2.64 g (7.1 mmol. 65 %), yellow solid, $C_{20}H_{20}ClNO_4$. ESI-MS: m/z (M-H$^+$, cation) for $C_{20}H_{21}ClNO_4^+$, calculated 374.1, found 374.0; ^{1}H-NMR (300 MHz, DMSO-d6) δ (ppm): 1.15 (t, 3H, J = 7.14 Hz), 1.3 (m, 2H), 1.6 (m, 4H), 2.3 (t, 2H, J = 7.14 Hz), 4.0 (m, 4H), 7.9 (m, 2H), 8.3 (m, 1H), 8.5 (m, 2H). The compound was synthesized according to the literature and all NMR data are analogue.

6.2.6 Synthesis and Characterization of (6)

$C_{20}H_{20}ClNO_4$	C_2H_7NO	$C_{22}H_{26}N_2O_5$
373.11 g/mol	61.05 g/mol	398.18 g/mol
1 eq	2 eq	
5		**6**
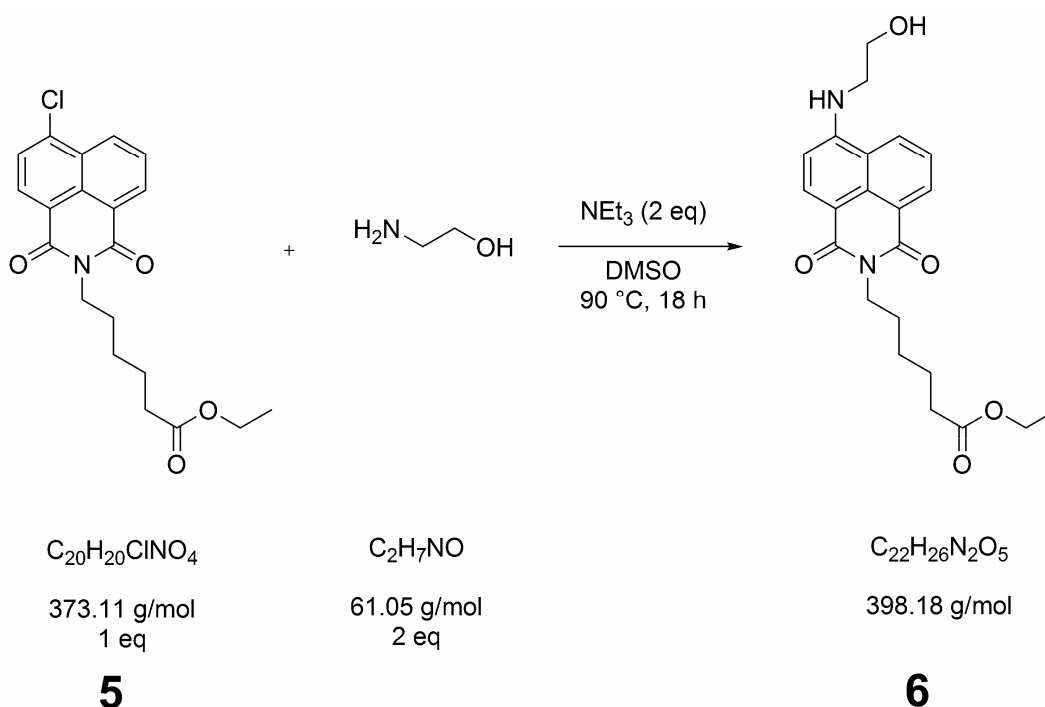
A yellow solution of 2 g (5.36 mmol) of **5**, 647 µL (10.72 mmol) of ethanolamine and 1.486 mL (10.72 mmol) of triethylamine in 20 mL of DMSO was stirred at 90 °C for 18 hours. The hot brown solution was poured into 150 mL of cold water, after three hours the resulting precipitate was filtered off and washed three times with cold water. The brown crude product was recrystallized from ethyl acetate. The crystals were filtered off the solution, washed with cold ethyl acetate and dried over solid KOH in a desiccator. Yield: 1.53 g (3.84 mmol, 72 %), brown-yellow solid, $C_{22}H_{26}N_2O_5$, melting point: 110 °C. ESI-MS: m/z (M-H$^+$, cation) for $C_{22}H_{27}N_2O_5^+$, calculated 399.2, found 399.0. ^{1}H-NMR (300 MHz, CDCl$_3$) δ (ppm): 1.2 (t, 3H, J = 7.13 Hz), 1.45 (m, 2H), 1.7 (m, 4H), 2.3 (t, 2H, J = 7.41 Hz), 3.1 (s(b), 1H), 3.7 (m, 2H), 4.1 (m, 6H), 5.9 (m, 1H), 6.6 (d, 1H, J = 8.5 Hz), 7.45 (t, 1H, J = 7.96 Hz), 8.0 (d, 1H, J = 8.23 Hz), 8.25 (d, 1H, J = 8.23 Hz), 8.4 (d, 1H, J = 7.13 Hz). The compound was synthesized according to the literature and all NMR data are analogue.

6.2.7 Synthesis and Characterization of (7)
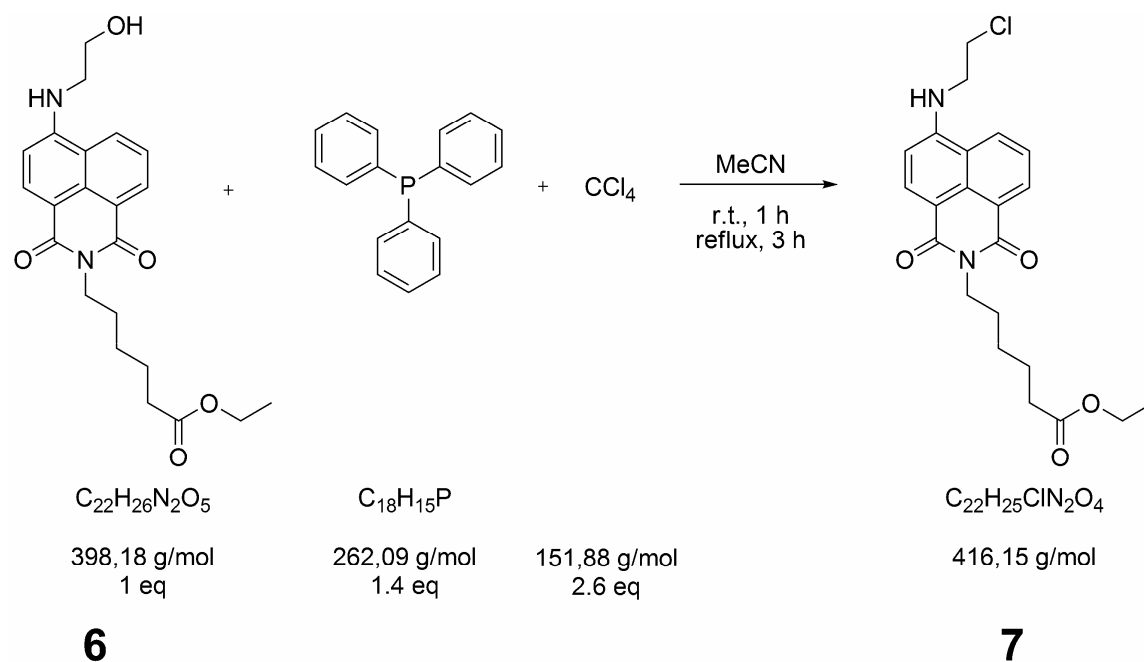
A suspension of 4.0 g (10 mmol) of **6**, 3.69 g (14 mmol) of triphenylphosphine and 2.513 mL (26 mmol) of tetrachloromethane in 30 mL of acetonitrile was stirred at room temperature for one hour and refluxed for three hours afterwards. The solution was cooled to room temperature, the golden precipitate was filtered off and washed three times with cold acetonitrile. The crude product was recrystallized from ethyl acetate. The golden crystals were filtered off the solution and dried over solid KOH in the desiccator. Yield: 2.135 g (5.13 mmol, 51 %), golden powder, $C_{22}H_{25}ClN_2O_4$, melting point: 150 °C. ^{1}H-NMR (300 MHz, DMSO-d6) δ (ppm): 1.1 (t, 3H, J = 7.14 Hz), 1.3 (m, 2H), 1.6 (m, 4H), 2.3 (t, 2H, J = 7.13 Hz), 3.8 (q, 2H, J = 5.49 Hz, 11.25 Hz), 3.9 (t, 2H, J = 6.32 Hz), 4.0 (m, 4H), 6.85 (d, 1H, J = 8.51 Hz), 7.6 (m, 1H, P(O)Ph$_3$), 7.7 (t, 1H, J = 8.24 Hz), 7.9 (t, 1H, J = 5.49 Hz), 8.25 (d, 1H, J = 8.51 Hz), 8.42 (d, 1H, J = 7.13 Hz), 8.65 (d, 1H, J = 7.68 Hz). The compound was synthesized according to the literature and all NMR data are analogue.

6.2.8 Synthesis and Characterization of (8)

$C_{22}H_{25}ClN_2O_4$

416.15 g/mol
1 eq

7

$C_8H_{12}N_2$

136.10 g/mol
1.2 eq

$C_{30}H_{36}N_4O_4$

516.27 g/mol

8

120 mg of **7** (0.29 mmol) and a catalytic quantity of sodium iodide were dissolved in ethyl acetate and the mixture was refluxed for 4 h. The solution was filtered to remove sodium chloride. 47 mg of N,N-dimethyl-*p*-phenylene diamine (0.35 mmol) and 48.4 mg of K_2CO_3 (0.35 mmol) were added and the mixture was refluxed for 16 h afterwards. After cooling to room temperature, K_2CO_3 was filtered off and the solution was evaporated to dryness. The crude product was purified by column chromatography (2 cm diameter, 20 cm length) on silica with n-hexane/DCM (1:9, v/v), DCM and DCM/MeOH mixtures (gradient from 99:1 to 95:5, v/v). Yield: 28 mg (0.054 mmol, 19 %), ochre solid, $C_{30}H_{36}N_4O_4$, melting point: 64 °C. HR-EI-MS: m/z [M$^{+\cdot}$, radical cation] for $C_{30}H_{36}N_4O_4^{+\cdot}$, calculated 516.27366, found 516.27345. ^{1}H-NMR (300 MHz, DMSO-d6): δ (ppm) 1.15 (t, 3H, J = 6.86 Hz), 1.33 (m, 2H), 1.57 (m, 4H), 2.27 (t, 2H, J = 7.41 Hz), 2.7 (s, 6H), 3.5 (d, 2H, J = 2.75 Hz), 3.55 (m, 3H), 4.0 (m, 4H), 5.1 (t, 1H, J = 6.04 Hz), 6.58 (d, 2H, J = 9.06 Hz), 6.63 (d, 2H, J = 9.06 Hz), 6.8 (d, 1H, J = 8.5 Hz), 7.68 (t, 1H, J = 4.94 Hz), 8.25 (d, 1H, J = 8.51 Hz), 8.42 (d, 1H, J = 7.14 Hz), 8.7 (d, 1H, J = 8.51 Hz). ^{13}C-NMR (600 MHz, DMSO-d6): δ = 14.06,

24.18, 25.90, 27.30, 33.31, 41.72, 42.21, 42.31, 59.60, 103.81, 107.73, 113.46, 115.34, 120.15, 121.84, 124.26, 128.57, 129.40, 130.67, 134.22, 140.65, 143.05, 150.64, 162.88, 163.72, 172.80 ppm.
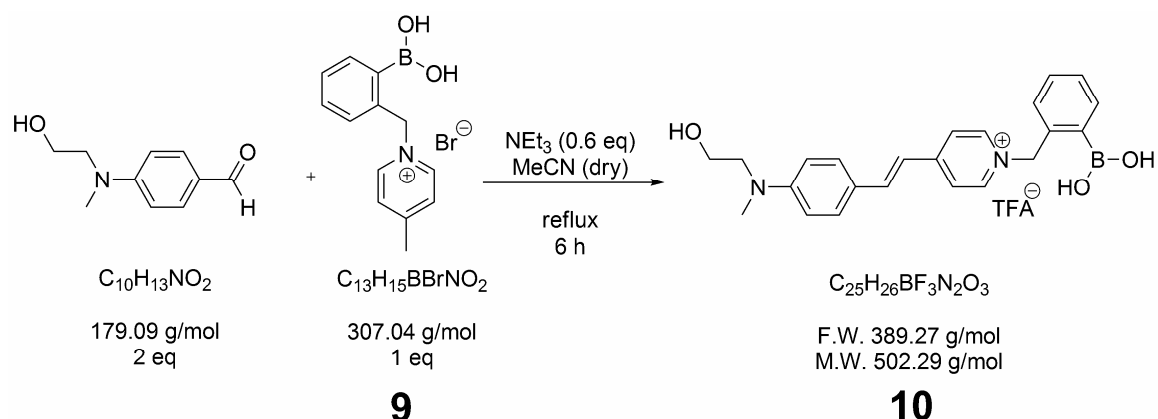
6.2.9 Synthesis and Characterization of (9)
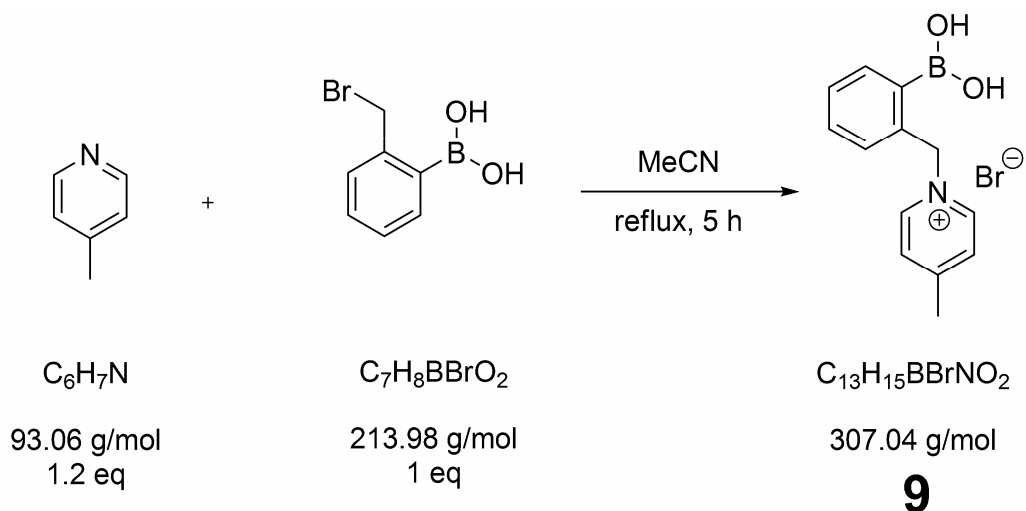
117 µL (1.2 mmol) of 4-picoline was slowly added to a colourless suspension of 214 mg (1 mmol) of 2-(bromomethyl)phenylboronic acid in 10 mL MeCN. After the reaction mixture was refluxed for 5 hours it was cooled to room temperature, the solvent was evaporated and dried in vacuum. The crude product was washed three times with cold ethyl acetate and dried in a desiccator over solid KOH. Yield: 301 mg (8.13 mmol, 98%), colourless powder, $C_{13}H_{15}BBrNO_2$; ^{1}H-NMR (300 MHz, DMSO) δ (ppm): 2.6 (s, 3H), 5.9 (s, 2H), 7.3 (d, 1H, J = 7.2 Hz), 7.5 (m, 2H), 7.8 (d, 1H, J = 7.1 Hz), 8.0 (d, 2H, J = 6.3 Hz), 8.6 (s, 2H), 8.9 (d, 2H, J = 6.6 Hz). The compound was synthesized according to the literature and all NMR data are analogue.

6.2.10 Synthesis and Characterization of (10)

$C_{10}H_{13}NO_2$
179.09 g/mol
2 eq

9
$C_{13}H_{15}BBrNO_2$
307.04 g/mol
1 eq

10
$C_{25}H_{26}BF_3N_2O_3$
F.W. 389.27 g/mol
M.W. 502.29 g/mol

200 mg (0.65 mmol) of **9**, 233 mg (1.3 mmol) of N-Methyl-N-(2-hydroxyethyl)-4-aminobenzaldehyde and 54 µL (0.39 mmol) of triethylamine were placed in a 50 mL round bottom flask. Some molsieve (3 Å) was added and the compounds were dissolved in 15 mL of dry MeCN. After the reaction mixture had refluxed for 6 hours it was cooled to room temperature, filtered off, evaporated and dried in vacuum. The crude product was purified by preparative HPLC. Yield: 5.6 mg (0.01 mmol, 2 %), red solid, $C_{25}H_{26}F_3BrN_2O_5$; ^{1}H-NMR (300 MHz, CD$_3$CN) δ (ppm): 3.1 (s, 3H), 3.5 (t, 3H, J = 6.0 Hz), 3.7 (t, 2H, J = 6.0 Hz), 5.8 (s, 2H), 6.8 (d, 2H, J = 9.1 Hz), 7.0 (d, 1H, J = 16.2 Hz), 7.4 (d, 1H, J = 7.1 Hz), 7.5 (t, 2H, J = 8.2 Hz), 7.5 (s, 1H), 7.6 (s, 1H), 7.7 (d, 1H, J = 16.2 Hz), 7.8 (d, 2H, J = 6.9 Hz), 8.0 (d, 1H, J = 7 Hz), 8.5 (d, 1H, J = 7.1 Hz); IR $\bar{v}$ (cm^{-1}): 1439 (B-O). The compound was synthesized according to the literature with the exception of the workup with preparative HPLC. All NMR data are analogue.

6.2.11 Synthesis of Pinacol Boronic Esters for MS Characterization

The respective boronic acid (1 eq), pinacol (1 eq) and excess calcium sulphate are placed in a flask and 10 mL of acetonitrile/toluene (2:1, v/v) is added. The mixture is refluxed for 3.5 h, filtered off to remove calcium sulphate and the filtrate is evaporated to dryness.[1] A small amount is submitted to mass spectrometry analysis.

6.2.12 General Procedure for the Synthesis and Characterization of ((1,10-Phenanthrolin-5-ylamino)methyl)phenylboronic Acids

$C_{12}H_9N_3$

195.08 g/mol
1 eq

$C_7H_7BO_3$

150.05 g/mol
1.3 eq

$C_{19}H_{16}BN_3O_2$

329.13 g/mol

11a/b
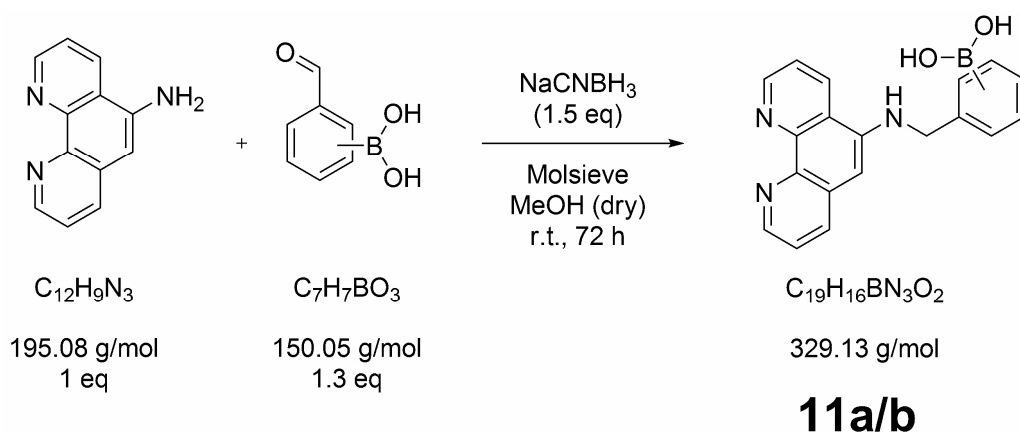
800 mg (4.1 mmol) of 1,10-phenanthrolin-5-amine, 738 mg (4.92 mmol) of formylphenylboronic acid and molsieve (3 Å) were placed in a 100 mL two-necked flask and were dissolved in 50 mL of dry MeOH. The yellow suspension was stirred for 5 hours at room temperature to form the imine. Afterwards, 386 mg (6.15 mmol) of sodiumcyanoboron hydride was added in four portions and the solution was stirred for further 67 hours. The reaction mixture was filtered off to remove the remaining molsieve and the filtrate was evaporated. The crude product was purified on basic alumina with DCM and DCM/MeOH mixtures (95:5, 93:7, 90:10 and 80:20, v/v) to yield a solid after solvent removal and drying over solid KOH in a desiccator. In case of **11a**, the product was crystallized from chloroform/acetonitrile (8:2, v/v).

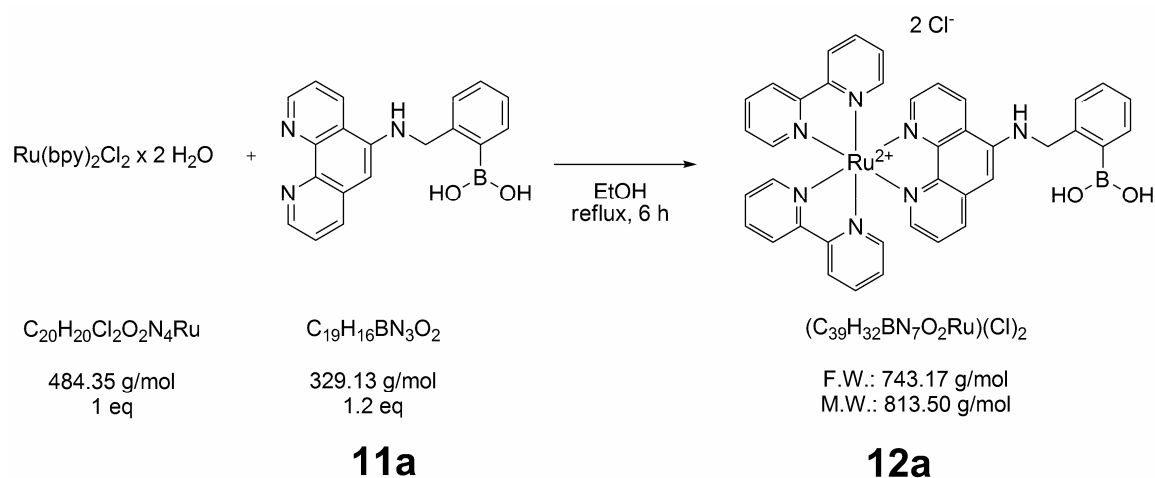(a) 2-((1, 10-phenanthrolin-5-ylamino)methyl)phenylboronic acid **(11a)**

Yield: 371.9 mg (1.13 mmol, 28 %), yellow solid, $C_{19}H_{16}BN_3O_2$; Elemental analysis Calc.: C 69.33 %, H 4.90 %, N 12.77 %; found: C 69.06 %, H 4.98 %, N 12.88 %; EI-HR-MS: m/z (M$^+$, cation) for $C_{25}H_{26}BN_3O_2$ pinacol ester derivative, calculated 411.2118, found 411.2118. ^{1}H-NMR (300 MHz, DMSO-d6) δ (ppm): 4.7 (d, 2H, J = 5.48 Hz), 6.65 (s, 1H), 7.1 (t, 1H, J = 5.49 Hz), 7.2 – 7.3 (m, 2H), 7.4 (d, 1H, J = 7.14 Hz), 7.45 (dd, 1H, J = 4.4 Hz), 7.55 (d, 1H, J = 6.86 Hz, 1.37 Hz), 7.75 (dd, 1H, J = 4.12 Hz), 8.0 (d, 1H, J = 7.96 Hz, 1.65 Hz), 8.25 (s, 2H), 8.65 (d, 1H, J = 4.11 Hz, 1.84 Hz), 8.8 (d, 1H, J = 8.78 Hz, 1.37 Hz), 9.05 (d, 1H, J = 4.11 Hz, 1.37 Hz); ^{13}C-NMR (300 MHz, DMSO-d6) δ (ppm): 46.99, 98.93, 122.05, 122.14, 123.17, 125.73, 126.35, 128.66, 130.25, 130.31, 133.10, 133.18,

140.46, 141.56, 142.58, 144.93, 145.95, 149.28; ^{11}B-NMR (400 MHz, DMSO-d6) δ (ppm): 32.7 (s(b)); IR $\bar{\nu}$ (cm^{-1}): 1397 (B-O), 1223 (B-N).

(b) 3-((1, 10-phenanthrolin-5-ylamino)methyl)phenylboronic acid **(11b)**

Yield: 339.3 mg (69 %), orange solid, $C_{19}H_{16}BN_3O_2$; ESI-MS: m/z (MH$^+$, cation) for $C_{25}H_{26}BN_3O_2$ pinacol ester derivative, calculated 412.22, found 412.0; ^{1}H-NMR (300 MHz, DMSO-d6) δ (ppm): 4.6 (d, 2H, J = 5.49 Hz), 6.6 (s, 1H), 7.3 (m, 2H), 7.5 (m, 2H), 7.7 (t, 1H, J = 5.21 Hz), 7.78 (q, 1H, J = 4.67 Hz, 8.51 Hz), 7.98 (d, 1H, J = 8.23 Hz), 8.65 (d, 1H, J = 4.12 Hz), 8.9 (d, 1H, J = 8.51 Hz), 9.05 (d, 1H, J = 4.39 Hz); ^{13}C-NMR (300 MHz, DMSO-d6) δ (ppm): 46.65, 98.61, 121.97, 123.20, 127.00, 127.35, 128.27, 128.81, 130.38, 132.40, 132.56, 137.99, 140.32, 141.53, 144.85, 145.95, 149.30.

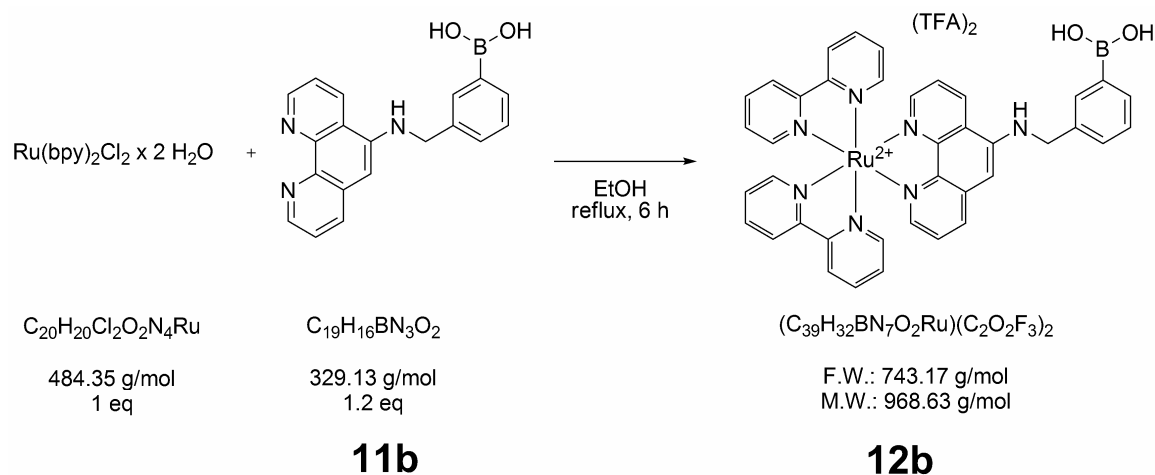### 6.2.13 Synthesis and Characterization of (12a)

$Ru(bpy)_2Cl_2 \times 2\ H_2O$

$C_{20}H_{20}Cl_2O_2N_4Ru$
484.35 g/mol
1 eq

$C_{19}H_{16}BN_3O_2$
329.13 g/mol
1.2 eq

11a

EtOH reflux, 6 h

$(C_{39}H_{32}BN_7O_2Ru)(Cl)_2$
F.W.: 743.17 g/mol
M.W.: 813.50 g/mol

12a

198 mg (0.38 mmol) of cis-dichloro(2,2´-bipyridine)ruthenium(II) and 150 mg (0.46 mmol) of **11a** were dissolved in 15 mL of dry ethanol and refluxed for 6 hours. The solvent was evaporated, the remaining oil was dissolved in 2 mL of ethanol and poured into 100 mL of cold tert. butylmethyl ether (TBME). The precipitate was filtered off, dried at 70 °C and was pure enough for further application. Yield: 168 mg (0.21 mmol, 45 %), red solid, $[C_{39}H_{32}BN_7O_2Ru](Cl)_2$; ^{1}H-NMR (300 MHz, CD$_3$CN) δ (ppm): 5.6 (s, 2H), 7.14 (s, 1H), 7.20 (m, 3H, J = 6.04 Hz), 7.40 (m, 3H), 7.46 (m, 1H, J = 5.22 Hz), 7.53 (m, 2H, J = 5.76 Hz, 8.78 Hz), 7.65 (m, 2H, J = 5.21 Hz), 7.80 (t, 3H, J = 6.59 Hz), 7.95 (t, 3H, J = 7.7 Hz), 8.04 (m, 3H, J = 5.5 Hz), 8.07 (m, 1H, J = 1.23 Hz), 8.17 (d, 1H, J = 8.2 Hz), 8.47 (m, 5H,
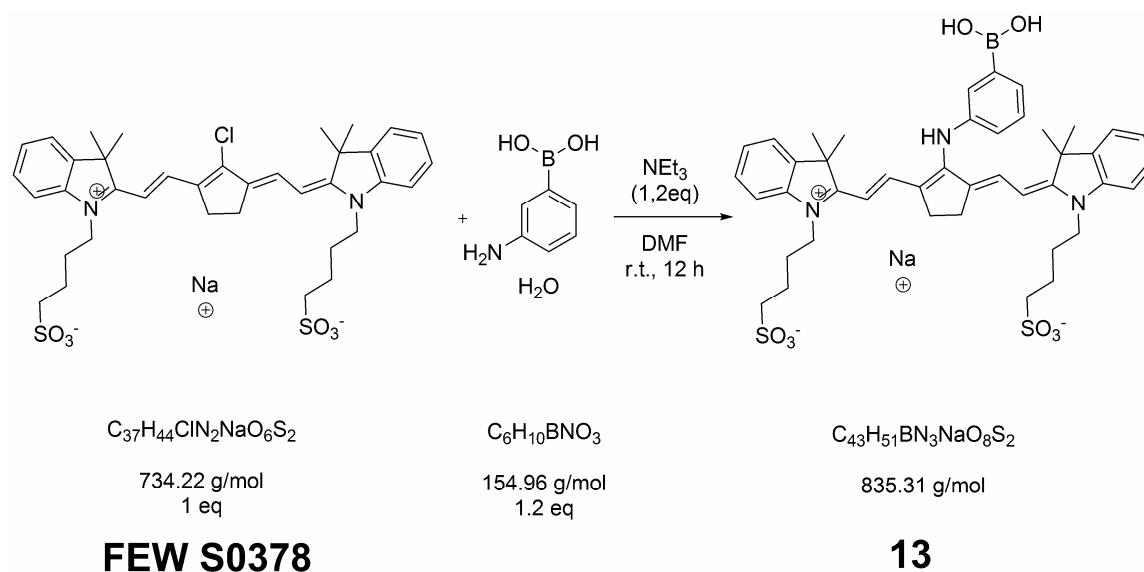
J = 8.8 Hz, 3.3 Hz), 8.60 (d, 1H, J = 8.5 Hz); ^{13}C-NMR (400 MHz, CD$_3$CN, Et$_2$OxBF$_3$ external) δ (ppm): 43.5, 104.4, 124.98, 125.09, 125.11, 125.15, 125.20, 125.76, 126.80, 128.35, 128.43, 128.45, 128.50, 132.48, 133.84, 134.72, 138.57, 138.69, 138.71, 142.92, 145.49, 145.50, 148.48, 149.29, 152.78, 152.86, 152.96, 153.13, 158.02, 158.04, 158.26; ^{11}B-NMR (400 MHz, CD$_3$CN, Et$_2$OxBF$_3$ external) δ (ppm): -0.52.

6.2.14 Synthesis and Characterization of (12b)

11b

C$_{20}$H$_{20}$Cl$_2$O$_2$N$_4$Ru
484.35 g/mol
1 eq

C$_{19}$H$_{16}$BN$_3$O$_2$
329.13 g/mol
1.2 eq

12b

(C$_{39}$H$_{32}$BN$_7$O$_2$Ru)(C$_2$O$_2$F$_3$)$_2$
F.W.: 743.17 g/mol
M.W.: 968.63 g/mol

161 mg (0.31 mmol) of cis-dichloro(2,2´-bipyridine)ruthenium(II) and 85 mg (0.26 mmol) of **11b** were dissolved in 15 mL of dry EtOH and refluxed for 6 hours. The solvent was evaporated, the remaining solid was dissolved in water, NH$_4$PF$_6$ was added in excess and the precipitate was filtered off. The red solid was purified on basic alumina with n-hexane/DCM (25:75, 10:90, v/v), DCM and DCM/MeOH mixtures (95:5, 93:7, 90:10 and 80:20, v/v) to obtain a red solid after removing the solvent and drying over solid KOH in the desiccator. Finally, the product was purified with preparative HPLC to remove impurities that could not be removed by column chromatography. Yield: 25 mg (0.26 mmol, 10 %), red solid, [C$_{39}$H$_{32}$BN$_7$O$_2$Ru](C$_2$O$_2$F$_3$)$_2$; ESI-MS: m/z (M$^+$, cation) for C$_{45}$H$_{42}$BN$_7$O$_2$Ru pinacol ester derivative, calculated 824.35 , found 412 (m/2z); ^{1}H-NMR (400 MHz, DMSO-d6, TMS external) δ (ppm): 4.5 (m, 2H), 6.85 (s, 1H), 7.35 (m, 3H), 7.65 (m, 7H), 7.8 (m, 4H), 8.05 (m, 3H), 8.15 (m, 3H), 8.8 (m, 5H), 9.1 (m, 3H); ^{13}C-NMR (400 MHz, DMSO-d6) δ (ppm): 46.7, 98.5, 123.9, 124.3, 124.4, 124.9, 126.1, 127.7, 131.6, 132.6, 133.6, 137.6, 137.8, 140.6, 143.9, 146.2, 147.6, 151.1, 151.3, 151.7, 156.5, 156.6, 156.8; ^{11}B-NMR (400 MHz, DMSO-d6, TMS external) δ (ppm): 28.2.

6.2.15 Synthesis and Characterization of (13)

C$_{37}$H$_{44}$ClN$_2$NaO$_6$S$_2$

734.22 g/mol
1 eq

FEW S0378

C$_6$H$_{10}$BNO$_3$

154.96 g/mol
1.2 eq

C$_{43}$H$_{51}$BN$_3$NaO$_8$S$_2$

835.31 g/mol

13

500 mg (0.68 mmol) of **S0378**, 126.5 mg (0.82 mmol) of 3-aminophenylboronic acid monohydrate and 115 µL (0.82 mmol) of triethylamine were placed in a 50 mL round bottom flask. The green solution was stirred for 12 hours at room temperature thereby changing its colour to blue. Then it was poured into 50 mL of tert.-butylmethyl ether (TBME) and the product precipitated. The precipitate was filtered off, washed three times with 10 mL TBME and dried over solid KOH in the desiccator. Yield: 550 mg (0.66 mmol, 97 %), blue solid, C$_{43}$H$_{51}$BN$_3$NaO$_8$S$_2$, thermal decomposition 200 °C; ESI-MS: m/z (MH$^+$, cation) for C$_{43}$H$_{52}$BN$_3$O$_8$S$_2$$^+$, calculated 813.3, found 813.4; ^{1}H-NMR (300 MHz, DMSO-d6) δ (ppm): 1.3 (s, 11H), 1.7 (m, 9H), 2.8 (s(b), 4H), 3.9 (m, 4H), 5.65 (d, 2H, J = 13.18 Hz), 7.0 (t, 2H, J = 7.41 Hz), 7.18 (d, 2H, J = 7.96 Hz), 7.25 (t, 2H, J = 7.69 Hz), 7.4 (d, 2H, J = 7.41 Hz), 7.5 (d, 2H, J = 6.58 Hz), 7.65 (d, 2H, J = 13.18 Hz), 7.8 (d, 1H, J = 5.76 Hz), 7.9 (s, 1H); ^{13}C-NMR (300 MHz, DMSO-d6) δ (ppm): 8.4, 22.4, 25.4, 25.5, 27.0, 42.0, 45.0, 47.0, 51.0, 97.0, 109.0, 122.0, 123.0, 127.0, 127.4, 128.01, 128.02, 129.0, 131.0, 132.5, 135.0, 140.0, 143.0, 162.0, 167.0; IR $\overline{\nu}$ (cm^{-1}): 1378 (B-O).

6.2.16 Synthesis and Characterization of (14)
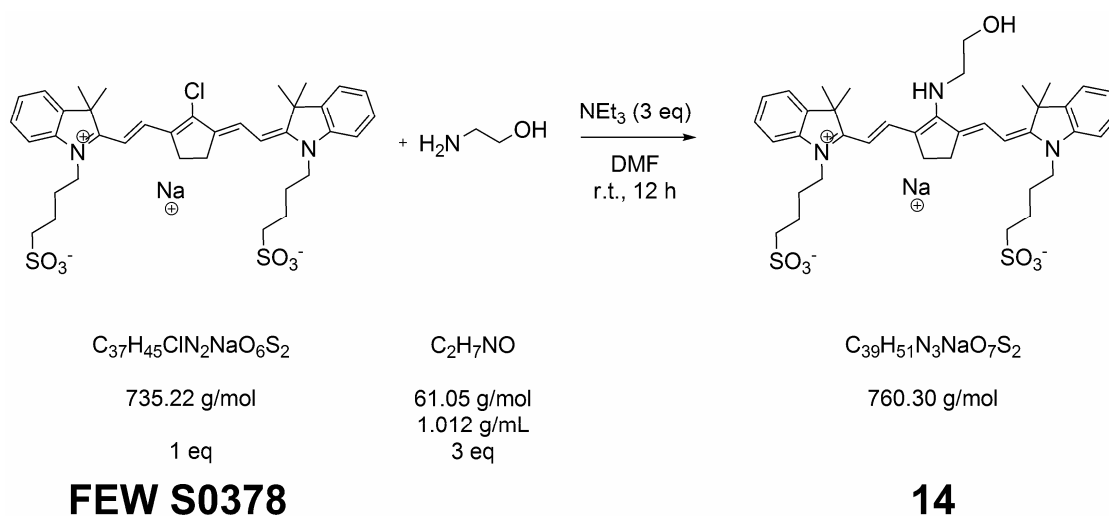
500 mg (0.68 mmol) of **S0378**, 123 µL (2.04 mmol) of ethanolamine and 283 µL (2.04 mmol) of triethylamine were dissolved in 10 mL of DMF. The solution was stirred at room temperature for 12 h and at 90 °C for 1 h. The solution was cooled to room temperature, poured into 100 mL of cold tert.-butylmethyl ether (TBME) and the resulting precipitate was filtered off, washed three times with 20 mL of cold TBME and dried in a desiccator over solid KOH. Yield: 479 mg (0.63 mmol, 93 %), black solid, $C_{39}H_{51}N_3NaO_7S_2$, HR-LSI-MS: m/z (M$^+$, cation) for $C_{39}H_{52}N_3O_7S_2^+$, calculated 738.3241, found 738.32603; ^{1}H-NMR (300 MHz, DMSO-d6) δ (ppm): 1.6 (s, 12H), 1.75 (s(b), 8H), 2.7 (s, 4H), 2.85 (t, 1H, J = 5.49 Hz), 3.6 (m, 1H), 3.8 (s(b), 4H), 3.92 (s(b), 4H), 5.15 (m, 1H), 5.35 (s(b), 1H), 5.6 (d, 2H, J = 12.62 Hz), 7.05 (t, 2H, J = 7.41 Hz), 7.35 (d, 2H, J = 7.96 Hz), 7.28 (t, 2H, J = 7.41 Hz), 7.45 (d, 2H, J = 7.13 Hz), 7.85 (s(b), 1H), 7.95 (d, 2H, J = 12.62 Hz), 9.0 (s(b), 1H); ^{13}C-NMR (300 MHz, DMSO-d6) δ (ppm): 22.53, 25.28, 25.91, 27.55, 41.08, 42.16, 42.24, 46.96, 48.56, 50.81, 57.34, 59.65, 96.16, 108.99, 109.30, 121.91, 122.17, 125.89, 127.99, 139.75, 142.87, 165.31, 166.05. IR $\bar{v}$ (cm^{-1}): 3417-3264 (O-H and N-H), 3052 (C-H unsaturated), 2928 (C-H saturated), 1604-1484 (C-H, aromatic), 1381-1269 (S-O, sulfonic acid), 1130 (S-C, sulfonic acid).

6.2.17 Attempted Purification of the Purple Decomposition Product

$C_{39}H_{51}N_3NaO_7S_2$

F.W. 736.96 g/mol
M.W. 760.30 g/mol

14
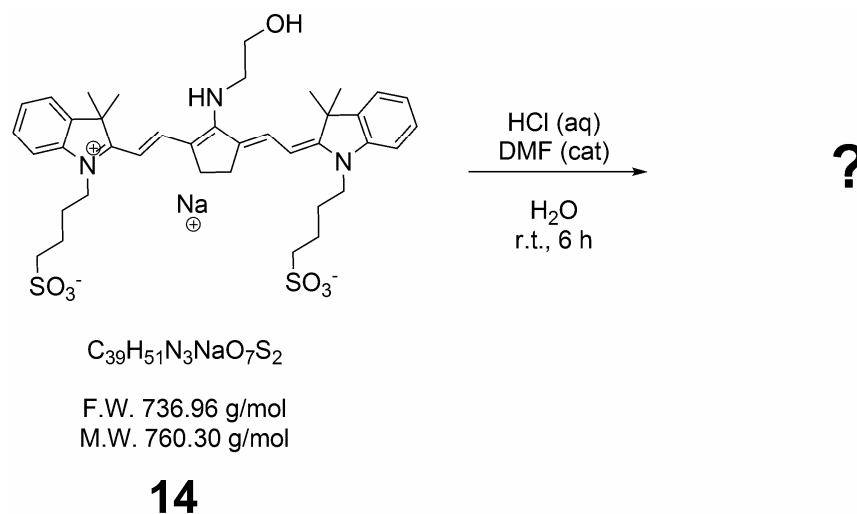
200 mg (0.26 mmol) of **14** were dissolved in 1 ml of DMF and the solution was added to a mixture of 10 mL of bidest. water and 1 mL of 37% (w/w) hydrochloric acid. The solution was stirred at room temperature for 6 hours, evaporated and purified with preparative HPLC (details see below). Yield: 1.2 mg, HR-ESI-MS: m/z (MH^{+}, radical cation) for $C_{39}H_{52}N_3O_8S_2$, calculated 754.3196, found 754.3190. IR $\bar{\nu}$ (cm^{-1}): 3400-3200 (O-H and N-H), 3060 (C-H, unsaturated), 2929 (C-H, saturated), 1673 (C-O, ketone), 1625-1523 (C-H, aromatic), 1389-1265 (S-O, sulfonic acid), 1132 (S-C, sulfonic acid).

6.2.18 Preparation of the H$_2$O$_2$ Sensor

(a) Activation of HP Green

4 mg of HP Green, dissolved in 100 µL DMSO, was added to a solution of 2.6 mg of DCC in 100 µL DMSO. Then, 1.5 mg of NHS in 100 µL DMSO was added to the reaction mixture and was shaken for 18 hours at room temperature to form the NHS active ester. The solution was used as obtained.

(b) Immobilization on O-(2-aminoethyl)-cellulose with 1% (w/w) HP Green

200 mg of O-(2-aminoethyl) cellulose was placed in a round bottom flask and suspended in 10 mL of phosphate buffer (pH 9, 10 mM). The suspension was put in an ultrasonic bath

for ten minutes and 150 µL of the activation cocktail was added. The reaction mixture was incubated for 24 hours at 37 °C. Then, the particles were centrifuged and washed three times with bidistilled water. The particles were suspended again in ethyl acetate and refluxed for 24 hours. Finally the particles were centrifuged, washed three times with ethyl acetate and dried at 50 °C.

(c) Immobilization on polystyrene particles (PS, size 5 µm) with 1% (w/w) HP Green

2 mL of a PS suspension (50 mg/mL) in PBS was diluted with 3 mL of phosphate buffer (pH 9, 10 mM) and 100 µL NaOH (0.1 M). Then, 75 µL of the activation cocktail was added and the reaction mixture was incubated for 24 hours at 37 °C. Finally, the particles were centrifuged and washed three times with bidistilled water and ethanol.

(d) Preparation of the sensor membrane

The corresponding amount of particles is placed in an Eppendorf cup and suspended in 1 mL of a 0.1 M $Na_2S_2O_4$ solution and incubated at 37 °C over night. The particles were centrifuged and washed two times with bidistilled water and ethanol. Afterwards 1 mL of Hydrogel D4 (2.5 % w/w in ethanol/water) was added and the particles were placed in an ultrasonic bath for 20 minutes. The sensor cocktail was spread over Mylar with a knife coating device and dried at room temperature for twenty minutes. Circular sensor spots (20 mm in diameter) were punched out and stored in 1 M $Na_2S_2O_4$ solution over night.

6.2.19 Preparation of the Sensor for Acidic Gases

2.5 g of Hypan hydrogel were added to 47.5 g of dry DMSO to obtain a 5% (w/w) stock solution that was stirred for 20 h at 80 °C. 1 g of PS was dissolved in 21.3 mL ($\cong$ 19 g at 20 °C) of anhydrous THF to give a 5% (w/w) stock solution. For the sensor cocktail, 2 mg of aminocyanine **14** were dissolved in 900 µL of dry DMSO and 100 µL of the viscous Hypan solution was added. The cocktail was shaken at 60 °C for twenty minutes and spread on Mylar with a knife-coating device. The "wet" sensor was dried for twenty minutes at room temperature followed by 18 h at 50 °C. The PS layer was directly spread on the Hypan layer with the knife-coating device. The sensor was dried at room temperature and stored at 50 °C. Each layer has a thickness of around 6 µm.

6.3 Sample Preparation, Instrumentation and Additional Data

6.3.1 Cyclic Voltammetry (CV)

Cyclic voltammograms were acquired on a CHI 660a potentiostat (CH Instruments, www.chinstruments.com) with homemade electrodes. CV measurements were performed against a silver/silver chloride reference electrode with a platin counter electrode and a platin auxiliary electrode. Concentrations of the fluorophores and parameters are given below.

(a) **HP Green** and probe **8**

10 mL of 50 µM stock solutions of HP Green and probe **8** in PBS of pH 7.4 (10 mM; 154 mM NaCl) were subjected to CV measurements. Parameters: Init E (V) = 0.2; High E (V) = 0.8; Low E (V) = -0.2; Init P/N = P; Scan Rate (V/s) = 0.1; Segment = 6; Sample Interval (V) = 0.002; Quiet Time (sec) = 2; Sensitivity (A/V) = 1e-4;

(b) Aminocyanine fluorophores **13** and **14**

10 mL of 500 µM stock solutions of probe **13** and **14** in phosphate buffer of pH 9.5 (25 mM; 100 mM NaCl) were subjected to CV measurements. Parameters: Init E (V) = 0; High E (V) = 1; Low E (V) = -0.8; Init P/N = P; Scan Rate (V/s) = 0.1; Segment = 6; Sample Interval (V) = 0.002; Quiet Time (sec) = 2; Sensitivity (A/V) = 1e-4;
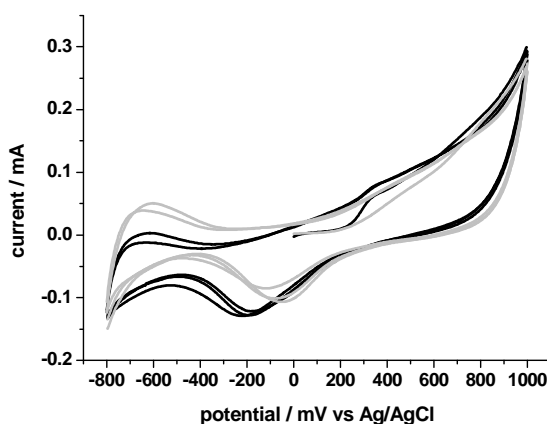

Figure 6.1. Cyclic voltammogram of probes **13** (black) and **14** (grey) in buffer of pH 9.5.

6.3.2 High Performance Liquid Chromatography (HPLC)

Analytical RP-HPLC was carried out on the Agilent 1100 series (Waldbronn, Germany) consisting of a binary pump (G1312A), an autosampler (G1313A), a DAD detector (DAD G1315B) and a Luna C18(2) column (particle size 3 μm, 150 x 2.00 mm) from Phenomenex (Aschaffenburg, Germany). A small amount of crude or purified product was dissolved in MeOH (β = 1 mg/mL). A binary elution system consisting of (A) TFA/H$_2$O (0.0059%, w/w) and (B) TFA/MeCN (0.0059%, w/w) was used with the following gradient: 5-98% B in 20 min at a flow rate of 0.3 mL/min.

Preparative RP-HPLC was carried out on the Agilent 1100 series (Waldbronn, Germany) consisting of two separate pumps (PrepPump G1361A), an autosampler, a Luna C18(2) column (particle size 10 μm, 250 x 21.2 mm), a DAD detector (DAD G1315B) and a fraction collector (AFC G1364A). The crude product was dissolved in the respective solvent and filtered through polytetrafluoroethylene syringe filters (0.2 µm). A binary elution system consisting of (A) TFA/H$_2$O (0.0059 w/w) and (B) MeCN was used at a flow rate of 21 mL/min. The fractions (6 mL) were collected and, after evaporation of MeCN, the product was lyophilized (more details are given at the respective chromatogram).

(a) Hemicyanine dye **10**: β = 40 mg/mL in MeOH; Gradient: 3% B for 5 min, 3-98% B in 15 min, 98% B for 10 min. Detection: 254 nm in absorption (blue) and 600 nm in fluorescence ($\lambda_{exc.}$ 476 nm, red).
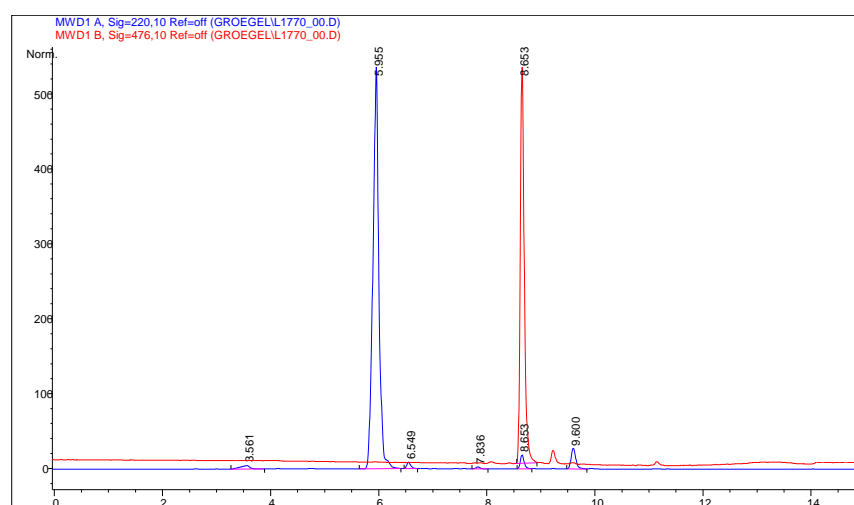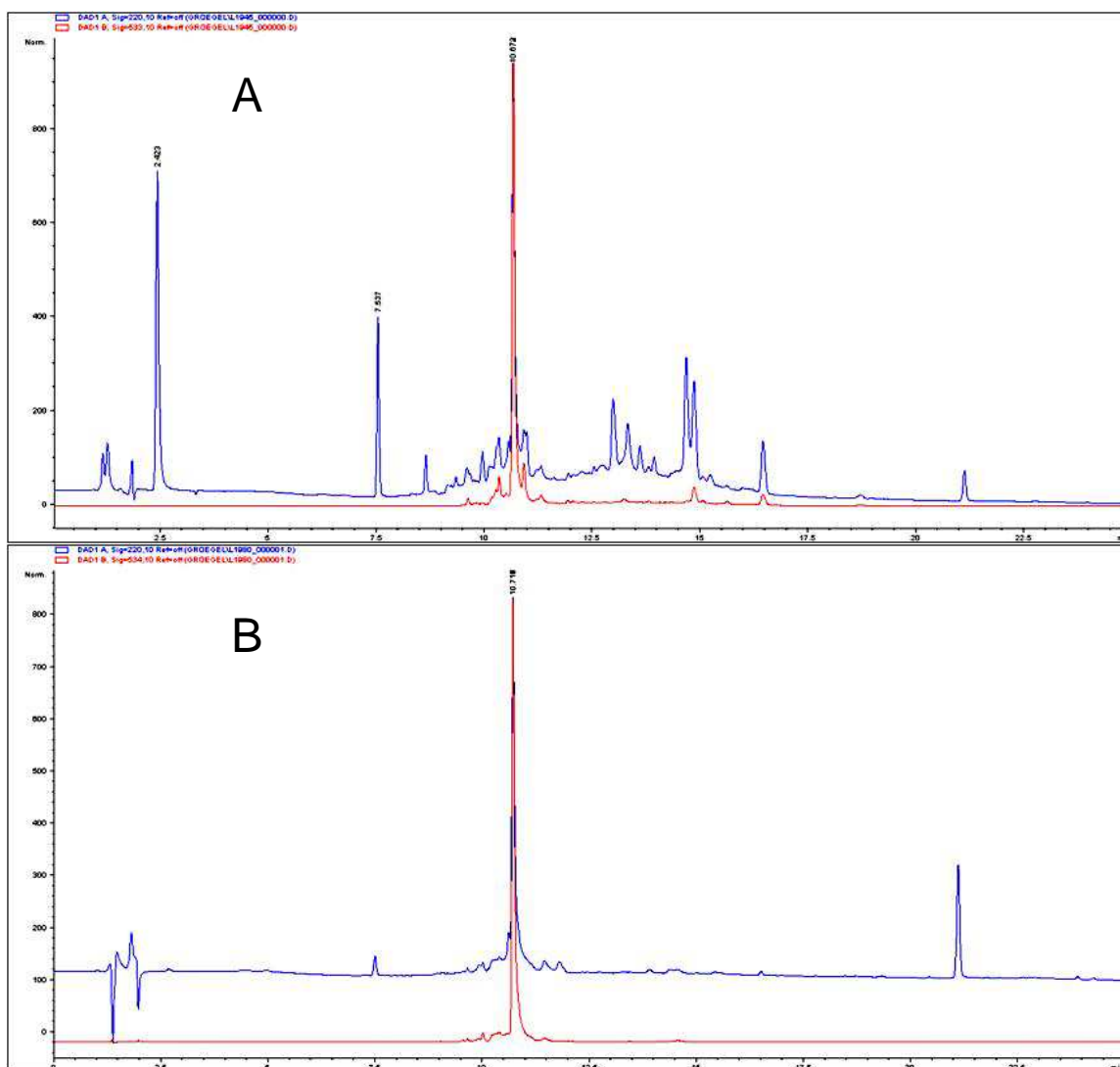

Figure 6.2. Analytical chromatogram of the crude product of **10** before purification by preparative HPLC.

(b) Ruthenium(II)-probe **12b**: β = 1 mg/mL in MeCN; Gradient: 3-98% B in 20 min.
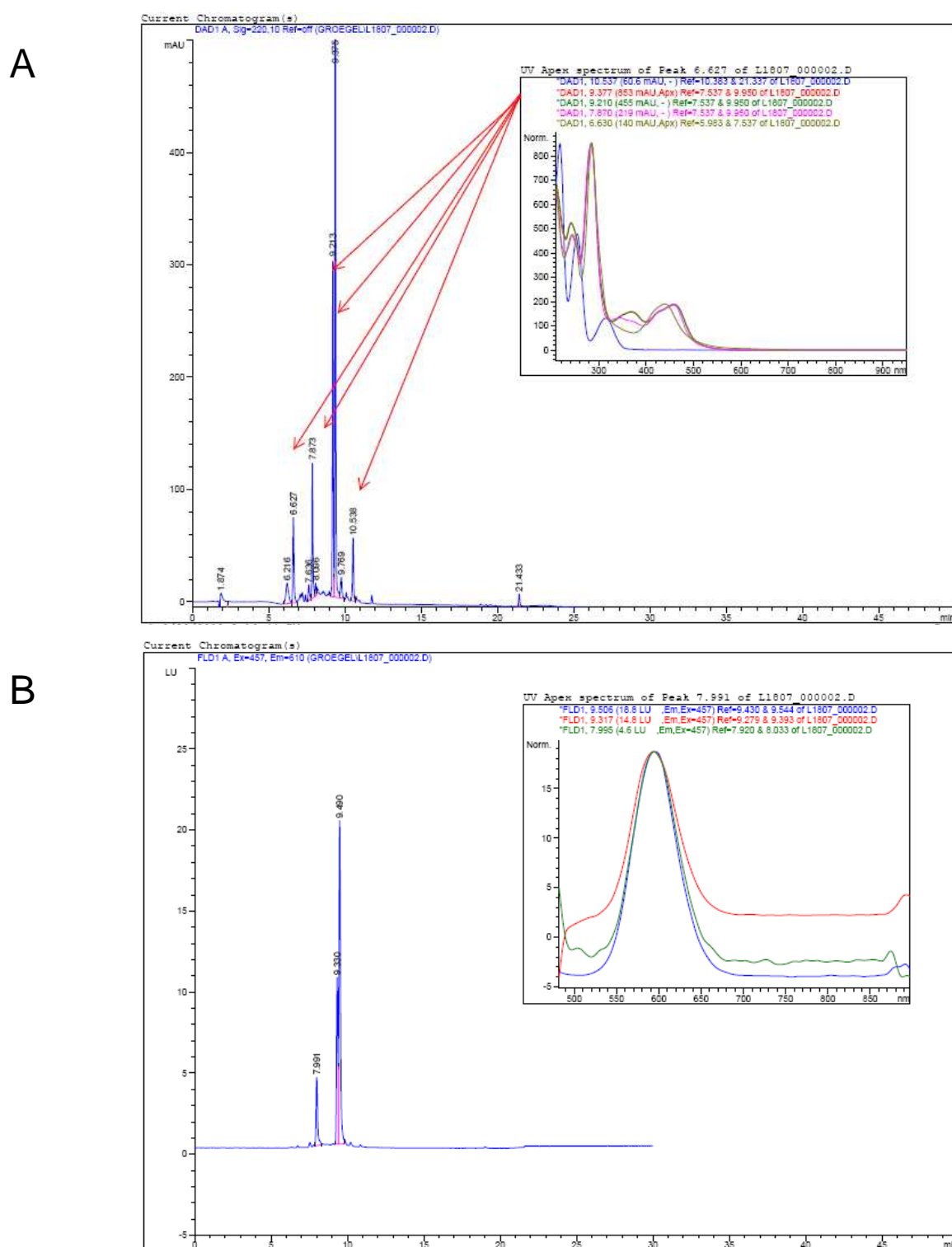
Figure 6.3. Analytical chromatograms of the crude product of **12b** before purification with preparative HPLC. A: Detection at 220 nm (UV detector, blue). B: 612 nm (Fluorescence, λ$_{exc.}$ 457 nm, blue).

(c) Purple decomposition product: β = 5 mg/mL in MeOH; Gradient: 5-98% B in 20 min. UV detection was done at the absorption wavelengths of 220 and 534 nm.


Figure 6.4. Analytical chromatograms of the purple product with detection at λ_{abs} = 220 nm (blue) and λ_{abs} = 534 nm (red). A: crude product; B: purified product. Background signal at t_r = 21.0 – 21.5 min.

6.3.3 Experimental Procedure for the Spectroscopic Characterization of HP Green and Probe 8

(a) Preparation of stock solutions of the dyes

Stock solutions of all compounds were prepared freshly in 10 mM phosphate buffered saline (PBS) of pH 7.4 with the exception of HP Green and probe **8**, which were each dissolved in PBS/DMSO (9:1, v/v).

(b) Sample preparation for fluorescence spectra and time traces/Additional spectra
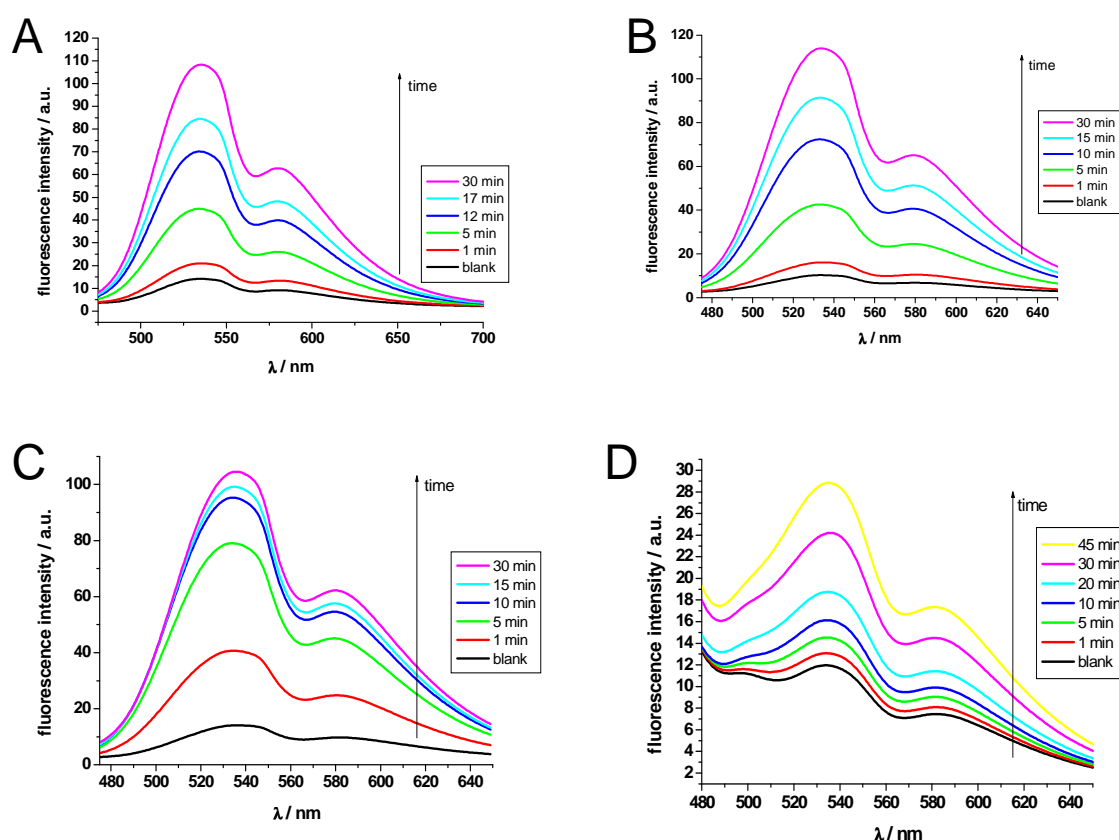
Figure 6.5. Temporal development of the emission spectra of HP Green (10 µM) and HRP (0.1 U/mL) in PBS of pH 7.4 at 30 °C. A: Presence of HP (10 µM). B: Presence of GOx (1 U/mL) and D-glucose (100 µM). C: Presence of LOx (1 U/mL) and L-lactate (20 µM). D: Temporal development of the emission spectra of probe **8** (10 µM) and HP (1 mM) in phosphate buffer (10 mm) of pH 7 (no HRP added).

Fluorescence spectra and time traces were acquired on a JP 6300 fluorimeter in quartz cuvettes *(a) without HRP*, *(b) with HRP and HP* and *(c) with HRP, oxidase and substrate* with the following experimental parameters: Excitation: 450 nm, bandwidth 5 nm; emission: 534 nm, bandwidth 5 nm; PMT voltage: 350 V; *(a)* 30 µL of HP Green (1 mM), 30 µL of HP (of various concentration) and 2,940 µL of PBS; *(b)* 30 µL of HP Green (1 mM), 30 µL of HRP (10 U/mL), 30 µL of HP (of various concentration) and 2,910 µL of PBS; *(c)* 30 µL of HP Green, 30 µL of HRP (10 U/mL), 30 µL of oxidase (100 U/mL), 30 µL of substrate (of various concentration) and 2,880 µL of PBS. Blank measurements were carried out without the addition of HP, glucose and L-lactate, respectively.

(c) Sample preparation for calibrations

Calibration measurements were performed in 96-well microtiterplates (MTPs; from GreinerBioOne, www.gbo.de, 8 wells per concentration) on a GENios Plus MTP reader (from Tecan, www.tecan.com) using a 430 nm excitation and 535 nm emission filter *(d) without HRP*, *(e) with HRP and HP* and *(f) with HRP, oxidase and substrate*. The other parameters were as follows: Gain: 80; number of flashes: 100; lag time: 0 µs, integration time: 40 µs; fluorescence top; temperature: 30 °C; *(d)* 10 µL of HP Green (250 µM), 10 µL of HP (of various concentration) and 230 µL PBS; *(e)* 10 µL of HP Green (250 µM), 25 µL of HRP (1 U/mL), 10 µL of HP (of various concentration) and 205 µL of PBS; *(f)* 10 µL of HP Green (250 µM), 25 µL of HRP (1 U/mL), 10 µL oxidase (25 U/mL), 10 µL of substrate (of various concentration) and 195 µL of PBS. Fluorescence intensities (I) were measured after 6 and 11 min, respectively and referenced against a blank (I_0) at the corresponding point in time. The corresponding blank values were obtained with solutions without HP, glucose or L-lactate, respectively. Error bars are calculated from standard deviations, possible outliners were identified with a Q-test (test value 0.51).

6.3.4 Experimental Procedure for Fluorescence Imaging of Hydrogen Peroxide in NRK Cells

(a) Preparation of the stock solution of HP Green

4 mg of HP Green (8.42 mmol) were dissolved in 100 µL DMSO and transferred to 9.9 mL of PBS (pH 7.4, 12 mM) containing 1 mM Ca^{2+}, 0.5 mM Mg^{2+} and 1 g/L glucose (further

referred to as PBS^{++}). This stock solution of HP Green was diluted to 2 mL with PBS^{++} to achieve concentrations of 8, 50 and 800 µM, respectively. The volume fraction of DMSO in the cell experiments was kept below 1‰.

(b) Cellular uptake of HP Green

For routine culture, normal rat kidney cells (NRK-52 E, DSMZ, www.dsmz.de) were kept in a humidified cell culture incubator at 37 °C with 5% CO_2. Cells were cultured in Dulbecco's modified Eagle medium with 4.5 g/L D-glucose supplemented with 5% (v/v) fetal calf serum, 100 µg/µL penicillin/streptomycin and 2 mM L-glutamine. Cells were cultured in Petri dishes and confluent cell monolayers were exposed to 2 mL of HP Green in PBS^{++} for 20 min at 37 °C, washed three times with PBS^{++}, and finally covered with 2 mL of PBS^{++}.

(c) Fluorescence Imaging Experiments and Analysis

Fluorescence imaging studies of a fixed local position were performed with an upright epifluorescence microscope Eclipse 90i equipped with a water immersion objective NIR Apo 60x/1.0 W and a DS-Fi1 high-definition CCD camera (Nikon, www.nikoninstruments.eu). Fluorescence was excited with a mercury vapour lamp in combination with a 465-495 nm excitation filter. Emission light was collected between 515-555 nm after passing a dichroic mirror of 505 nm. Images were analyzed *via* the Image J and Adobe Photoshop software. The intensity of HP Green is well reflected by the mean values of the histograms.

(d) Histograms

Figure 6.6. Histograms of the total images (red: mean curve of control)
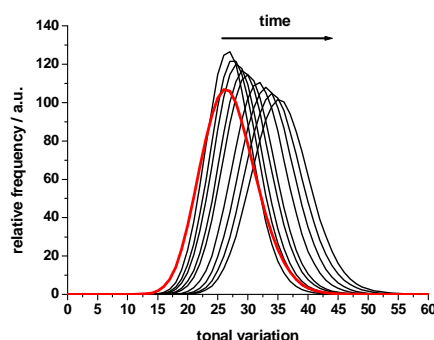
(e) Fluorescence images of NRK cells with different concentrations of HP Green
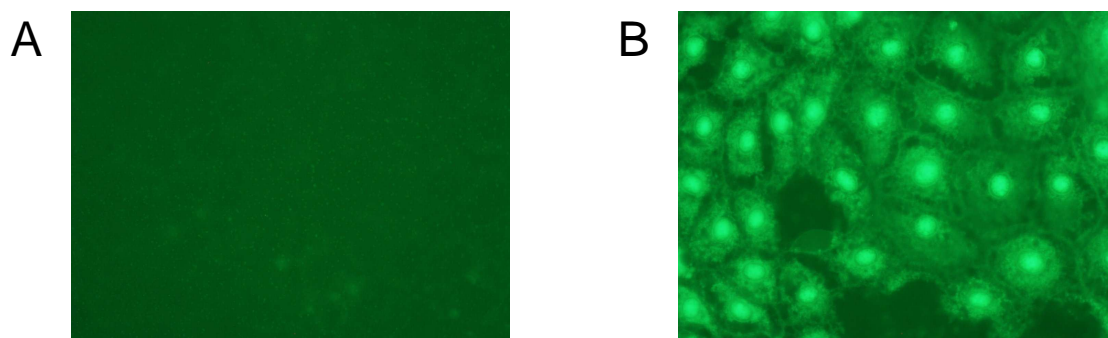
Figure 6.7. Images of NRK cells incubated with HP Green. A: 8 µM stock solution. B: 800 µM stock solution.

(f) Fluorescence images of HP Green (50 µM) in NRK cells in the presence of hydrogen peroxide

Figure 6.8. Images of NRK cells incubated with HP Green and 100 µM HP over time.

(g) Fluorescence images of HP Green in NRK cells without hydrogen peroxide

0 min	**10 min**	**20 min**
30 min	**40 min**	**50 min**
60 min	**70 min**	**80 min**
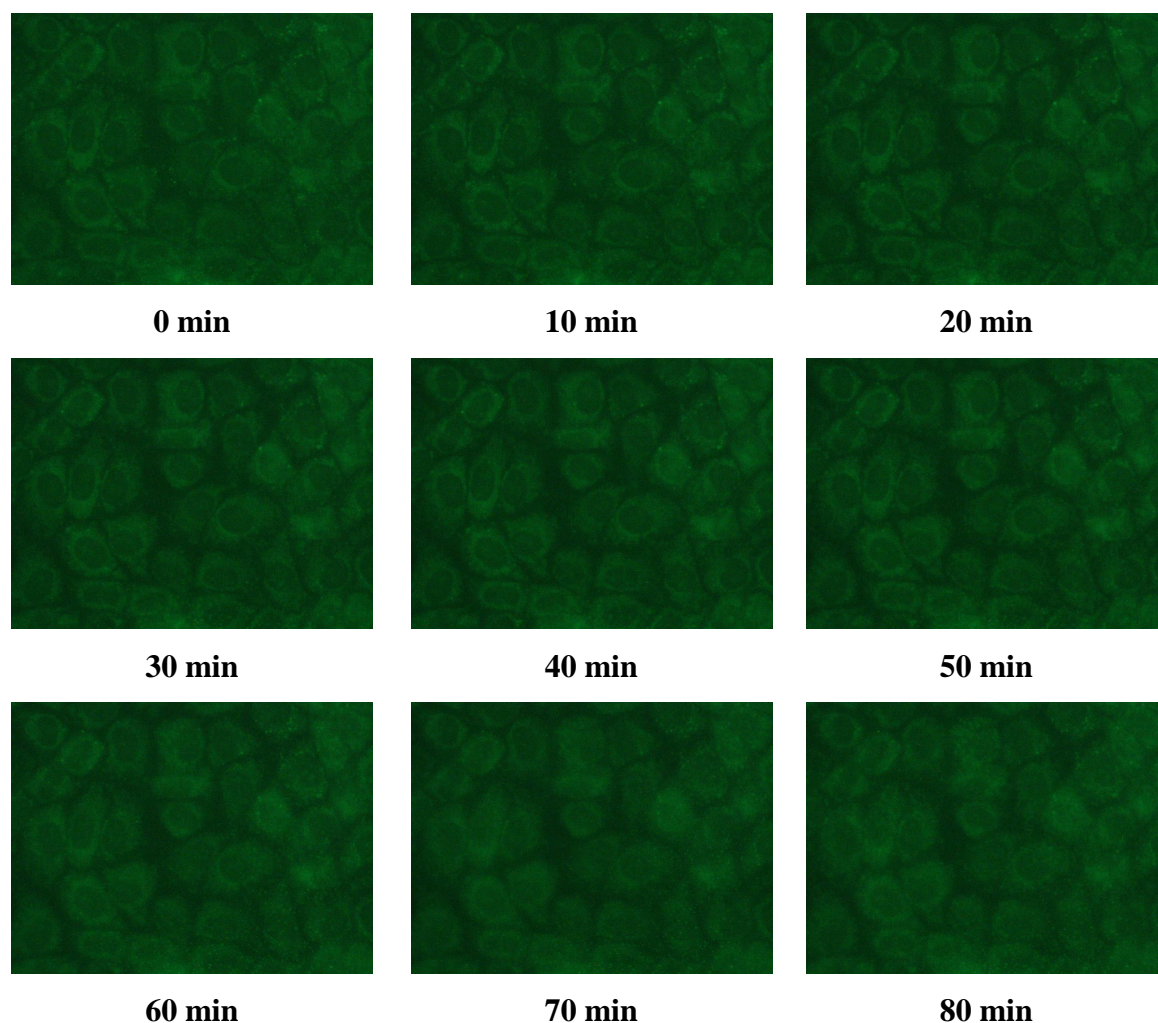
Figure 6.9. Images of NRK cells incubated with HP Green without HP over time.

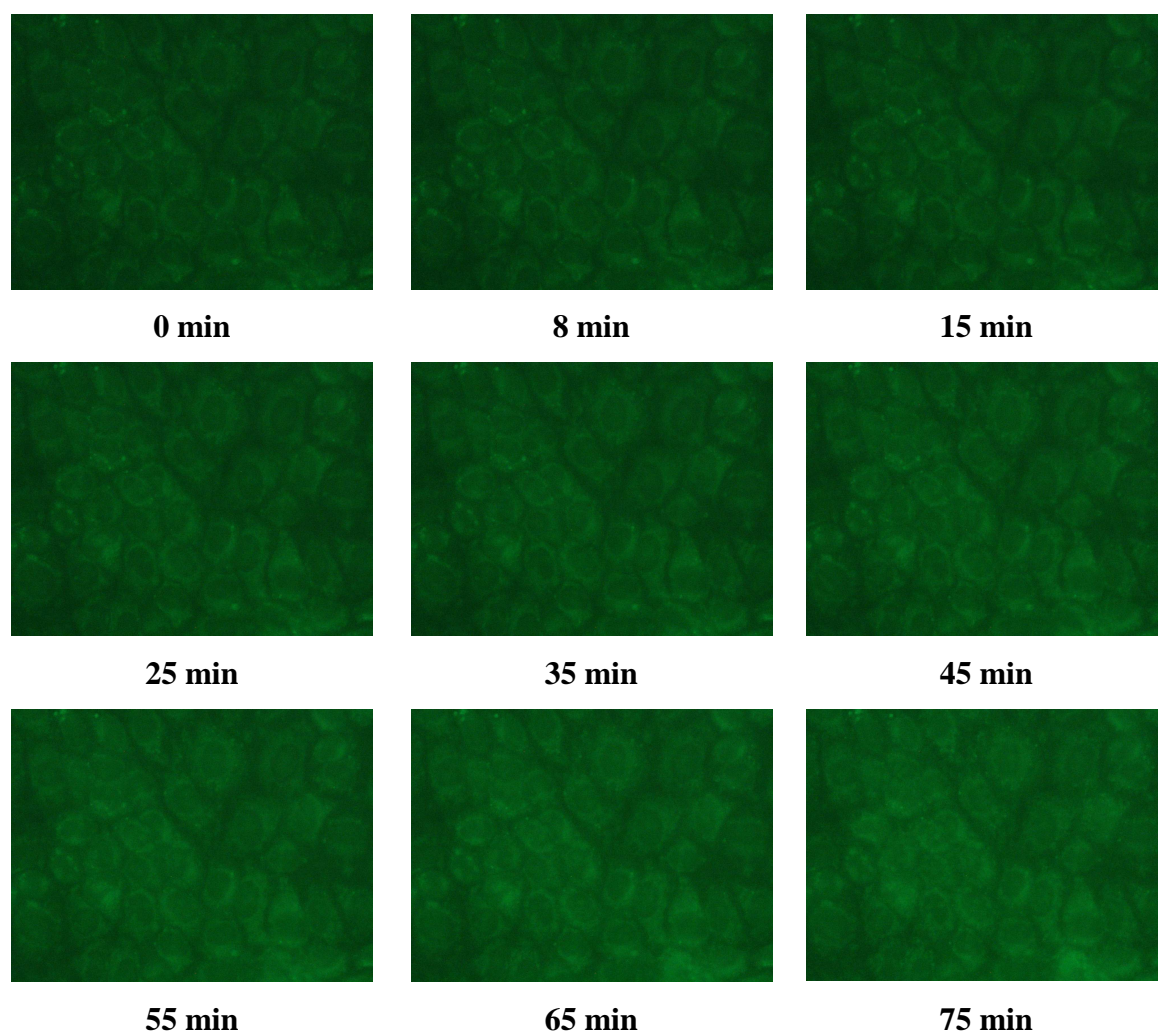### 6.3.5 Instrumental Settings to Determine the Fluorescence of HP Green on Particles/Additional Spectra

Fluorescence emission spectra of the particles were acquired on an Aminco Bowman AB2 luminescence spectrometer with the following experimental parameters: Excitation: 450 nm, bandwidth 8 nm; emission: 530 nm, bandwidth 8 nm; PMT voltage: 760 V (for PAN and PS particles), 665 V (for AC particles).
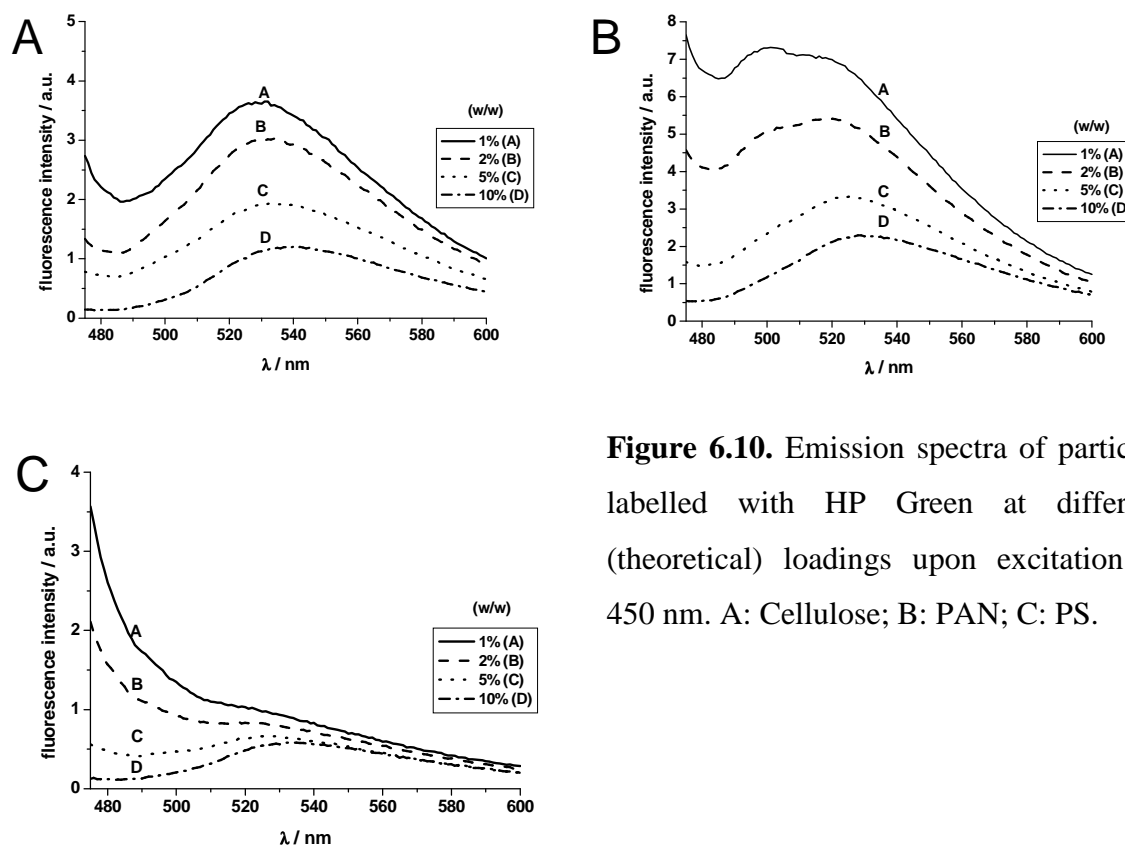
Figure 6.10. Emission spectra of particles labelled with HP Green at different (theoretical) loadings upon excitation at 450 nm. A: Cellulose; B: PAN; C: PS.

6.3.6 Instrumental Settings for Spectral Investigation of the H_2O_2 Sensor

Sensors were placed in a powder cell with quartz window connected to a Minipuls 3 peristaltic pump (Gilson Inc, www.gilson.com). Fluorescence emission spectra of the sensors were recorded on a FP-6300 spectrofluorometer (JASCO, www.jasco.de) with the following experimental parameters: excitation: 450 nm, bandwidth 5 nm; emission bandwidth 5 nm; PMT voltage: medium; the cell was fixed in a modified FDA-430 solid sample holder. Time trace measurements were acquired with the following experimental parameters: excitation: 450 nm, bandwidth: 5 nm; emission: corresponding emission maximum wavelength, bandwidth: 10 nm; PMT voltage: medium; resolution: 5 s.

6.3.7 Experimental Procedure for the Spectroscopic Characterization of Probes 10, 12a, 12b and 13 in Lactate Assays

(a) Preparation of stock solutions of dyes

3.2 mg of **10** were dissolved in 2.07 mL phosphate buffer (pH 7, 10 mM) for a 3.3 mM stock solution. 1.56 mg of **12a** and 1.86 mg of **12b**, respectively, were dissolved in phosphate buffer (pH 7, 10 mM) to obtain stock solutions with a final concentration of 400 µM.

(b) Preparation of lactate stock solutions for experiments in microtiter plates

448.24 mg of either D- or L-lactate were dissolved in 100 mL phosphate buffer (pH 7, 10 mM) to obtain stock solutions with a final concentration of 40 mM. Afterwards, they were diluted to receive the respective solutions for the calibration experiments.

(c) Preparation of sugar stock solutions for experiments in microtiter plates

9 mg either of glucose, fructose or galactose were dissolved in 10 mL phosphate buffer (pH 7, 10 mM) to give a 5 mM stock solution. Afterwards they were diluted to receive new stock solutions for the interference experiments.

(d) Preparation of MTP for calibration of **10** with D-lactate and L-lactate and experimental parameters

Calibration measurements were performed in 96 well MTP-plates from GreinerBioOne (www.gbo.de, 4 wells per concentration) on a GENios Plus MTP-reader from Tecan (www.tecan.com) using a 485 nm excitation and 612 nm emission filter. Further parameters: Gain: 103; Number of flashes: 5; Lag time: 0 µs, Integration time: 40 µs; shake duration before measurement: 10 s.

Blank: 7.6 µL of **10** and 242.2 µL of phosphate buffer (pH 7, 10 mM)

Test-x: 7.6 µL of **10**, 50 µL of D/L-lactate-**x** and 192.4 µL of phosphate buffer (pH 7, 10 mM)

(e) Preparation of MTP for interference of saccharides on **10** and D-lactate and experimental parameters

Interference measurements were performed in 96 well MTP-plates from GreinerBioOne (www.gbo.de, 4 wells per concentration) on a GENios Plus MTP-reader from Tecan (www.tecan.com) using a 485 nm excitation and 612 nm emission filter. Further parameters: Gain: 96; Number of flashes: 5; Lag time: 0 µs, Integration time: 40 µs; shake duration before measurement: 10 s.

Blank: 8 µL **10**, 50 µL D-lactate and 192 µL phosphate buffer (pH 7, 10 mM)

Test-Sugar: 8 µL **10**, 50 µL D-lactate, 50 µL sugar and 142 µL phosphate buffer (pH 7, 10 mM)

(f) Preparation of MTP for calibration of **12a**/**12b** with D-lactate and L-lactate and experimental parameters

Calibration measurements were performed in 96 well MTP-plates from GreinerBioOne (www.gbo.de, 8 wells per concentration) on a GENios Plus MTP-reader from Tecan (www.tecan.com) using a 485 nm excitation and 612 nm emission filter. Further parameters: Gain: 200; Number of flashes: 100; Lag time: 50 µs, Integration time: 50 µs; time between move and flash: 10 ms; shake duration before measurement: 50 s.

Blank: 5 µL **12a**/**12b** and 195 µL phosphate buffer (pH 7, 10 mM)

Test-x: 5 µL **12a**/**12b**, 10 µL D/L-lactate-**x** and 185 µL phosphate buffer (pH 7, 10 mM)

(g) Preparation of MTP for interference of saccharides on **12a** and D-lactate or L-lactate and experimental parameters

Interference measurements were performed in 96 well MTP-plates from GreinerBioOne (www.gbo.de, 4 wells per concentration) on a GENios Plus MTP-reader from Tecan (www.tecan.com) using a 430 nm excitation and 612 nm emission filter. Further parameters: Gain: 94; Number of flashes: 100; Lag time: 0 µs, Integration time: 40 µs; shake duration before measurement: 45 s.

Blank: 12.5 µL **12a**, 10 µL D/L-lactate and 177.25 µL phosphate buffer (pH 7, 10 mM)

Test: 12.5 µL **12a**, 10 µL D/L-lactate, 50 µL saccharide and 127.25 µL phosphate buffer (pH 7, 10 mM)

6.3.8 Calculation of Selectivity Values

Table 6.1. Selectivity for D-lactate or L-lactate of probe **10**

c(lactate) / µM	Increase (D)	Increase (L)	Selectivity
1	5.41	0.11	**49**
10	7.38	0.23	**32**
100	8.58	2.13	**4**
1000	9.35	4.79	**2**

Table 6.2. Selectivity for D-lactate or L-lactate of probe **12a** and **12b**, respectively.

	12a			**12b**		
c(lactate)	Increase	Increase	Selectivity	Increase	Increase	Selectivity
µM	(D)	(L)		(D)	(L)	
1000				18.24	14.42	**1.3**
750				17.26	14.5	**1.2**
500				17.03	12.68	**1.3**
250	15.43	17.18	**0.9**	11.83	10.52	**1.1**
100	14.82	14.14	**1.0**			
75	11.32	13.88	**0.8**	7.13	10.5	**0.7**
50	10.71	5.967	**1.8**	4.786	9.767	**0.5**
20	6.930	1.139	**6.1**	0.003	9.447	**3.3E-4**

Table 6.3. Selectivity for *ortho*- (**12a**) or *para*-phenylboronic acid (**12b**) to D/L-lactate.

	D-lactate			**L-lactate**		
c(lactate) /	Increase	Increase	Selectivity	Increase	Increase	Selectivity
µM	(*ortho*)	(*meta*)		(*ortho*)	(*meta*)	
1000		18.24			14.42	
750		17.26			14.5	
500		17.03			12.68	
250	15.43	11.83	**1.3**	17.18	10.52	**1.6**
100	14.82			14.14		
75	11.32	7.13	**1.6**	13.88	10.5	**1.3**
50	10.71	4.786	**2.2**	5.967	9.767	**0.6**
20	6.930	0.003	**2,234**	1.139	9.447	**0.12**

6.3.9 Emission Spectra for Probe 13 upon Interaction with D-Lactate or L-Lactate
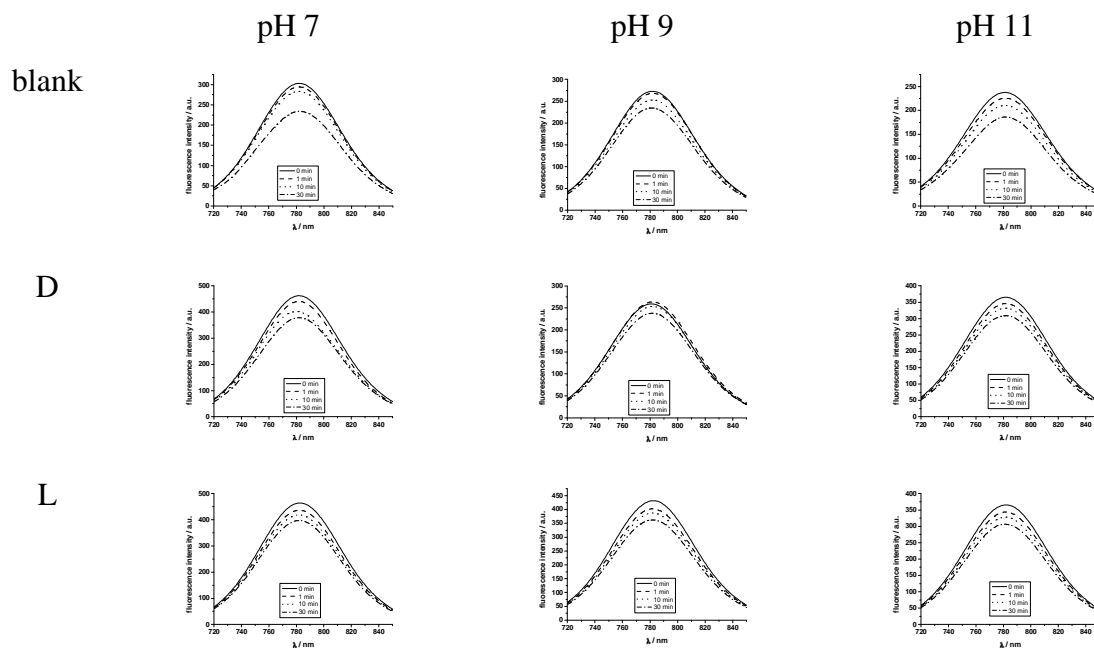
Figure 6.11. Emission spectra that were used to establish Table 4.7.

6.3.10 Additional Emission Spectra of Aminocyanine 13

pH 5   pH 6
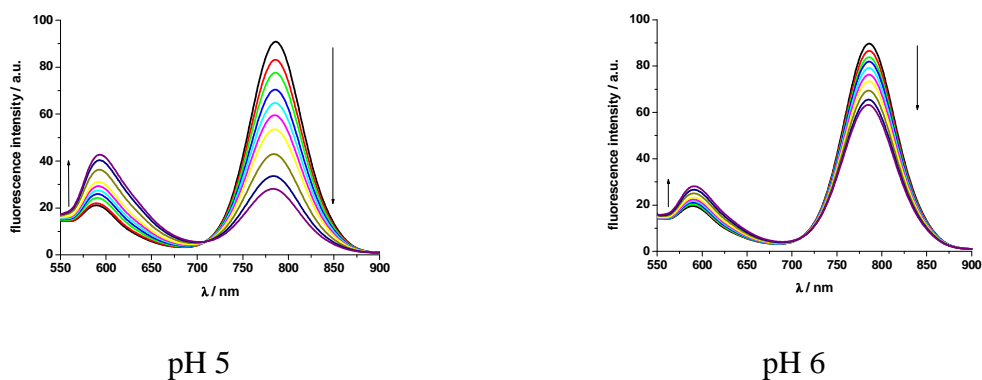
Figure 6.12. Time-dependent emission spectra of **13** (10 µM) in phosphate buffered solutions of varying pH after 0, 10, 20, 30, 40, 50, 60, 120, 190 and 240 min, respectively. Excitation at 527 nm.

pH 7   pH 8

Fig. 6.12. continued.

6.3.11 Additional Emission Spectra of Aminocyanine 14

pH 5   pH 6

pH 7   pH 8

Figure 6.13. Time-dependent emission spectra of **14** (10 µM) in phosphate buffered solutions of varying pH after 0, 10, 20, 30, 60, 120, 180 and 240 min, respectively. Excitation at 512 nm.
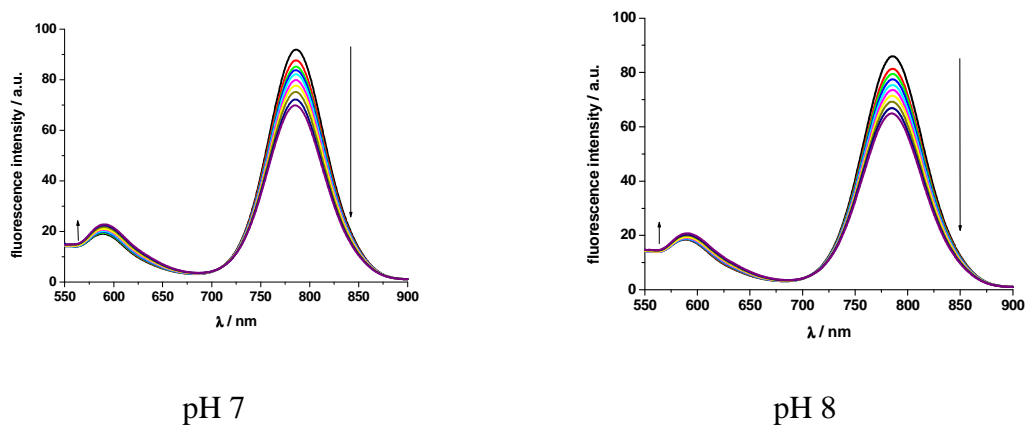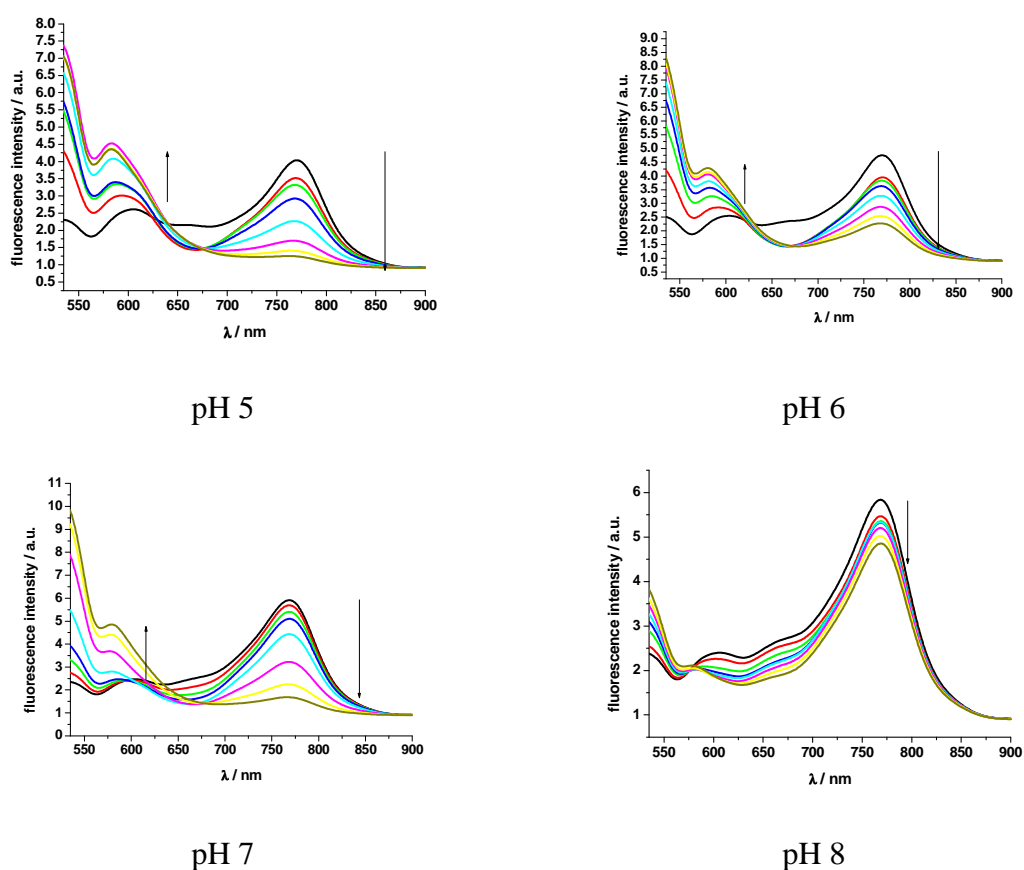
6.3.12 Determination of Molar Absorbance and Fluorescence Quantum Yield

Molar absorption coefficients ε were determined by dissolving the respective fluorophore in three different concentrations in the respective solvent according to the "dry weight determination" method.[2] The quantum yields (QY) of **HP Green** (28.6 µM in PBS) and probe **8** (5 µM in PBS) were determined relatively against the reference dye fluorescein (1.9 µM in 0.1 M NaOH) whose QY is reported to be 0.95.[3, 4] QYs of hemicyanine **10** (3.4 µM) and the ruthenium(II) probes **12a** (6.8 µM) and **12b** (4.16 µM) were determined in air-saturated water relatively against the reference dye $Ru(bpy)_2Cl_2$ x 6 H_2O (4.2 µM), whose QY is reported to be 0.028.[5]

6.4 Literature

1. Q. Jiang, M. Ryan, P. Zhichkin, Use of in situ isopropoxide in the metal-halogen exchange of arylboronates. *J. Org. Chem.*, **2007**, 72, 6618 – 6620.

2. J.-S. Hong, J. C. Rabinowitz, Molar extinction coefficient and iron and sulphide content of clostridial ferredoxin. *J. Biol. Chem.*, **1970**, 245, 4982 – 4987.

3. M. Grabolle, M. Spieles, V. Lesnyak, N. Gaponik, A. Eychmüller, U. Resch-Genger, Determination of the fluorescence quantum yield of quantum dots: suitable procedures and achievable uncertainties. *Anal. Chem.*, **2009**, 81, 6285 – 6294.

4. J. H. Brannon, D. Madge, Absolute quantum yield determination by thermal blooming. Fluorescein. *J. Phys. Chem.*, **1978**, 82, 705 – 709.

5. K. Nakamaru, Synthesis, luminescence quantum yields, and lifetimes of trischelated ruthenium(II) mixed-ligand complexes including 3,3´-dimethyl-2,2´-bipyridyl. *Bull. Chem. Soc. Jpn.*, **1982**, 55, 2697 – 2705.

7. Summary

7.1 In English

Novel fluorescent probes and methods are presented that enable the determination of lactate and hydrogen peroxide (HP). The first part (chapter 2) describes the design and preparation of two fluorescent probes for HP. The naphthalimide fluorophores **5** (which is referred to as **HP Green**) and **8** have either a *p*-anisidine (HP Green) or N,N-dimethyl-*p*-phenylene diamine (**8**) group attached as a redox active moiety. Both PET probes display absorption around 450 nm and emission at 534 nm. HP Green turned out to be more stable on air and to be more suitable for experiments under physiological conditions. PET from the redox moiety to the fluorophore is suppressed after oxidation with HP, and HP Green displays a moderate increase in fluorescence (of up to 11%) in a range of 10 to 250 µM of HP. The effect, however, is increased significantly in presence of horseradish peroxidase (HRP), and fluorescence rises up to 11-fold. HRP decreases the incubation time (30 min *vs.* 11 min) and shifts the dynamic range to much lower concentrations (100 nM to 5 µM) with a limit of detection (LOD) of 64 nM of HP. This closely matches the one of the well established Amplex Red probe (LOD 50 nM). L-Lactate detection affords lactate oxidase (LOx) in combination with HP Green and HRP to yield a fast enzymatic assay (6 min). The dynamic range is from 0.5 to 10 µM of L-lactate with a LOD of 162 nM, which is 6-fold lower than methods that apply Amplex Red (LOD 1 µM). Furthermore, a D-glucose assay with glucose oxidase was established. After 11 min of incubation, the dynamic range is from 2 to 30 µM and the LOD is 0.64 µM, which is 3-fold lower than the respective Amplex Red system (2 µM). HP Green also was applied as an *in-vitro* probe for imaging of HP in NRK cells. In addition, the feasibility of a reusable chemosensor for HP is shown, in which a reductive agent can regenerate HP Green so to enable quasi-continuous monitoring of HP (chapter 3).

The second part aims at the development of probes that directly bind lactate upon covalent interactions (chapter 4). *Ortho-* and *meta*-phenylboronic acids, respectively, are connected to either a hemicyanine fluorophore (**10**) or ruthenium(II) complexes (**12a/b**). Upon excitation at 460 nm, all fluorophores emit red light around 610 nm and differed in their response to both lactate enantiomers. The experiments hint at boronic acids being suitable to the detection of lactate and to differentiate between the two enantiomers at concentrations from 20 µM to 75 µM and 500 µM to 1000 µM for probes **12a** and **12b** and

1 µM to 1000 µM for probe **10**. The presence of saccharides is to be avoided owing to their strong interference. The cyanine dye **13** features interesting spectral properties as the blue dye changes its colour to purple in acidic aqueous solutions (Chapter 5). Another similar cyanine derivative **14** displays the same spectral changes but they occur faster, here. Hence, the purple decomposition product of **14** was isolated with preparative HPLC and its molecular weight was determined to be 754.3 g/mol. The dye displayed absorption at 534 nm and two emission maxima at 547 and 588 nm. Finally, a colorimetric sensor for acidic gases was developed. It was exploiting the chameleon properties of **14** in presence of gaseous hydrochloric acid. The sensor slowly changes its colour from blue to purple upon exposition to low amounts of gaseous HCl (0.1 µbar), and high partial pressures of HCl can accelerate the response to less than 30 min. The irreversible, disposable sensor layer may be used as an indicator for inappropriate storage conditions or as a long-term dosimeter for workplace monitoring.

7.2 In German

Im Rahmen dieser Arbeit werden neue fluoreszierende Farbstoffe und Methoden vorgestellt, die die Bestimmung von Laktat und Wasserstoffperoxid (HP) ermöglichen.

Der erste Teil (Kapitel 2) beinhaltet die Synthese und analytische Anwendung zweier neuer fluoreszierender Farbstoffe für den Nachweis von HP. An die Naphthalimid-fluorophore **5** (welcher als **HP Green** bezeichnet wird) und **8** sind entweder *p*-Anisidin (HP Green) oder N,N-Dimethyl-*p*-phenylendiamin (**8**) als redoxaktive Gruppen gebunden. Die beiden PET Farbstoffe zeigen Absorptionsmaxima um 450 nm und Emissionsmaxima bei 534 nm. HP Green ist an Luft stabiler und für Messungen unter physiologischen Bedingungen der bessere Farbstoff. Die Oxidation durch HP unterdrückt den PET von der redoxaktiven Gruppe zum Fluorophor und ein schwacher Anstieg der Fluoreszenz (bis zu 11%) ist im Konzentrationsbereich von 10 bis 250 µM HP zu beobachten. Jedoch wird dieser Effekt durch Zugabe von Meerrettich Peroxidase (HRP) enorm verstärkt, wodurch die Fluoreszenz um das elffache steigt. HRP verkürzt die Inkubationszeit (von 30 min auf 11 min) und verschiebt den dynamischen Bereich des Farbstoffs zu weitaus niedrigeren Konzentrationen (0,1 bis 5 µM HP), wobei eine Nachweisgrenze (LOD) von 64 nM HP erreicht wird. Diese liegt im Bereich des besten gängigen Fluoreszenzfarbstoffs zum Nachweis von HP, dem Amplex Red (LOD 50 nM). Zur enzymatischen Bestimmung von L-Laktat werden Laktatoxidase (LOx), HP Green und HRP in eine Probe gegeben. Dies

ermöglicht einen schnellen Assay (6 min) mit einem dynamischen Bereich von 0,5 bis 10 µM L-Laktat. Die LOD ist mit 162 nM um das sechsfache niedriger als bei Amplex Red basierten Methoden (LOD 1 µM). Desweiteren wurde ein enzymatischer Assay für D-Glucose mit Hilfe von Glucoseoxidase entwickelt. Nach einer Inkubationszeit von 11 min kann Glucose von 2 bis 30 µM bestimmt werden. Die Nachweisgrenze beträgt 0,64 µM und liegt damit um einen Faktor von 3 niedriger als das entsprechende Amplex Red System (LOD 2 µM). HP Green wurde auch mit Zellen inkubiert und nach Aufnahme HP *in-vitro* über Fluoreszenzmikroskopie visualisiert. Zusätzlich wird die Machbarkeit eines wieder verwendbaren Chemosensors für HP gezeigt, der nach Regeneration von HP Green mit einem Reduktionsmittel eine quasi-kontinuierliche Messung von HP ermöglicht (Kapitel 3).

Der zweite Teil beinhaltet die Entwicklung von Farbstoffen, die direkt über kovalente Wechselwirkungen an Laktat binden (Kapitel 4). Dazu werden *ortho-* bzw. *meta-*Phenylboronsäuren entweder an einen Hemicyaninfarbstoff (**10**) oder an Ruthenium(II)-komplexe gebunden (**12a,b**). Nach Anregung bei 460 nm emittieren alle Fluorophore rotes Licht um 610 nm, unterscheiden sich aber bezüglich ihrer Wechselwirkung mit beiden Laktat-enantiomeren. Die Experimente zeigen, dass Boronsäuren geeignet sein können um Laktat nachzuweisen und zwischen beiden Enantiomeren zu differenzieren, aber nur zwischen 20 bis 75 µM im Falle von Verbindung **12a** bzw. von 0,5 bis 1 mM für Verbindung **12b** sowie von 1 bis 1000 µM für Fluorophor **10**. Sacharide müssen aufgrund ihrer erheblichen Störung des Fluoreszenzsignals aus dem Reaktionsgemisch fern gehalten werden. Der blaue Cyaninfarbstoff **13** zeigt interessante spektrale Eigenschaften da er seine Farbe in sauren wässrigen Lösungen zu purpurrot ändert (Kapitel 5). Ein weiteres, ähnliches Cyaninderivat **14** geht dieselben spektralen Änderungen ein, allerdings laufen sie hier schneller ab. Das purpurrote Zersetzungsprodukt von **14** wurde mit präparativer HPLC isoliert und sein Molekulargewicht zu 754,3 g/mol bestimmt. Der Farbstoff absorbiert bei 534 nm und besitzt zwei Emissionsmaxima bei 547 und 588 nm. Damit wurde ein colorimetrischer Sensor für saure Gase entwickelt, welcher sich des Farbumschlags von **14** in Gegenwart von gasförmiger Salzsäure bedient. Der Sensor ändert seine Farbe langsam und irreversibel von blau nach purpurrot, wenn er niedrigen HCl Mengen (0,1 µbar) ausgesetzt ist. Hohe Partialdrücke an HCl verkürzen das Ansprechverhalten auf weniger als 30 min. Die Sensorschicht könnte als Indikator für falsche Lagerbedingungen in Verpackungen dienen oder als Langzeitdosimeter zur Kontrolle der Exposition mit sauren Gasen am Arbeitsplatz verwendet werden.

8. Curriculum Vitae

Name:	Dominik Berndt Michael Grögel
Date of Birth:	April 16th 1982
Place of Birth:	Deggendorf
Family Status:	single

Doctorate, University of Regensburg	2007/12 – present
Ph.D. Thesis, Institute for Analytical Chemistry, Chemo- and Biosensors	2007/12 – 2011/07
„*New fluorescent probes and assays for lactate and hydrogen peroxide*"	

Studies

Chemistry studies at the University of Regensburg	2002/10 – 2007/09
Chemistry Diploma	2007/09
Diploma Thesis, Institute of Organic Chemistry,	2007/01 – 2007/09
„*Synthesis of peptides related to the N- and C-terminal domains of the Id2 protein and their characterization*"	

School Education

General qualification for university entrance / baccalaureate	2001/06
Robert-Koch-Gymnasium Deggendorf	1992/09 – 2001/06

Languages

English, French and Italian

Work Experience

Warehouse employee, UPS Germany, Passau Agency	2001/10 – 2002/10

9. List of Publications

Journal Papers

1. X. Wang, H.-H. Gorris, J. A. Stolwijk, R. J. Meier, D. B. M. Groegel, J. Wegener, O. S. Wolfbeis, "Self-referenced RGB colour imaging of intracellular oxygen." *Chem. Sci.*, **2011**, 2, 901 – 906.

2. M. Schaeferling, D. B. M. Groegel, S. Schreml, "Luminescent probes for detection and imaging of hydrogen peroxide." *Microchim. Acta*, **2011**, 174, 1 – 18.

3. H.-H. Gorris, S. M. Saleh, D. B. M. Groegel, S. Ernst, K. Reiner, H. Mustroph, O. S. Wolfbeis, "Long-wavelength absorbing and fluorescent chameleon labels for proteins, peptides and amines." *Bioconjugate Chem.*, **2011**, DOI: 10.1021/bc200192k.

4. D. B. M. Groegel, M. Link, A. Duerkop, J. Wegener, O. S. Wolfbeis, "Novel PET probe for fluorescent detection and imaging of hydrogen peroxide." submitted.

Poster Presentations

1. *11th International Conference on Methods and Applications of Fluorescence: Spectroscopy, Imaging and Probes*, September **2009**, Budapest, Hungary;
   "A novel approach for the detection of D-lactate by using fluorescent hemicyanine dyes carrying a boronic acid." (Print in Book of Abstracts)

2. *3rd European Association for Chemical and Molecular Sciences (EuCheMS) Chemistry Congress*, August **2010**, Nuremberg, Germany;
   "Detection of D/L-lactate via luminescent boronic acids." (Print in Book of Abstracts)

Oral Presentation

1. *6th International Students Conference „Modern Analytical Chemistry"*, September **2010**, Prague, Czech Republic;
   "Blue to purple switch of conjugated cyanine dyes in a sensor for acid-containing gaseous environments." (Print in Book of Abstracts)

Erklärung

Hiermit versichere ich, dass ich die vorliegende Arbeit selbst verfasst und keine anderen als die angegebenen Quellen und Hilfsmittel verwendet habe.

Regensburg, den 18.7.2011

Dominik Grögel